Electroforming of Personalized Miniature Metal Parts using Additively Manufactured Molds

by

Hazem Fawzi Hamed

A Thesis submitted to the School of Graduate and Postdoctoral Studies in partial fulfillment of the requirements for the degree of

Master of Applied Science in Mechanical Engineering

Department of Mechanical and Manufacturing Engineering

Faculty of Engineering and Applied Sciences

University of Ontario Institute of Technology (Ontario Tech University)

December 2023

Thesis Examination Information

Submitted by: **Hazem F. Hamed**

Master of Applied Science in Mechanical Engineering

Thesis title:

Electroforming of Personalized Miniature Metal Parts using Additively Manufactured Molds

An oral defense of this thesis took place on December 8th, 2023 in front of the following examining committee:

Examining Committee

Chair of Examining Committee	Dr. Amirkianoosh Kiani
Research Supervisor	Dr. Jana Abou-Ziki
Examining Committee Member	Dr. Sayyed Ali Hosseini
Thesis Examiner	Dr. Ramona Fayazfar

The above committee determined that the thesis is acceptable in form and content and that a satisfactory knowledge of the field covered by the thesis was demonstrated by the candidate during an oral examination. A signed copy of the Certificate of Approval is available from the School of Graduate and Postdoctoral Studies.

Abstract

In response to evolving manufacturing trends favoring personalized, small-batch production, this thesis centers on the development of additively manufactured molds to facilitate the electroforming of personalized metal parts. The methodology encompasses standardized mold design, experimental procedures for mold development and electroforming, and a simulation model for visualizing and predicting the deposition process. The study provides critical design considerations and guidelines for electroforming within additively manufactured molds, successfully demonstrating the production of composite metal components in 2.5D and 3D configurations. Emphasizing cost efficiency and improved part quality, especially for limited-thickness metal components, the developed technique presents advantages over available metal additive manufacturing processes. Electroforming emerges as a versatile and robust metal additive manufacturing technique, expanding its application beyond traditional limitations of thin-walled hollow structures, 2D components and applications at the nanoscale.

Keywords: Electroforming; Metal; Additive Manufacturing; Mold Design; Design Guidelines.

Author's Declaration

I, Hazem F. Hamed, hereby declare that this thesis consists of original work of which I have authored. This is a true copy of the thesis, including any required final revisions, as accepted by my examiners. I authorize the University of Ontario Institute of Technology (Ontario Tech University) to lend this thesis to other institutions or individuals for the purpose of scholarly research. I further authorize University of Ontario Institute of Technology (Ontario Tech University) to reproduce this thesis by photocopying or by other means, in total or in part, at the request of other institutions or individuals for the purpose of scholarly research. I understand that my thesis will be made electronically available to the public.

Hazem Hamed

Statement of Contributions

I performed the research work flow, established the methodology, executed most of the experimental work, interpreted the results, and wrote the manuscript. Mohammadali Aghili performed the electroforming experiments. Jana Abou-Ziki and Rolf Wüthrich conceptualized the research, conducted reviews and edits to the manuscript, and provided supervision throughout the research process.

Hamed, Hazem; Wüthrich, Rolf; Abou-Ziki, Jana. (2023) "Electroforming of Additively Manufactured Conductive Molds for the Manufacture of Miniature Metal Parts." Proceedings of the Canadian Society for Mechanical Engineering (CSME) Annual Conference, Université de Sherbooke, May 2023. In Press.

Chapters 3, 4, 5, and 6 of this thesis are currently being prepared for submission to respected journals in the field as two separate articles.

Acknowledgements

I would like to begin by acknowledging the guidance and mentorship provided by my supervisor Dr. Jana Abou-Ziki, and my co-supervisor Dr. Rolf Wüthrich. Your expertise, patience, and dedication have been pivotal in the completion of this thesis, pushing me beyond my perceived limits.

I extend my heartfelt gratitude to my family for their unconditional support. Your sacrifices and encouragement have been the driving force behind my academic journey. I would not be able to achieve any accomplishments in my life without you. My dear mother, I cannot express how much I love you. I dedicate this work to you!

To my closest friend and colleague, Marwan Eldiasty, thank you for being a constant source of motivation and for the countless hours of discussion, collaboration, and encouragement. My sincere gratitude also goes out to my fellow lab colleagues, namely Zahraa Bassyouni, and Seyed Mahmoud Seyedi Sahebari, for the cherished time we spent together in the lab and your generous help and support during the work. I would also like to thank Mohammad Aghili for conducting the electroforming experiments.

Lastly, I deeply appreciate the teachers, mentors, and individuals who selflessly shared their knowledge, wisdom, and encouragement. While I can't thank each one individually, I am committed to passing on the lessons and kindness to those who may seek it.

Table of Contents

List of Tables

List of Figures

Abbreviations

ABS Acrylonitrile Butadiene Styrene.

AM Additive manufacturing.

CAD Computer-Aided Design.

Cu Copper.

CVS Chemical Vapor Smoothing.

FDM Fused Deposition Modeling.

LIGA German acronym for lithography, electroforming, and molding.

MP Mass Personalization.

STL Standard Tessellation Language.

Chapter 1

Introduction

1.1 Background

Over the past century, mass production has revolutionized manufacturing, significantly reducing costs by distributing production overhead across identical parts. Despite its efficiency and cost reduction benefits, mass production is limited in flexibility. In the 1980s, mass customization emerged as a natural progression, allowing customers to customize products from predefined options, leading to re-configurations of manufacturing lines.

In contemporary manufacturing, there is a discernible shift towards producing smaller batches of personalized products [1]. This transition aligns with just-in-time manufacturing principles and responds to the increasing demand for customization, rapid prototyping, and the emergence of personalization as a distinct concept. Unlike mass customization, personalization involves active customer participation in product design, often resulting in very small batch sizes, ideally one unit. However, this trend poses challenges to traditional mass production methods, which are not adequately suited for such niche, personalized production, leading to increased expenses.

Addressing this challenge, digital manufacturing, often referred to as Industry 4.0, stands out as a promising solution [2]. In digital manufacturing, cyber-physical systems are employed to provide the required flexibility. These systems facilitate the swift and efficient adaptation of production lines to accommodate customer design in-

puts. They integrate various functions, including computer-aided design, simulation, visualization, and analytics [3]. The significance of digital manufacturing becomes more evident as both product complexity and manufacturing processes become more intricate. Within this context, Additive Manufacturing (AM) processes stand out as a promising manufacturing technology to meet the requirements of personalized small-batch-size production. These processes contribute significantly by essentially providing "complexity for free" through virtual means.

Contrary to traditional manufacturing, AM excels in intricate part design and rapid lead times. Moreover, it maintains cost-efficiency for single, complex, or customized items, with a consistent cost per unit regardless of volume or complexity. Despite these advantages, AM faces several challenges across various aspects. Material choice, especially in the metal category, remain somewhat limited. The current technology permits the printing of only a limited array of materials, which constrains the full utilization of AM capabilities. Additionally, post-processing steps are often essential to achieve mechanical attributes and surface quality comparable to those achieved with traditional manufacturing methods. This supplementary phase extends the production time and add complexity to the process.

Electroforming, traditionally used for forming parts on mandrels, has recently garnered attention for additive manufacturing of metal parts [4–6]. The distinction between electroforming and electroplating centers on the intended purpose of the deposited metal. Electroplating involves adding a metallic coating to an existing part, serving either decorative or protective functions. In contrast, electroforming results in metallic components of higher thicknesses manufactured by utilizing the electroplating process to deposit metal onto or around a master form. Electroforming offers significant advantages when compared to traditional manufacturing methods. It enables the production of components that would be challenging or even impossible to create using conventional techniques. Key advantages include high dimensional accuracy and consistency, atomic-scale deposition, tunable mechanical properties, low

surface roughness, and cost efficiency [7–9].

Despite its precision and surface quality advantages, electroforming presents several engineering limitations. These include time-intensive deposition processes, material restrictions, challenges in separating the electroform from the mandrel, and non-uniform deposition thicknesses. Furthermore, possible undesired voids can build-up during the electroforming process resulting in a rough and uneven surface with reduced mechanical properties, and difficulties in replicating high-aspect-ratio micro/nano-structures due to limited ion transport within micro-channels.

Traditionally limited in literature to the fabrication of thin-walled hollow structures, 2D components, LIGA (German acronym for lithography, electroforming, and molding) process, and applications at the nanoscale, electroforming has undergone an exploration in this study. This work aims to adapt the electroforming, exploring its capacity to produce solid and composite structures in both 2.5D and 3D configurations, spanning across micro and macro scales. Noteworthy applications presented in this work boast thicknesses surpassing 1000 μm, a significant feat considering electroforming's historical challenge in achieving surface uniformity at such thicknesses.

Crucially, the methodologies developed for mold design, experimental application, and the simulation model not only overcome this challenge but also lay the foundation for realizing true mass personalization across a spectrum of applications. This positions electroforming as a promising candidate to evolve into a dependable, robust, and versatile metal additive manufacturing technique. The rest of this thesis delves into the intricacies of these advancements and their implications, shedding light on the potential role of electroforming in modern manufacturing.

1.2 Thesis Objective

This thesis aims to establish a set of design procedures for creating modular molds, enabling the electroforming of 2.5D and potentially 3D metal components, specifically with thicknesses exceeding 1000 µm. This involves the utilization of Fused Deposition Modeling (FDM) for fabricating the molds, followed by electroforming to additively manufacture the intended metal components. The study is designed to investigate the potential for achieving mass personalization of metal structures across both macro and micro scales through this low-cost additive manufacturing approach.

To accomplish these objectives, the methodology is divided into several key aspects. Initially, it involves the development of a mold design capable of accommodating the electroforming of intricate metal parts with varying shapes and geometries. Subsequently, an experimental process was developed covering every aspect from the CAD design of the part to its actual manufacture via electroforming. Throughout the research, multiple geometric features are explored to assess the feasibility and efficiency of the fabrication process. This investigation aims to define crucial design considerations, especially for components that exhibit diverse geometries and features.

A simulation model is also introduced to facilitate the visualization of the electroforming process across a range of structures. This model not only saves time but also serves as a guiding tool for more efficient experimental trials. Moreover, the simulation is a necessary tool to achieve true mass personalization. By employing this manufacturing approach, the full potential of FDM printing can be leveraged to fabricate intricate mold geometries while simultaneously producing a large number of parts via electroforming. This can be achieved without incurring supplementary costs tied to design changes initiated by customers. This fabrication method holds the potential to significantly reduce per-unit cost as production volume expands within the realm of mass personalization. Additionally, it offers the capacity for additively manufacturing metal parts with low cost.

1.3 Thesis Outline

The thesis is structured into seven chapters, each serving a distinct purpose. Chapter 1 introduces the research, its objectives, and the outline of the proposed work. Chapter 2 provides the necessary theoretical background, covering topics such as mass personalization, additive manufacturing, and electroforming, while highlighting their associated challenges and opportunities.

Chapter 3 discusses the research methodology, highlighting the mold design, the process overview and the experimental setups used for FDM printing and electroforming. Chapter 4 focuses on assessing the viability of the fabrication approach by electroforming relatively thick copper structures in various geometries, thereby establishing important design considerations for the process.

Chapter 5 focuses on the study and simulation of the electrochemical deposition process of copper. This simulation serves as a time-saving tool and offers guidance for more effective experimental trials. In Chapter 6, the thesis explores the applications of electroforming in the FDM printed molds to produce 2.5D and 3D metal parts. Lastly, Chapter 7 summarizes the key findings presented in the thesis and explores potential avenues for future research.

Chapter 2

Literature Review

2.1 Mass Personalization

Developments in digital manufacturing, in addition to the continuing paradigm change in industrial production, are altering not just traditional methods of production, but also the way customers are served. Manufacturing organizations struggle with the challenges of differentiating themselves from competitors and implementing creative strategies to serve their customer needs [2]. Thus, several businesses are implementing the manufacture of personalized products with more client collaboration. Moreover, personalized products have recently grown in appeal among customers, many of whom feel that manufacturers must tailor their products in order to satisfy all of their latent requirements because mass-produced parts frequently fall short of expectations [10].

Mass Personalization (MP) is the process of design and manufacturing of custom products tailored to the customers' preferences with the efficiency of mass production. To exploit the benefits of MP, the manufactured products must be unique to the customers' needs while still achieving economies of scale through efficient and optimized production processes. While MP provides on-demand products to the customers and answers their diversifying needs, it presents a significant challenge to the companies. For manufacturing organizations to effectively adopt MP, they need to use advanced manufacturing technologies and flexible automation lines that can produce those customized products in an efficient and cost-effective manner. Moreover, they

need to overcome many operational difficulties across multiple departments. Some of these operational challenges are difficulty in forecasting due to the constant changes in the production demands and bill of materials, lack of sufficient flow of product information across departments, and customer-management relationship to facilitate co-creation [11].

Along with the operational difficulties, MP also brings new design challenges, that necessitates designers to adapt the approach of product design in the MP context. Products ought to become adaptable to meet particular customer requirements, and the design process should involve customers more closely in order to elicit those demands. Approaching product development with traditional design techniques and conventional production mindset has various considerations which are not always applicable to flexible manufacturing systems. As a result, traditional design techniques may fall short planning for product variability in the MP context. Thus, designing for MP necessitates a distinct viewpoint and methodology in order to fully leverage manufacturing flexibility and really respond to user demands [2].

2.1.1 Evolution of Mass Personalization

Although MP has been receiving great recognition, primarily in the last two decades, personalized products have a significantly old history in the manufacturing industry. Made-to-order or personalized products were a staple of craft production, yet they were beyond the reach of the majority [12]. Even though industrial manufacturing has mostly taken the place of this kind of production, it still persists today. There have been several paradigm shifts throughout the history of industrial production, depicted in figure 2.1, most of which have been influenced by market conditions or consumer requirements and desires, and facilitated by technology advances [13].

Products were made-to-order, at a premium expense and with restricted accessibility. In addition, there were no manufacturing systems related to the craft production, and products were confined to localized regions, thus such manufacturing paradigm

was not scalable [14]. Subsequently, to meet rising product demand, the emergence of large-scale production systems with flexible assembly lines altered the paradigm to Mass Production [15]. Mass production is the automated manufacturing of standardized products at a low cost and high volume, without any involvement of the customer.

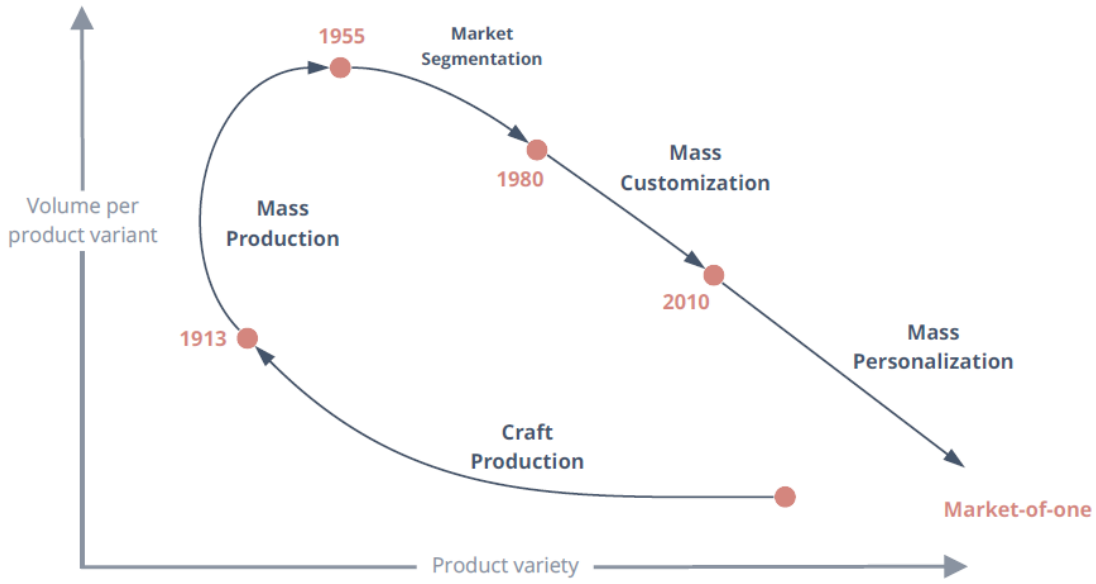

Figure 2.1: Comparison of the volume-variety of the produced products in manufacturing paradigms. Figure reprinted from [2].

Mass production, with its capacity for affordable, high-volume manufacturing, has historically provided products to the masses. However, this approach often sacrificed product uniqueness in favor of a one-size-fits-all model. Companies concentrated on promoting, selling, and distributing these mass-produced items, believing that supply would naturally generate demand. Nevertheless, as markets in various sectors began to mature and saturate around the 1950s, businesses started shifting their focus from products to markets.

Following the notion that the fundamental goal of a company should be the satisfaction of their consumers [16]. Market segmentation was the inevitable next step as the focus on markets grew, and it was the first step towards product variety. Mar-

ket segmentation divides the market into segments with different demand functions, necessitating modifications to products and marketing strategies to account for these variations. As a result, companies started to form according to market sectors and to provide various niche product options. Moreover, the market started to focus more on the consumers and their specialized demands as the need for product diversity increased [15]. Hence, the mass customization paradigm emerged in the 1980s to answer the diverse customer needs.

Mass customization allows customers to choose tailored product features while maintaining cost efficiency, driven by adaptable manufacturing technologies. This shift in customer engagement from selection to active configuration has potential[17]. However, mass customization faces challenges including low adoption rates due to complex and costly modularity and limited customer interest in specific configurations, thus constraining product diversity [13].

Presently, an ongoing industrial transformation is underway, which has the potential to render products both accessible and personalized. Mass-produced goods often fall short of meeting individualized customer requirements. Therefore, companies, driven by global competition and evolving market dynamics, seek ways to produce personalized products at costs comparable to mass production [18]. This industrial transformation aligns with the demand for customized products and Industry 4.0 vision of smart manufacturing, characterized by responsive, autonomous, and on-demand processes using highly intelligent cyber-physical systems [19].

Digital manufacturing combines flexible production methods with information systems to efficiently provide customized products while maintaining mass production efficiency. This innovation has led to the emergence of MP, which offers unique products tailored to individual customers' needs, distinguishing itself from traditional Craft Production methods that tend to be more labor-intensive and costly due to craftsmanship.

In addition, MP emphasizes the accessibility of personalized products, making it a

compelling and feasible approach for businesses [20]. The process of product differentiation commenced with market segmentation and was followed by mass customization striving to fulfill individualized needs of customers [21]. Meeting personal needs necessitates a comprehensive understanding of individual customers, which consequently transforms the customer's role in the design process from mere configuration to active co-creation [22]. With the evolvement of manufacturing paradigms, there have been substantial transformations in product design [13].

According to Koren et al. [23], there are three fundamental actions inherent in all manufacturing paradigms: design, fabricate and sell. What sets these paradigms apart is the sequence and the participants involved in these actions. In Craft Production, the order follows sell-design-fabricate, where the craftsman assumes both the role of designer and manufacturer. In the realm of mass production, however, product design becomes a distinct professional activity, leading to a shift in the order of operations to design-fabricate-sell. This is accompanied by the presence of standardized products meticulously designed by professionals and held in stock.

Mass customization and mass personalization necessitate customer involvement, thereby shifting the sequence of operations to design-sell-make. In Mass Customization, the manufacturer designs all module variants, and the product is manufactured once the customer selects from the provided options. On the other hand, MP entails active customer engagement in the design process to understand the individual needs [13] and effectively transmit that to the design stage becomes crucial.

Consequently, when designing products for MP, careful consideration should be given to incorporating variety through fundamental design and structural modifications, while ensuring the meaningful participation of customers in the design process. Table 2.1 summarizes the main differences between mass production, mass customization, and mass personalization in terms of the market, customer, product, and manufacturing system.

Mass Customization focuses on a select market segment, leveraging mass efficiency

Table 2.1: A comparison between mass production, mass customization, and mass personalization. Adopted from [2, 15]

Point of Comparison	**Mass Production**	**Mass Customization**	**Mass Personalization**
Market	Market for all	Market of few	Market of one
Customer demand	Generic customer requirements	Specific requirements of a market sector	Personalized needs
Customer role	Purchase	Configure and purchase	Design, configure, and purchase
Customer involvement	Limited to no participation	User configuration	User co-creation
Value proposition	Fixed product	Product options variety	Tailored products
Product alteration	No change	Modifications based on available selections	Changeable and adaptable
Manufacturing System	Standardized assembly lines	Re-configurable manufacturing systems	On-demand manufacturing

to offer diverse product configurations. In contrast, MP aims for individualized products, prioritizing value creation over efficiency. However, there exists a threshold beyond which the cost of value creation outweighs the benefits.

Modifications in the design inputs can lead to the emergence of additional production expenses, which can be systematically categorized using Ishikawa's 6M methodology, as depicted in figure 2.2. Within the measurement category, augmented manufacturing costs arise due to the production of small batches of distinct products to achieve mass personalization.

Giving customers the freedom to actively change the design introduces supplementary material expenses, which subsequently impact the sustainability of the supply chain [24]. Moreover, alterations in design lead to augmented manufacturing expenses in the machining procedures. For instance, specialized tools necessary for producing a personalized product can no longer be applied across a significant number of other products. In addition, the production of personalized items escalates the expenses associated with manufacturing procedures such as assembly, part transfer, design, and post-processing [25].

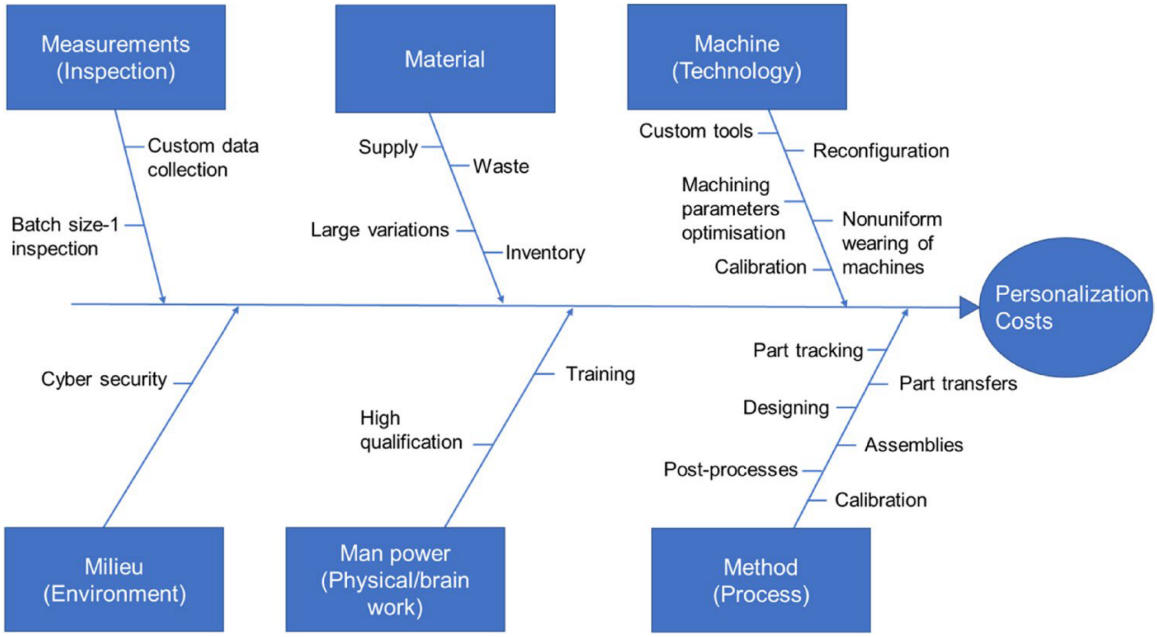

Figure 2.2: The supplementary expenses associated with personalized parts production, systematically categorized based on the Ishikawa's 6Ms. Figure reprinted from [26].

Previous studies done by Boer and Dulio [26], and Abdul Kudus [24] affirm that personalization does enhance customer value, but their willingness to pay for this added value can range up to 30% more compared to mass-produced alternatives. The Deloitte consumer review [25] similarly reports that approximately one-third of customers are only willing to pay a 10% premium for personalized products, while another third is willing to pay an additional 20% to 40%. These findings encompass

various product categories such as clothing, footwear, jewelry, electronic gadgets, and homeware.

Notably, medical products represent an exception, where the added value holds greater significance, and customers may prefer personalized products irrespective of the cost due to associated health benefits. However, for other consumer durables, targeting mass efficiency remains crucial in attracting customers. The key cost drivers in MP are the design personalization process and manufacturing. The flexibility afforded by digital manufacturing is an essential prerequisite for MP, while the automation of design personalization plays a vital role in achieving mass efficiency.

2.1.2 Manufacturing Processes for Mass Personalization

Mass Production and Mass Customization predominantly rely on conventional production methods, where flexibility in the supply chain and assembly processes allows for diverse product configurations [27]. In the context of Mass Customization, product differentiation is achieved through the utilization of modular and common components, offering variation to customers [28]. On the other hand, MP requires flexibility at the manufacturing's lowest level.

Since each manufacturing paradigm has distinct objectives, the production tools, processes, and their characteristics also diverge; craft production, rooted in traditional practices, relies on processes such as manual labor, machining, and a diverse range of fabrication tools. Unlike mass production, craft production involves limited or no reliance on tooling, granting greater flexibility in the workflow and facilitating the introduction of new products and customization of designs. However, due to its manual nature, craft production exhibits lower throughput and is not easily scalable [29]. Conventional mass production, however, relies on traditional manufacturing methods such as injection molding, casting, forming, or stamping, which necessitate costly tooling and significant lead time for creation, setup, and refinement.

Efficiency can be enhanced through the implementation of assembly lines and au-

tomation. Once established, this mode of production enables the rapid production of thousands of units within a short time-frame, with the fixed costs distributed across these units, resulting in low unit costs. However, mass production processes are inflexible, and implementing design changes incurs substantial expenses due to the need to modify tooling and adapt the manufacturing process.

Mass customization relies on cutting-edge and emerging technologies to gather data, generate designs, fabricate parts, and assemble products. It employs manufacturing processes that eliminate the need for tooling or utilizes low-volume rapid tooling for traditional processes, thereby reducing costs. Depending on the complexity of the product and the level of development required, the time to market for mass customization may exceed that of mass production. Nevertheless, modifications to the product design are cost-effective and straightforward, enabling customization and facilitating adaptation to market demands. Moreover, many enterprises embrace the concept of modularity, incorporating a range of standardized mass-produced components that can be assembled in various configurations, modified, and combined with custom parts to produce the final product. This approach boosts throughput and ensures manageable costs [30].

The case is different regarding MP, as each individual product can have its own design, material, and complexity, thus there's no specific machining methods or manufacturing processes that can apply in this case. However, the advent of Industry 4.0 integrates information and communication technologies into manufacturing, facilitating the development of intelligent and adaptable processes within smart factories. The industry 4.0 framework envisions the capability to produce personalized products that are both affordable and timely. Such intelligent manufacturing endeavors enable the realization of mass personalized production through highly flexible processes [31].

According to Lu et al. [19], smart manufacturing is characterized as an operational framework that is fully integrated, collaborative, and responsive. It encompasses real-time adjustments to address evolving demands and conditions within the factory,

supply network, and customer requirements. This is achieved through data-driven comprehension, reasoning, planning, and execution of all facets of manufacturing processes. Advanced sensing, modeling, simulation, and analytics technologies play a crucial role in facilitating this comprehensive approach.

Digital manufacturing technologies play a pivotal role in the smart manufacturing paradigm, enabling data-driven and adaptable production. This encompasses a range of processes, both additive and subtractive, that are under the control of computer-based systems. These systems integrate various functionalities such as computer-aided design (CAD), simulation, visualization, and analytics [32]. The value of digital manufacturing becomes increasingly apparent as the complexity of both the product and its manufacturing processes intensifies [18].

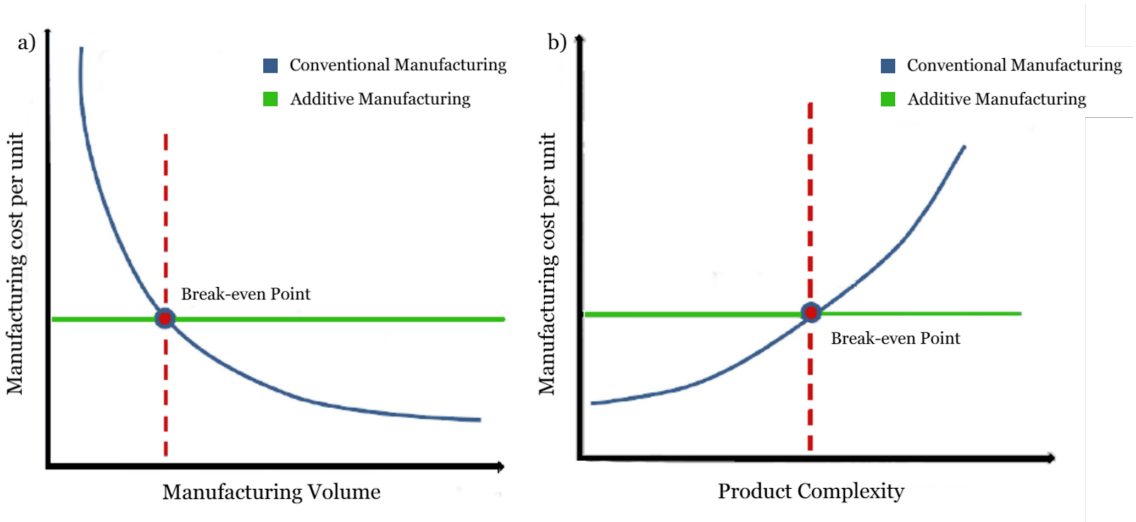

Figure 2.3: A graph illustrating the contrast between additive manufacturing and traditional manufacturing in relation to (a) production volume and (b) product complexity versus manufacturing cost per unit. Adapted from [3].

Within this context, Additive Manufacturing processes emerge as notable contributors, effectively offering "complexity for free" through virtual means [33]. By employing layer-by-layer material deposition and eliminating the need for dedicated tooling, additive manufacturing processes present new possibilities in design, such as optimizing lightweight structures, incorporating hierarchical arrangements, and

consolidating parts [34].

This enhance design freedom and flexibility and also facilitate product differentiation through fundamental design modifications, thereby unlocking significant potential for MP. Consequently, additive manufacturing processes hold particular significance among the array of digital manufacturing technologies, as they enable the realization of MP.

Moreover, additive manufacturing offers the advantage of maintaining low costs for producing batches of single, complex, and personalized products. In conventional machining methods, the manufacturing volume and product complexity significantly influence the product manufacturing cost. However, additive manufacturing technologies operate differently, where the cost per unit remains constant irrespective of the volume or complexity, as demonstrated in figure 2.3. Consequently, the future landscape of manufacturing low-cost products will no longer solely rely on mass production.

2.2 Additive Manufacturing

Additive manufacturing (AM) is a cutting-edge technique that involves the blending of materials through processes like fusion, binding, or solidification of liquid resins and powders. This innovative method constructs parts layer by layer, employing 3D computer-aided design (CAD) modeling to create intricate and precise three-dimensional objects. AM processes excel at fabricating components based on 3D computer data or Standard Tessellation Language (STL) files, which contain detailed information about the object's geometry [35]. This technology proves highly advantageous in scenarios demanding low production volumes, intricate design complexity, and frequent design changes. One of the key strengths of AM lies in its capability to produce complex parts by circumventing the design constraints that often accompany traditional manufacturing methods. This enables the creation of intricate, custom-made components with unparalleled efficiency [36].

Until now, the technology commonly referred to by various names, such as rapid prototyping, rapid manufacturing, 3D printing, desktop manufacturing, and solid freeform fabrication (SFF), has evolved significantly since its commercialization in the mid-1980s and early 1990s. In its early stages, the technology was primarily utilized for creating concept models and prototypes. However, as the technology advanced and gained acceptance, its applications expanded to include the production of functional parts and components. Notably, as recently as 2004, a mere 8% of all parts manufactured using this technology were attributed to the production of actual end-use parts [37]. This statistic highlights the initial focus on prototyping and concept development, with production applications gradually gaining momentum over time.

Despite its numerous advantages, AM also faces several challenges and disadvantages in various aspects. The selection of materials remains somewhat limited, particularly in the metal category. The current technology allows for the printing of only a narrow range of materials, which hinders the full realization of AM's potential. Moreover, post-processing procedures are often necessary in AM to attain mechanical properties and surface finishing comparable to those achieved through traditional manufacturing processes. This additional step can increase production time and complexity. Furthermore, the cycle times for repetitive part production in AM tend to be longer, and cost reductions may not be as apparent when compared to conventional manufacturing methods [38].

A multitude of additive manufacturing processes are now available, each varying in how they deposit layers to create parts, their operating principles, and the materials they can use. Some methods involve melting or softening materials to produce layers, such as selective laser melting (SLM), selective laser sintering (SLS), and fused deposition modeling (FDM). On the other hand, some methods cure liquid materials, like stereolithography (SLA). Each of these methods comes with its own set of advantages and drawbacks. As a result, certain companies provide the option to choose

Table 2.2: Classification of additive manufacturing processes according to ASTM. Adopted from [39, 40].

Process Category	**Technology**	**Materials**
Material Extrusion	Fused Deposition Modelling (FDM) Fused Filament Fabrication (FFF)	Polymers Sand
Vat Photo-polymerization	Stereolithography (SLA) Digital Light Processing (DLP)	Polymers Sand Wax
Material Jetting	PolyJet and MultiJet Printing (MJP)	Polymers Metals Wax
Binder Jetting	Powder Bed and Inkjet Head (PBIH) Plaster-based 3D Printing (PP)	Polymers Metals Glass
Powder Bed Fusion	Selective Laser Sintering (SLS) Selective Laser Melting (SLM) Laser Beam Melting (LBM)	Polymers Metals Ceramics
Sheet Lamination	Laminated Object Manufacturing (LOM) Ultrasonic Consolidation (UC)	Polymers Metals
Directed Energy Deposition	Direct Laser Deposition (DLD) Laser Metal Deposition (LMD) Direct Metal Deposition (DMD)	Powders Metals

between powder-based or polymer-based materials for building the object. Table 2.2 depicts the classification of additive manufacturing processes according to the Amer-

ican Society for Testing and Materials (ASTM), known as ASTM F2792-12(2018). This standard provides a comprehensive categorization of additive manufacturing processes based on their fundamental characteristics.

When selecting an additive manufacturing technique, several key considerations come into play. These include the machine's printing speed, the cost of both the machine and the printed prototype, and the range and cost of materials available [41].

2.2.1 Fused Deposition Modeling

In this research, Fused Deposition Modeling (FDM) is the primary focus among all the different AM processes. FDM stands out as a widely adopted technique in industries. This preference stems from several significant advantages it offers, including low maintenance costs, a diverse array of available materials, cost-effectiveness even for complex geometries, as well as its environmentally friendly nature and ease of operation, requiring minimal to no supervision. FDM process involves fabricating three-dimensional models by incrementally adding materials layer by layer in the form of filaments [42].

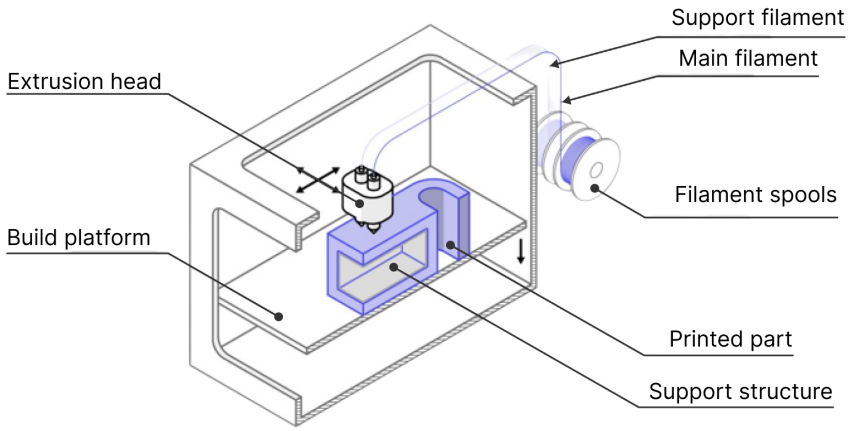

Figure 2.4: A schematic depicting the principal components of an FDM printer. Adapted from [43].

A temperature-regulated extrusion head is composed of a liquefier nozzle responsible for extruding the semi-liquid thermoplastic material. This material is then deposited in the form of precise layers on a fixture-less base table. To ensure optimal performance, the temperature inside the chamber is carefully maintained at a level lower than the melting temperature of the filament. As a result, the deposited filament swiftly solidifies upon adherence to the previous layer, leading to a highly transient heat transfer process [44]. This controlled cooling and layer-by-layer deposition are critical aspects of the FDM process, contributing to the accurate fabrication of three-dimensional models. A schematic showing the working principle of FDM process is shown in figure 2.4.

In FDM process, achieving the desired final mechanical properties, surface roughness, and geometric accuracy of the built parts presents a challenge, as they depend on a variety of process parameters and machine settings. Several process parameters, such as layer thickness, print speed, infill density, raster angle, and raster width, play a direct role in influencing the surface roughness, strength, and overall quality of the fabricated FDM parts. However, obtaining an accurate and smooth surface is often challenging due to the staircase effect. While it may not be possible to completely eliminate the staircase effect, it can be mitigated to some extent by employing optimal process parameter settings or adopting post-processing techniques [45].

Acrylonitrile Butadiene Styrene polymer (ABS), Polylactic acid (PLA), Nylon, Polyether-ether-ketone (PEEK), and Polycarbonates (PC) rank among the popular materials frequently employed in FDM printing [46]. In this research, ABS is the material of choice for additive manufacturing due to the following characteristics. ABS filament holds the distinction of being the most widely used 3D printing plastic. Its applications span across various industries, including the production of car bodywork, appliances, and mobile phone cases. This thermoplastic material contains a base of elastomers derived from polybutadiene, rendering it flexible and highly resistant to shocks. ABS exhibits opacity, and its surfaces possess a smooth and glossy finish.

The material's weldability through chemical processes utilizing acetone further adds to its versatility. For 3D printing, ABS is heated within the temperature range of 210^{o}C to 250^{o}C [47]. It boasts impressive toughness, enabling it to endure temperature variations from -20^{o}C to 80^{o}C with ease. However, it is non-biodegradable and has a tendency to shrink upon exposure to air, necessitating the heating of the printing platform to prevent warping. To limit particle emissions during ABS printing, it is advisable to utilize a closed chamber 3D printer.

2.3 Electroforming

Electroforming, a process discovered by Jacobi in 1837 during the electrodeposition of copper onto a printing plate [48], has been a well-known technique for many years. Electroforming has been subject to various descriptions, yet ASTM B 832-93 offers a simple and concise definition: "Electroforming is the process of creating or replicating articles through electrodeposition onto a mandrel or mold, which is then separated from the deposited material". Consequently, this technique enables the fabrication of parts that are typically self-supporting once separated from the mandrel [49].

Electroforming technology is rooted in the principle of electroplating, which involves several fundamental components: cathode, anode, electrolyte, workpiece model for plating, and power supply, as depicted in figure 2.5. These elements collectively form the basis of the electroforming process. By applying an electric field force, metal anions from a metal salt solution migrate towards the cathode, transform into atoms, and deposit onto the surface of the cathode model. During this deposition process, there are no gaps between the ion and the core model surface, ensuring the preservation of the model's surfaces without causing any damage [50]. The distinction between electroforming and electroplating lies in the intended purpose of the deposited metal. Electroplating aims to apply a very thin metallic coating onto an existing part, serving both decorative and protective functions.

On the other hand, an electroformed product is a distinct metallic object created by

utilizing the electroplating process to deposit metal of pronounced thickness onto or against a master form. Its purpose is to function independently, serving a specific role [51]. Typically, for electroplating, the materials selected as model materials should possess conductive properties on their active surfaces. However, when it comes to electroforming, the range of options is much broader. The master form used in electroforming can be made of various materials, including conductive, non-conductive, and even light-resistant materials.

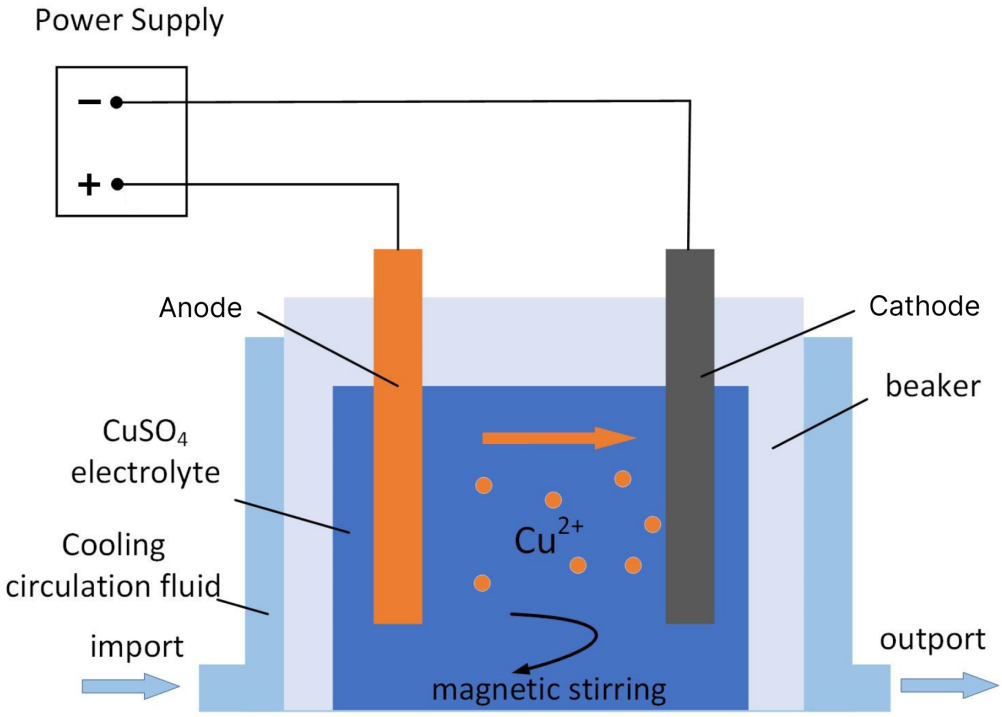

Figure 2.5: A schematic depicting the fundamental principles of the electroforming process. Figure reproduced from [52].

Electroforming products are primarily focused on achieving specific functional properties such as high hardness, however other mechanical properties differ according to the material composition of the used anodic material. Consequently, the composition of the solution and the operating conditions for electroforming significantly differ from those used in other processes. The electroforming process operates on the princi-

ple of accumulating atoms layer by layer, enabling the accurate replication of surface details from the model. In fact, the accuracy of electroforming depends entirely on the design precision of the master part, allowing for sub-micron level replication. This precise replication capability positions electroforming as a technique renowned for its accuracy [51].

To ensure the desired outcomes, it is crucial to effectively control the various parameters of the electroforming process. These parameters include the composition of the plating solution, pH level, temperature, presence of additives, and impurities. By adjusting these process parameters, the performance of the electroformed products can be controlled [50].

2.3.1 Electroforming Applications

The electroforming process offers remarkable advantages in the realm of micro and nano manufacturing. Compared to other conventional manufacturing technologies, micro/nano-electroforming exhibits several distinctive characteristics. High dimensional accuracy, process repeatability, and consistency in reproducing intricate surface features [50]. The process enables atomic-scale deposition, avoiding the adverse effects of cutting force, tool wear, and thermal energy transformation on the workpiece surface [53]. Furthermore, the mechanical properties can be finely tuned across a wide range through precise process control and solution adjustments. Electroforming delivers low surface finish and high form accuracy, making it applicable to a wide array of uses, including microfluidics, optics, functional surfaces, and high-precision aerospace components. It provides feature tolerance reaching up to 2 μm and surface roughness ranging from 1 to 20 nm in Ra [7].

These attributes position micro/nano-electroforming as an appealing choice for applications requiring meticulous precision, fine features, and superior surface characteristics. Its capabilities make it an invaluable technique in the field of advanced manufacturing, particularly for micro- and nano-scale applications.

The electroforming process, despite its numerous advantages, does have some engineering limitations that may impede its widespread adoption as a viable production process. These limitations include long deposition times, restrictions in the choice of material, and challenges associated with the separation of the electroform from the mandrel [41]. Furthermore, when forming large-area or thick components, flatness and surface uniformity are challenging to achieve. Other issues include complexity in residual stress which affects the structural integrity and performance of the final product, and difficulty in integrated replication of high-aspect-ratio micro/nano-structures due to the limited ion transportation within micro/nanochannels [54].

In practice, electroforming primarily utilizes materials like nickel, copper, iron, silver, gold, and a few other alloys. It has emerged as a significant technology in the micro-manufacturing field when compared to other viable processes, drawing attention from scientific and technical personnel as well as enterprises.

Electroforming finds applications in a variety of products [37], such as conventional record stampers, roughness standard samples, metal foils, metal meshes, perforated products like screen printing cylinders, filters, sieves, waveguides, reflectors, optical beam-bounding diaphragms, components for semiconductors and micro-systems technology, mini and micro-housings for shielding in electronics applications, and more. In the domain of mold manufacturing, electroforming is employed in the production of plastic molds, die and stamping dies, as well as Ni-Co alloy electroforming molds and Electrical discharge machining (EDM) electrodes. These diverse applications illustrate the versatility and relevance of electroforming in various industries. However, it is important to consider its limitations and suitability for specific production needs before implementing it as a manufacturing process.

2.3.2 Electroforming State-of-the-art

Electroforming, initially referred to as electrodeposition, had limited industrial application until the 1950s. During this period, studies on electrodeposition primar-

ily focused on fundamental aspects, leading to a relatively slow development of the electroforming process. However, in the early 2000s, there was a resurgence of interest in electroforming, accompanied by increased research efforts [55]. This renewed attention which coincided with the development of applications for micro-electromechanical systems (MEMS). During this stage, LIGA (the German acronym for lithography, electroplating, and molding) process provided significant opportunities for nano-electroforming applications in the microelectronics industry [56]. The convergence of these factors led to a notable advancement in electroforming technology, expanding its potential uses, and fostering further research and innovation in the field.

During last decades, remarkable advancements have taken place in the realm of electroforming. There has been substantial progress in the development of auxiliary technologies, as well as refinement and maturation of the parameters of the electroforming technique. These advancements have contributed to the enhanced capabilities and broader applications of electroforming. The primary issue encountered in conventional electroforming lies in the uneven distribution of the deposit thickness. This non-uniformity arises due to the influence of various contributing factors.

Achieving deposition uniformity is of utmost importance in the electroforming of micro/nano structures. Numerous methods have been discussed in the literature to enhance that. These approaches encompass the utilization of: pulse reverse current [57], rotated and moving cathodes [58], a second cathode [59], ultrasonic [60] and air-pressure agitation [61], an insulating shield [62], controlling the size, shape, and placement of the anode [63], adjusting electrolyte composites [64], and optimizing process parameters [65]. An essential parameter influencing deposit uniformity as well is the current density distribution [66]. Nevertheless, it is widely acknowledged that the current density experiences significant unevenness throughout the electroforming process, leading to pronounced effects on the surface quality, chemical composition, mechanical properties, and grain size of the electroformed deposits.

Figure 2.6 depicts the research articles on electroforming since the year 2000. As discussed, the majority of electroforming publications are focused on the LIGA process. Several of these publications delve into electroforming at the nano scale, while others are dedicated to optimizing electroforming process parameters and elevating the overall quality of electroformed components. However, there is a notable scarcity of research exploring the utilization of electroforming at the micro scale level and for depositing thick layers. Electroforming of thick deposit layers poses challenges due to the intricate nature of residual stress, which can adversely impact the structural integrity. Moreover, the limited ion transportation within micro channels further compounds the difficulty in achieving successful thick deposits [51].

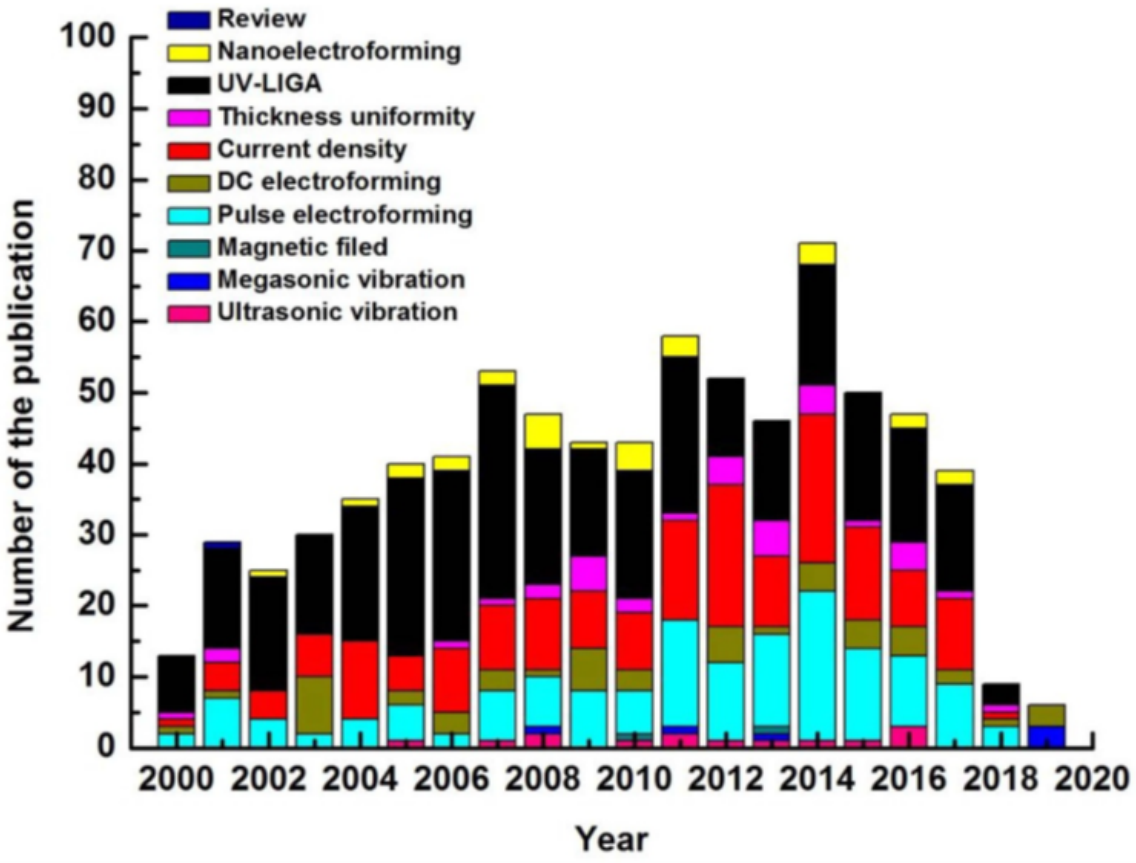

Figure 2.6: A figure illustrating research articles related to electroforming published from the year 2000 onwards. Figure sourced from [55].

In contrast to its traditional application of forming parts on mandrels, electroform-

ing has recently garnered increased attention within academia as a promising alternative to direct metal printing [54, 55]. The unique characteristics of electroforming offer a significant advantage in precision and the production of metal components, distinguishing it from other metal forming processes [54]. This shift in interest reflects the growing recognition of electroforming potential in advancing the field of metal manufacturing. Its ability to create intricate, high-precision components presents exciting possibilities for various industries, including micro-electronics, medical devices, and aerospace.

2.3.3 Electroforming/Electroplating and Additive Manufacturing

The concept of electroforming and electroplating on additively manufactured structures has received recent attention and has been steadily gaining momentum. Angel et al. [5] demonstrated the production of a solenoid inductor with low-frequency inductance through Fused Filament Fabrication and electrodeposition. Aghili et al. [6] successfully fabricated a 2D flexure mechanism utilizing additively manufactured molds.

Meanwhile, Matsuzaki et al. [4] investigated the feasibility of fabricating multi-material structures comprising resin and copper through the application of FFF and electroforming techniques. Furthermore, Phull et al. [67] explored the development of metal tooling by employing FDM in conjunction with nickel electroforming. The primary process steps encompass printing the desired mandrel or mold, activating the desired area for electroplating, conducting the electroplating/electroforming process, and separating the final part from the mandrel/mold.

However, the current applications for this technique are limited to producing hollow/thin-walled structures, 2D metal structures, and plastic/metal multi-material structures. Therefore, the current research aims to explore the viability of utilizing this affordable technology for mass personalized 2.5D and 3D metal structures at

the macro and micro scale. This indirect manufacturing process holds the potential to offer a cost-effective solution for fabricating precise metal parts while minimizing energy consumption and equipment investment costs.

Furthermore, electroforming yields higher quality surfaces compared to direct metal 3D printing, potentially addressing the issue of extensive post-processing required in other methods [13, 14]. This makes electroforming a promising approach for producing intricate and finely detailed metal structures at the macro/micro level.

In the present research, additive manufacturing along with electroforming have been used to create metal parts. The presented fabrication technique leads to cost reduction per unit as production volume scales up within the realm of mass personalization. This fabrication technique leverages the potential of generating intricate mold geometries through additive manufacturing and concurrently fabricating numerous parts through electroforming, without incurring supplementary costs attributed to design alterations driven by customer preferences.

Chapter 3

Methodology

In this work, molds have been designed and 3D printed to enable electroforming of multiple geometries and 2.5D structures. Parts in 2.5D configuration have three axes, with limited variability of features in the third axis. They involve multiple flat features at varying depths. However, 3D parts have complex shapes and features in all three dimensions. The overall methodology followed in this research is depicted in figure 3.1 and is formed of three primary aspects: Mold Design, Experimental Procedures, and Simulation and Modeling. The knowledge brought up from this research is applied into fabricating functional parts for various applications.

The first objective is introducing a modular mold design. The design should meet certain procedures to be suitable for electroforming. Additionally, the mold should be economically viable, eliminating the requirement for costly masks, while also having the capacity to achieve conductivity using a more affordable alternative. Subsequently, in this work an experimental process is developed that encompasses mold design and fabrication and then this mold is used to manufacture the desired part through electroforming. The overall fabrication process exhibits the main characteristics of cost-effectiveness, reliability, repeatability, and automation potential.

Throughout the research, an array of geometric features is explored to evaluate the feasibility and efficiency of the fabrication process. This investigation seeks to establish vital design considerations, particularly for components with diverse geometries

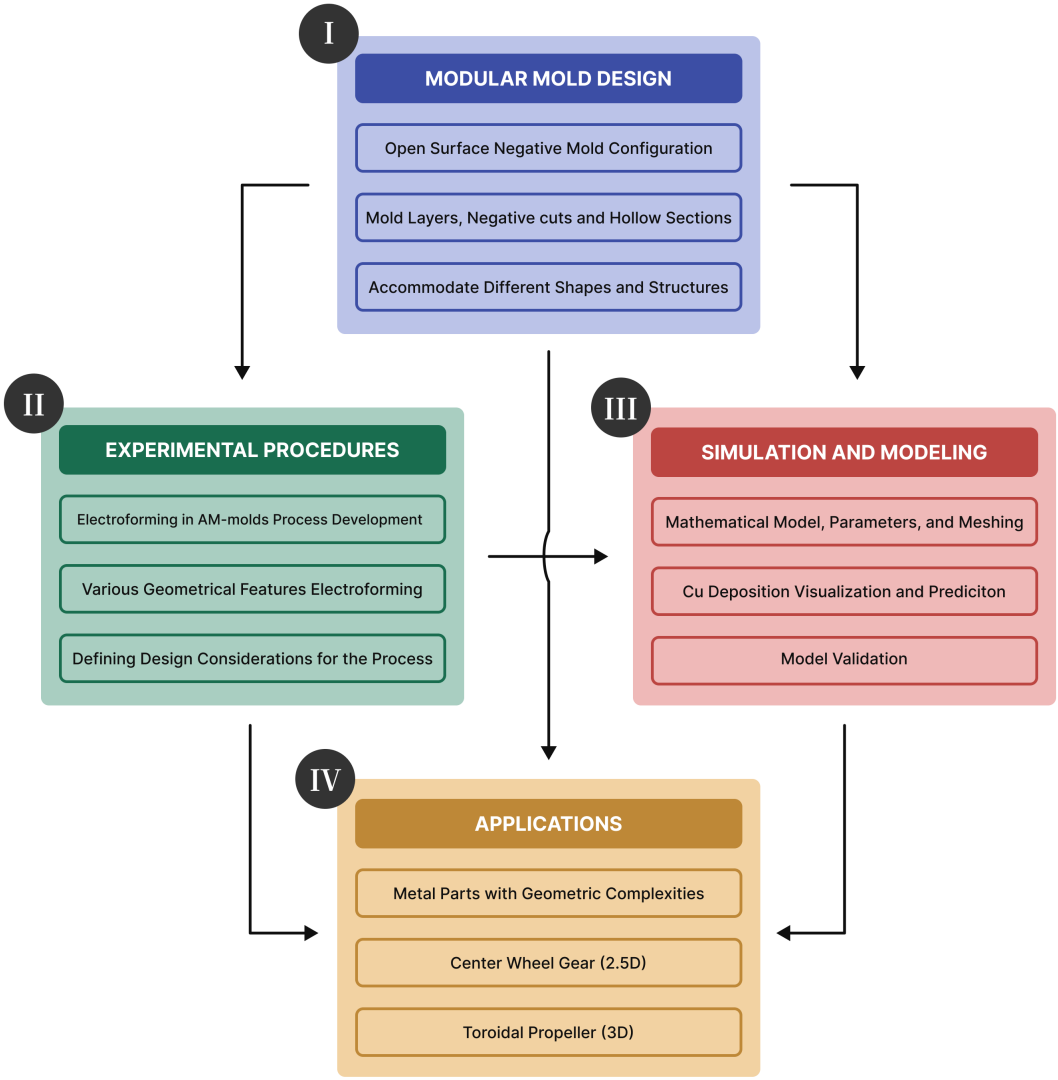

Figure 3.1: A schematic outlining the key aspects of the proposed work's methodology.

and features.

Following the development of the mold and the process, a simulation model is introduced. This model aids in visualizing and forecasting Cu growth within the mold. Its purpose extends beyond time-saving, as it also provides guidance for more efficient and determined experimental trials. Finally, subsequent to the development of a modular mold, the establishment of a fabrication process, and the definition of essential design considerations for the process, various applications of the proposed

method are introduced. These applications illuminate the capabilities of this process in manufacturing metal parts with intricate geometries and diverse dimensions along multiple axes.

In this chapter, an overview of the mold design and the process development for preparing additively-manufactured molds for electroforming is presented. Various aspects, including the modular mold design for electroforming, the application of conductive layers, the bonding procedures among the mold components, mold assembly methods, and a non-destructive strategy for part separation are discussed. Additionally, a detailed depiction of the experimental setups employed for both additive manufacturing and electroforming is presented, along with their respective parameters and operational conditions.

3.1 Mold Design

The primary step in attaining the thesis objective is mold development. This mold must be designed to facilitate the growth mechanism of the electroforming process and have the capacity to produce a variety of complex geometries, mainly 2.5D structures. To fulfill these criteria, the mold should exhibit specific characteristics:

- **Standardized Base Layer**: The molds developed must incorporate a consistent flat base layer (substrate) as the initiation point for the deposition process. While these molds are versatile in accommodating electroforming across diverse shapes and geometries, it is imperative that the resulting parts maintain a flat base in any of their three axes.

- **Facilitate Metal Ion Transfer**: The mold design must facilitate the efficient transfer of metal ions throughout the electroforming process.

- **Attain Uniform Conductive Surface**: It is essential to achieve a consistently conductive surface on the mold to ensure the effective deposition of copper atoms.

- **Facilitate Part Separation**: The mold should allow easy separation of the part without inducing any damage to the electroformed part.
- **Cost-effective Design and Manufacturing**: The mold design and manufacturing has to be simple, quick, and cost-efficient to be comparable to other processes.

The development process of this mold is undertaken with a comprehensive awareness of these challenges. First, a negative (female) mold configuration is selected to align with the intended shape of the desired product. The mold features an open-surface configuration, ensuring unobstructed metal ion transfer during electroforming. Additionally, Fused Deposition Modeling (FDM) additive manufacturing is chosen for mold fabrication. FDM is selected due to its inherent simplicity, cost-effectiveness, and ability to handle complex geometries, allowing for the production of modular molds of varying complexity.

The initial phase in designing the mold involves defining the geometry of the desired part. To determine the number of mold layers needed for manufacturing the desired part, the part geometry is assessed. This evaluation focuses on the part height along the z-axis and identifies substantial changes in its width along this axis. These width variations prompt the creation of additional layers. For instance, in the illustrated part in the figure 3.2, there is a single change in width along the z-axis, resulting in a division into two layers.

Second, identifying the negative cutouts and hollow sections within each layer. Given the mold negative configuration, corresponding positive counterparts are essential for accommodating these cutouts and hollow sections in the desired part. For instance, the desired part features two negative cutouts in its second layer and a cylindrical hollow shape spanning its entire depth. To address this, a positive shape with matching dimensions is incorporated into the second layer of the mold design to complement the negative cutouts. Furthermore, a cylindrical positive insert is

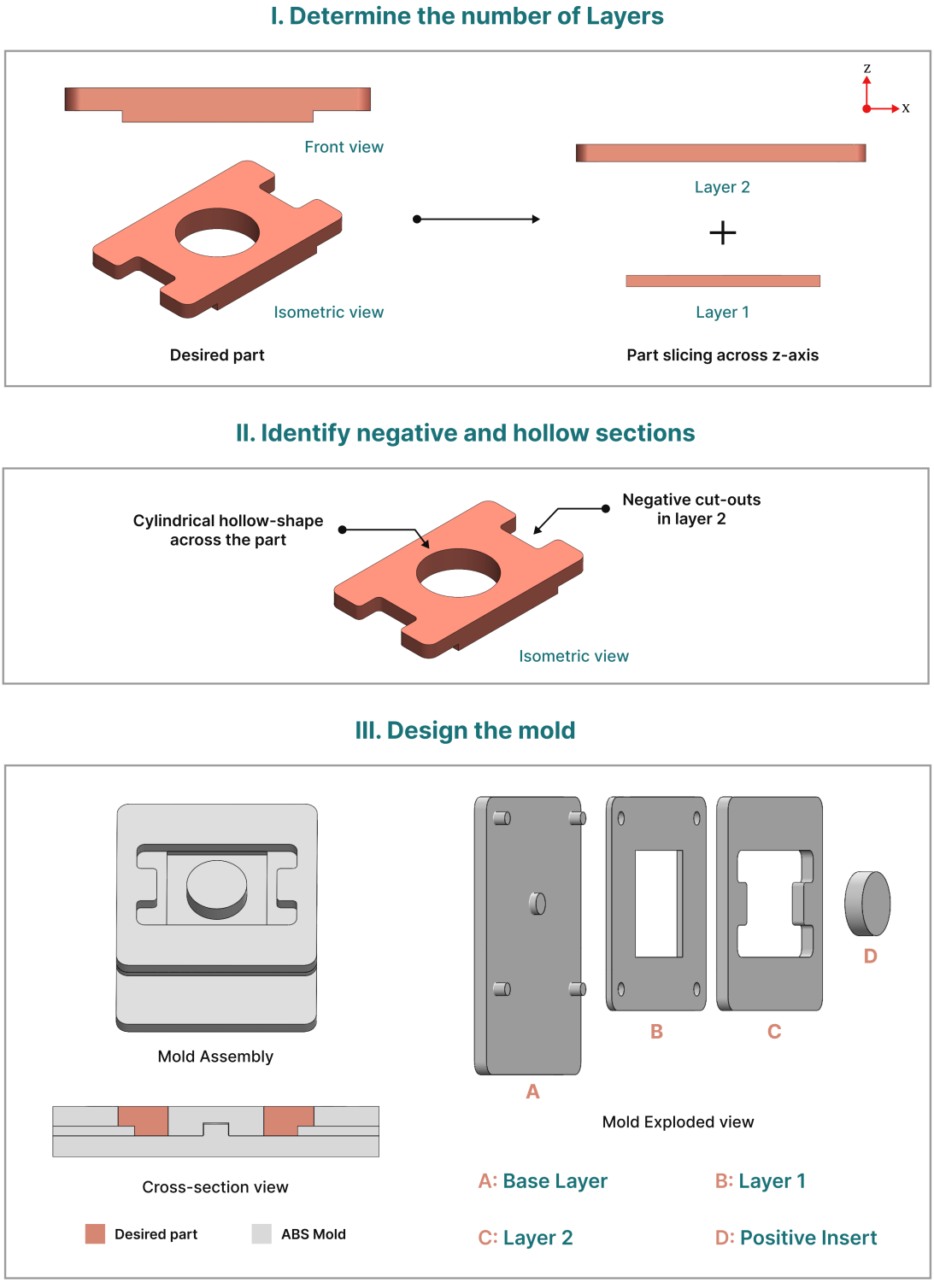

Figure 3.2: A schematic illustrating the methodology of mold design and development.

introduced, extending throughout the height of the desired part.

Having determined the number of layers and the negative cutouts in the desired part, the mold can be designed. In this process, all molds necessitate a foundational base layer that is coated by a conductive paint, mainly copper. To standardize the spraying process of the base, the base is chosen to be a flat rectangular part. The layers that are added on top of the base layer determine the shape of the mold and thus the part. For the desired part, a total of three layers are required: a base layer, layer one, and layer two. Layer one must match the dimensions of its corresponding section in the desired part. Copper electroforming commences on the base layer and proceeds until it attains the requisite thickness of layer one on the mold. Subsequently, copper growth continues at the base of layer one until it fills the required thickness of the second layer. The presence of the positive insert prevents the electroforming process from depositing copper on the cylindrical cutout.

Lastly, the base layer features four locator pins and a central positioning pin. These four locator pins serve to guarantee the accurate alignment and positioning of all mold layers during assembly. In contrast, the central pin is intended for positioning the positive insert that encounters the hollow cylindrical shape. A schematic illustrating and summarizing the mold design development is provided in figure 3.2.

3.2 Experimental Process Development

Establishing a robust foundation for any manufacturing technique necessitates the presence of a dependable process. To enable the electroforming of metal parts with varying shapes in an AM mold, several prerequisites must be met. These include the application of conductive coating to allow electroforming the part, solid bonding of the mold components during assembly, and using a non-destructive technique for part separation post-electroforming.

Moreover, the goal is to create an experimental process that spans all stages, from mold design and fabrication to the actual production of the desired part via

electroforming. This fabrication process must exhibit key attributes, notably cost-effectiveness, reliability, repeatability, and automation potential. Throughout the development of the experimental procedures, the focus remained on adhering to these procedures and finding suitable solutions for the encountered challenges. A schematic visualizing the procedures steps is depicted in figure 3.3

FDM Printing

Following the mold design technique previously outlined, the mold components are 3D printed using an FDM printer, with ABS material serving as the printing filament. Subsequently, the mold components undergo a dry test-fitting process to verify their alignment for assembly. Based on the experimental work done, the use of locator pins and positioning indents emerges as the most convenient technique for aligning the mold components in their designated positions during assembly. However, It is worth noting that alternative techniques can also be effectively employed depending on the designer's preference and requirements. More information regarding the printing parameters and the setup used is discussed in section 3.3

Conductive Coating

Ensuring a consistent conductivity in the targeted electroforming region is crucial, thus a silver-coated copper conductive paint is utilized. The chosen conductive paint, designated as (MG Chemicals 843AR Liquid) has relatively high conductivity (3 x 10^{-4} Ω.cm), fast drying time, and strong adhesion to most plastics. Several painting techniques underwent experimentation and evaluation to determine the most effective approach for establishing a conductive printed layer. Both brush-painting and spray-painting methods were subjected to comparison.

Brush painting offers the advantage of applying thicker paint coatings, potentially enhancing conductivity. However, it's crucial to underscore the advantages of spray painting. This method boasts various merits, including its rapid and automatable

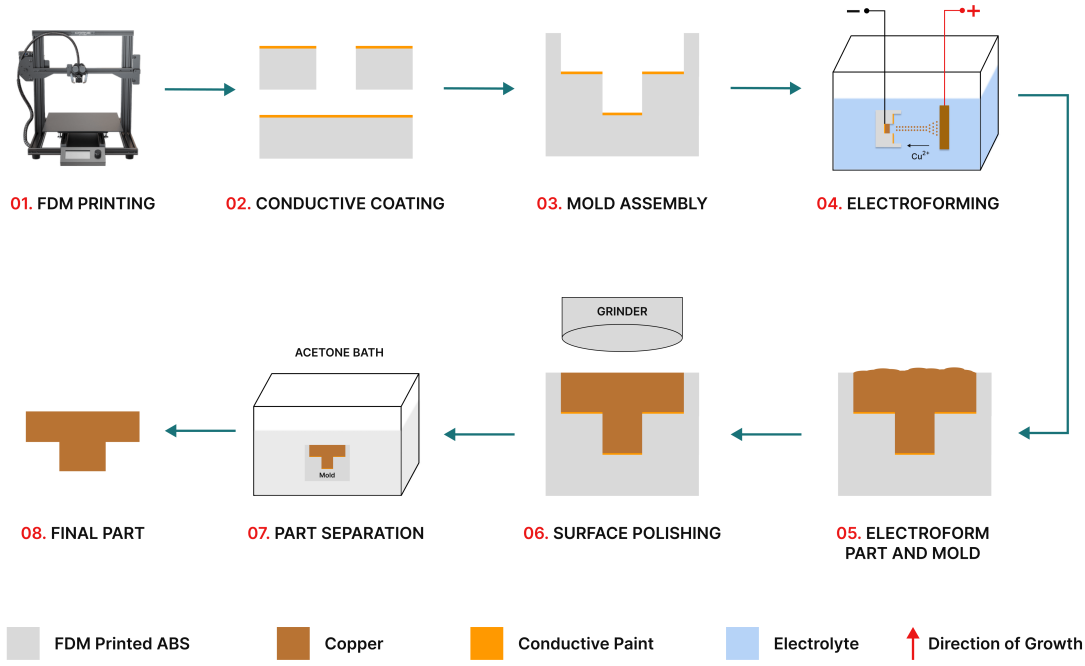

Figure 3.3: A schematic illustrating the steps followed in this work for part production with electroforming .

nature, quicker drying times compared to brush painting, and minimal impact on the molds surface roughness. Additionally, it ensures a more uniform and consistent application of paint across all mold components. Considering these benefits, the decision was made in favor of using spray painting over brush painting.

Regarding the application of the conductive layer, a high-volume low-pressure (HVLP) spray gun was employed. This particular spray gun has a nozzle tip diameter of 1.4 mm, a configuration that aligns with the recommendations of the paint manufacturer. During the application process, the paint is prepared, ensuring thorough mixing. Subsequently, the paint is dispensed through the HVLP spray gun using an air compressor line, with the air pressure regulated within the range of 30-35 PSI. A re-coating time of 3 minutes is allowed for the paint to cure before applying another coat. To attain a surface characterized by high electrical conductivity, it is recommended to apply a minimum of 3 coats of the conductive paint. The elec-

trical resistance of the mold components was assessed using a multi-meter, yielding resistance readings within the range of 0.3 to 0.6 ohms (Ω).

Mold Assembly

Various techniques are available for the process of bonding the layers. One approach involves glue bonding, where adhesive is applied to the layer's surface after the paint has dried, and then mechanical pressure is applied to bond the layers together. However, this method carries the risk of unintentionally introducing adhesive to areas that may affect the dimensions of the electroformed part. Alternatively, another method entails hot-pressing for mold assembly. In this technique, the mold components are bonded by subjecting them to both heat and pressure for a specific duration until secure bonding is achieved. Nevertheless, hot-pressing can lead to changes in the mold's dimensions due to the high temperatures involved.

Chemical bonding using acetone has been selected as the preferred method for bonding the mold components due to its straightforward and convenient application. This approach eliminates the necessity for heating or employing mechanical pressure during mold assembly. The incorporation of ABS as the chosen mold material, in conjunction with the use of acetone, a polar solvent, has effectively resolved several challenges in this process. When it comes into contact with ABS material, acetone triggers the formation of a sticky outermost surface. This phenomenon is utilized in bonding of the printed ABS components together. Acetone serves as a reliable bonding agent for the ABS layers, resulting in a highly strong bond. Following thorough drying of the paint, acetone is gently applied to the rear surface of each layer, and then pressed against the corresponding layer for couple seconds to achieve the bonding.

Electroforming Preparation

After the mold assembly is done, it is prepared for the electroforming process, which

will be discussed in detail in a later section 3.4. Following the electroforming phase, the mold goes through cleaning procedure using de-ionized water, followed by air drying. Due to electroforming tendency to result in surface irregularities, a polishing step becomes necessary to remove any surface imperfections from the exposed face of the mold (top surface area of the part). The sample outermost surface is polished (while still in the mold) using a reciprocating hand grinder to align the mold surface and the outermost part surface to be on the same plane, as depicted in steps 5 and 6 in figure 3.3 .

Surface Polishing

Sandpapers of 220 grit are employed to remove the material until the desired intersection is exposed. Subsequently, to achieve a smoother surface finish, the sample is subject to repeated polishing using 600 grit sandpapers. This step gradually refines the surface, enhancing its smoothness and eliminating any remaining imperfections. Once the polishing is complete, both the mold and the electroformed part are fully immersed in acetone to allow for easy separation of the electroformed part from the mold.

Part Separation

Last but not least, acetone demonstrates an impressive capability to completely dissolve ABS in just a matter of hours, a critical step in separating the part from the mold. Consequently, the component can be safely extracted from the mold without sustaining any damage. However, it is important to exercise caution while using acetone for bonding of the mold component, as an excessive application of acetone can lead to the dissolution of the layer, potentially affecting its thickness. Following the bonding of the mold components, an additional step involves applying varnish to the outer surfaces of the mold to insulate them, if desired. This insulation prevents deposition in unintended areas (outer side planes of the mold in this case) during the

electroforming process.

3.3 Fused Deposition Modeling Setup

A Creality Ender 3 Pro commercial FDM printer, shown in figure 3.4, was employed to manufacture the mold components. ABS material was chosen for its smooth surface finish and compatibility with acetone bonding. The quality and precision of the FDM part are critical for a successful electroforming process, capable of sub-micron replication [7]. Any flaws in the initial FDM part affect the final electroformed product. To ensure the best possible surface roughness and geometry, the FDM printing parameters were specifically optimized for ABS.

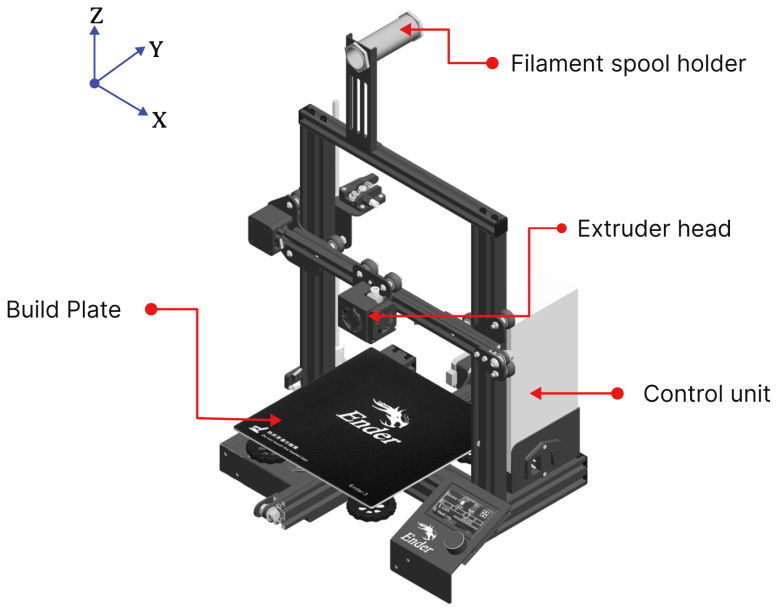

Figure 3.4: A CAD model representing the FDM printer employed in this study.

To ensure proper adhesion and prevent warping of the print layers, the printing process is carried out on a heated build plate with the temperature set to 95 °C, a printing glue is applied to the build plate, and a 3 mm brim was added to all printed parts. One crucial parameter in the FDM process is the printing layer thickness, which was set to 0.1 mm. This choice is based on the understanding that the layer

thickness height significantly contributes to approximately 85% of the FDM printed parts overall accuracy compared to other parameters. Furthermore, it has been determined that for FDM parts using ABS, the dimensional accuracy is found to be optimal when layer thicknesses range between 0.1 and 0.2 mm [68].

Table 3.1 Parameters of FDM printing.

Parameter	**Value**	**Unit**
Print Speed	30	mm/s
Layer Thickness	0.1	mm
Initial Layer Thickness	0.2	mm
Infill Density	50	%
Wall Thickness	1	mm
Extrusion Temperature	245	°C
Build Plate Temperature	95	°C
Nozzle Diameter	0.4	mm
Fan Speed (Cooling)	OFF	-

In this study, we employed specific printing parameters, illustrated in table 3.1. The printing speed was fixed at 30 mm/s, and the nozzle extruder temperature was set to 245 °C, aligning with manufacturer recommendations. A 50% infill density was chosen to manage geometrical deviations in the ABS printed parts [69]. After printing, the printer is allowed to cool down to ambient temperature, followed by detaching the parts from the printing plate and removing the attached brim. These steps contributed to the overall experimental process, ensuring precision and consistency in part production.

3.4 Electroforming Setup

To prevent electroforming on unintended areas, the external surfaces of the mold assembly were coated with varnish. A copper sheet with a rectangular shape, having dimensions of 80 mm × 160 mm, is employed as the counter electrode.

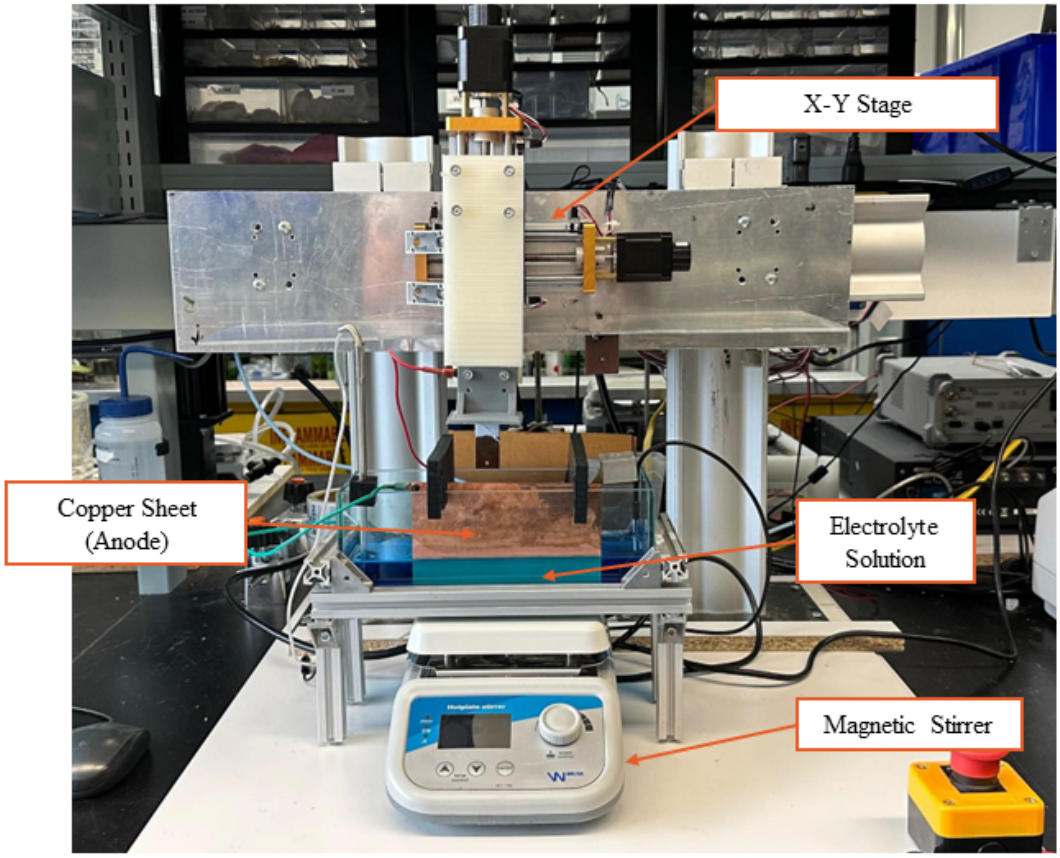

Figure 3.5: Electroforming experimental setup.

To ensure efficient mass transfer and uniform distribution of copper ions during the electroforming process, the mold assembly is subjected to reciprocating movement by an X-Y stage, maintaining parallel alignment with the counter electrode. The distance between the mold and the copper sheet is maintained at 5 mm. The experimental setup used for electroforming is depicted in figure 3.5.

The electroforming process is carried out in a solution composed of sulfuric acid and copper sulfate, without the use of any additives. In addition, the electrolyte

is steered by a magnetic rod to homogenize the solution and enhance the surface finish [70]. A pulsed deposition technique is implemented. This approach alternates between deposition pulses (at -150 mV vs. Cu) and polishing pulses (at +100 mV vs. Cu). Given the direct correlation between deposit thickness and the applied charge, the layer thickness in each pulse is effectively managed by maintaining a consistent deposition charge.

A fixed charge deposition approach is employed instead of a fixed-time deposition method. Deposition pulses continue until a charge of 1.33 C/cm^2 is passed in the electro-chemical circuit, which corresponds to a thickness of about 1 μm. Polishing pulses, on the other hand, last for 10% of the deposition charge. The deposition thickness is primarily influenced by two main parameters: the number of pulses and the surface area where the deposit is intended to grow.

This pulsed deposition process is essential in achieving high-quality thick deposits and preventing the formation of voids in the deposited material, as demonstrated in prior research [1] [71].

[1]The electroforming setup is located in Department of Mechanical, Industrial and Aerospace Engineering, Concordia University, Montreal, Quebec. All the electroformed parts mentioned in this thesis were manufactured in that facility. Moreover, the experimental parameters and conditions for electroforming were provided by the lab staff and their supervisor.

Chapter 4

Electroforming of Various Geometries

In this chapter, the focus transitions to a comprehensive exploration of the electroforming process in the developed mold. The primary objective is to assess the feasibility and viability of electroforming particularly in producing relatively thick copper structures exceeding 1000 μm in thickness. This assessment includes a wide range of various geometries, with the aim of establishing essential design considerations for the electroforming process. Moreover, electroforming of various geometries, shapes, and structures serves not only to validate the capabilities of the fabrication approach but also lays the foundation for the manufacturing of a diverse array of applications.

4.1 Geometrical Features Mold

To assess the feasibility of the presented fabrication approach, a simple mold is created with various geometrical features. The mold is composed of two distinct layers: a base layer (substrate), and a top layer (mask). The base layer measures 40 mm x 70 mm and has a thickness of 2 mm. To ensure secure mounting for the electroforming process, an extended piece is incorporated into the design. Additionally, four locator pins are included to ensure precise alignment and positioning of the top layer during assembly. The top layer, depicted in figure 4.1(a) is designed to encompass the

negative shapes of the intended features.

The chosen geometrical features include single v-grooves, double v-grooves, single bevels, double bevels, a straight 90° channel, multi-step channels, and holes with varying diameters ranging from 3 mm to 0.2 mm. Figure 4.1 illustrates the mold assembly and provides cross-sectional views of the various geometrical features incorporated in the design. The mold is fabricated using the process procedures outlined in the preceding chapter 3.

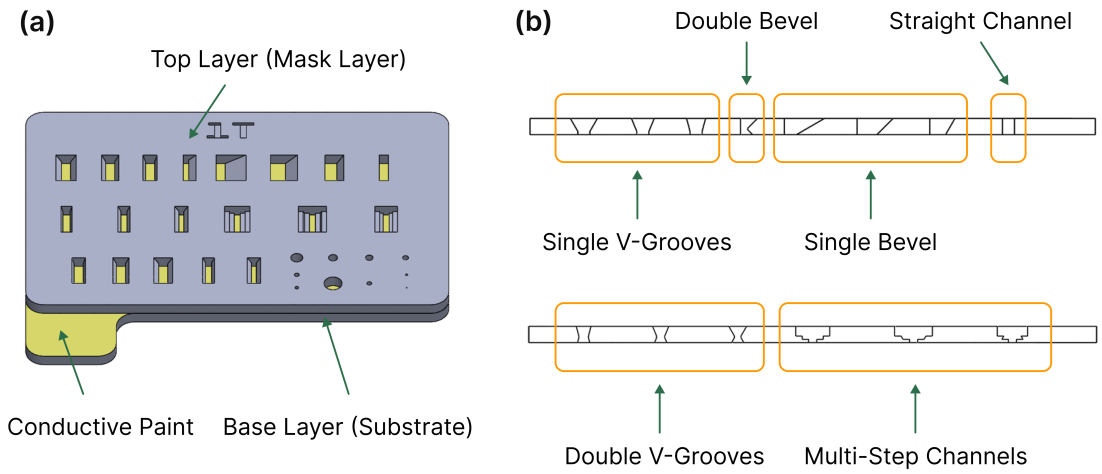

Figure 4.1: The geometrical features mold. (a) CAD model of the mold assembly, (b) cross-section illustrating various features of the top layer of the mold.

To accommodate diverse requirements, the single v-grooves, double v-grooves, and single bevels are designed with three different angles: 30°, 45°, and 60°. The multi-step channels, with various angles of 90°, 60°, and 120°, serve the purpose of identifying how the deposition process behaves when there are multiple steps with varying widths and angles at different thickness levels. This is done to understand how electroforming occurs for parts that have multiple thicknesses across their depths, i.e., 2.5D and 3D structures.

The incorporation of these varied geometrical features in the mold serves a specific purpose in the evaluation of the fabrication approach. By encompassing different

shapes, angles, and features, this mold is intended to comprehensively assess the capability of the fabrication process to produce intricate and diverse metal parts. Through careful examination, one can assess the essential design considerations when dealing with parts that exhibit a wide range of geometries and features, and how these geometries influence void formations, thickness variations, and surface uniformity in the electroformed parts. This understanding is instrumental in fine-tuning the design and fabrication process.

4.2 Quantifying true angles, thickness, and printing errors

As previously mentioned, the electroforming process is highly sensitive to accurately reproducing the intricate surface details of the master mold. Thus, an assessment of FDM printing errors becomes crucial for proper analysis of the electroforming outcomes. FDM printing, especially when dealing with micron-sized features, is inherently less precise in terms of dimensional accuracy, which may result in anticipated errors in the designed angles. To detect these errors and attain the actual printed angles, the mold top layer was printed using identical printing parameters. No attempts were made to achieve net-shape printing; however, this analysis was conducted to assess the behavior of the utilized FDM printer in printing ABS components.

Subsequently, the printed sample was divided into three sections, each displaying the cross-sections of the printed features. These specimens were then placed within a plastic mold and secured with a plastic support clip. For the casting of the mounting mold, blue-colored epoxy was employed, creating a visual contrast within the printed specimens. After the epoxy had cured, the mounting mold underwent polishing to gradually remove material unveiling the specimen's cross-section that displays the features.

Furthermore, the mold was mounted on a VHX-1000 digital microscope for analysis. To determine the actual angles printed through FDM printing, each individual

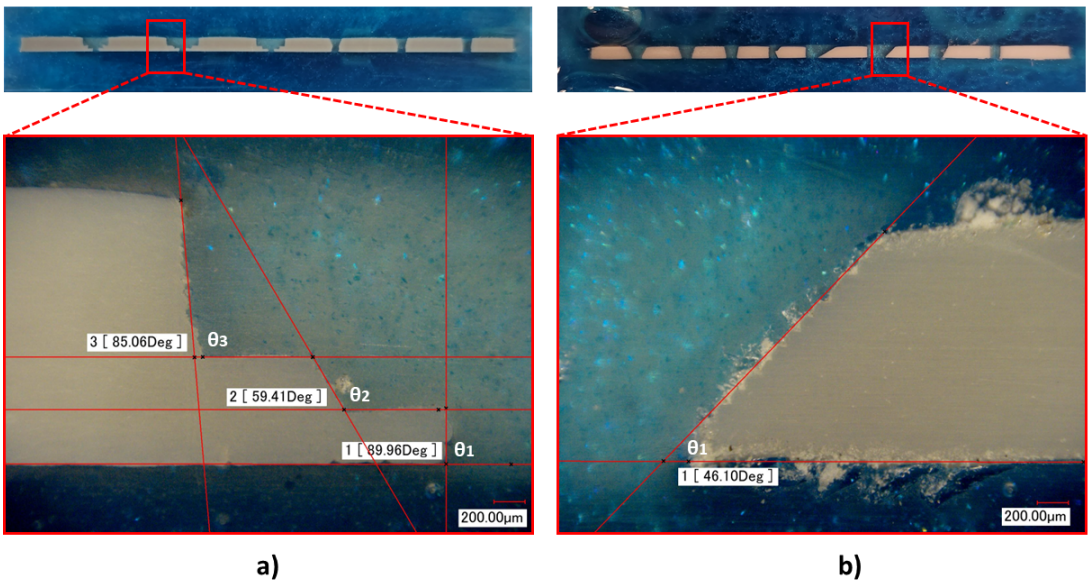

Figure 4.2: Measurements of actual feature angles. Microscopic view of a mounted specimen with (a) multi-step channel, and (b) 45° single bevel.

feature was separately examined. Figure 4.2 illustrates two of the specimens securely positioned within the epoxy mold subsequent to the polishing process. The examination of a specific feature, in this case, a multi-step channel, is presented under the microscope in figure 4.2(a). To measure the actual angle, perpendicular horizontal lines were constructed aligning with the base surface of each step in the feature. Then, vertical lines were constructed along the contours of each step, closely mirroring its shape. The angle of cross-section between the vertical and the horizontal lines determines the adjacent angle of each step.

The intended angles for the multi-step channel were designed as follows: a 90° angle for the first step, a second step at 120°, and a third step at 90°. However, the angles measured under the microscope correspond to the adjacent angles (θ) rather than the angles being directly measured. Thus, by subtracting the angles depicted in figure 4.2(a) from 180°, the actual angles can be deduced. Angles ($\theta 1$), ($\theta 2$), ($\theta 3$) are calculated to be approximately 90°, 120.6°, and 95° respectively. A similar approach was employed for the 45° single bevel, as illustrated in figure 4.2(b), resulting in an

actual angle measurement of 46.1°.

This identical technique was employed for all features across various specimens, allowing for the determination of their respective actual angles. By subtracting these actual angles from their corresponding designed values, the printing errors at each angle were calculated. Subsequently, the percentage errors for each angle were calculated using the formula specified in the following equation (4.1):

$$\% \, Error = (\frac{|Designed \, angle - Actual \, angle|}{Designed \, angle}) \times 100 \tag{4.1}$$

A total of 50 measured angles were employed to determine the error value of the printed angles. The calculated mean percentage error amounted to 7.670%. This implies that an average variation of approximately 4° can be expected when designing and printing angled structures using the aforementioned FDM printer, along with the indicated parameters. Similarly, the percentage error concerning the printing height (i.e., the thickness of the cross-section) was determined. For the analyzed sample, the designated thickness was 2000 μm. Through measurements of the actual height at different features within the mold, 38 distinct data points were gathered. By using the same equation 4.1, yet substituting the designed height and the actual one, the height percentage error for each data point was computed.

The calculated mean percentage error was found to be 5.249%, which suggests an average deviation of approximately 105 μm in the layer height when using the specified printing parameters. These calculated values hold significant relevance in this study, as they offer an estimated percentage error when fabricating molds with various structures. Furthermore, they contribute to a more precise evaluation of the electroformed features.

In summary, the FDM printer utilized in conjunction with the printing parameters plays a crucial role in determining the dimensional tolerance of the printed component. Opting for a higher quality or an industrial-grade FDM printer equipped with optimal

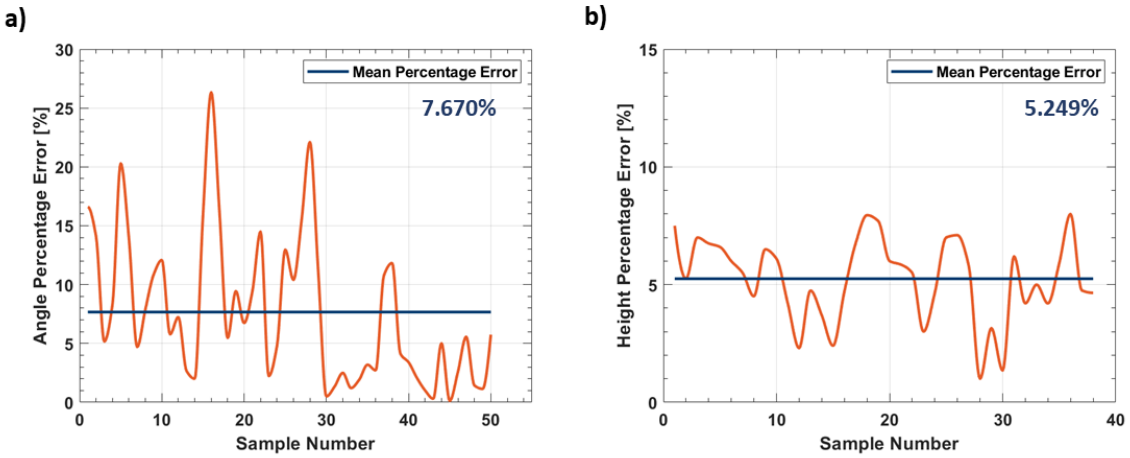

Figure 4.3: Plots depicting: (a) angle percentage error, and (b) height percentage error at each measured data point.

printing parameters for ABS can undeniably enhance the dimensional accuracy. A parameter that exerts substantial influence on achieving enhanced dimensional accuracy is the layer thickness. The implementation of a lower layer thickness value will dramatically decrease errors in both printed angles and thicknesses.

4.3 Electroforming Results and Discussion

The mold, incorporating diverse geometrical features, underwent electroforming process using the aforementioned setup. The deposition thickness is controlled by two main parameters; the number of pulses and the surface area where the deposit shall grow. Since the mold has different features with various surface areas, the total surface area of all the features, 2 cm^2, was used as an input for the process. Therefore, electroformed features have different deposition thickness. The exact thickness is not the primary concern, as the key objective is to ensure that these geometries are filled properly to evaluate the fabrication approach, and study the copper formation across different shapes and angles. The number of deposited pulses was set at 25,000 to ensure achieving thicknesses exceeding an average of 1200 µm in all the geometries. It took approximately 4 days and 4 hours, equivalent to 100 hours, for the mold to

complete the specified cycles.

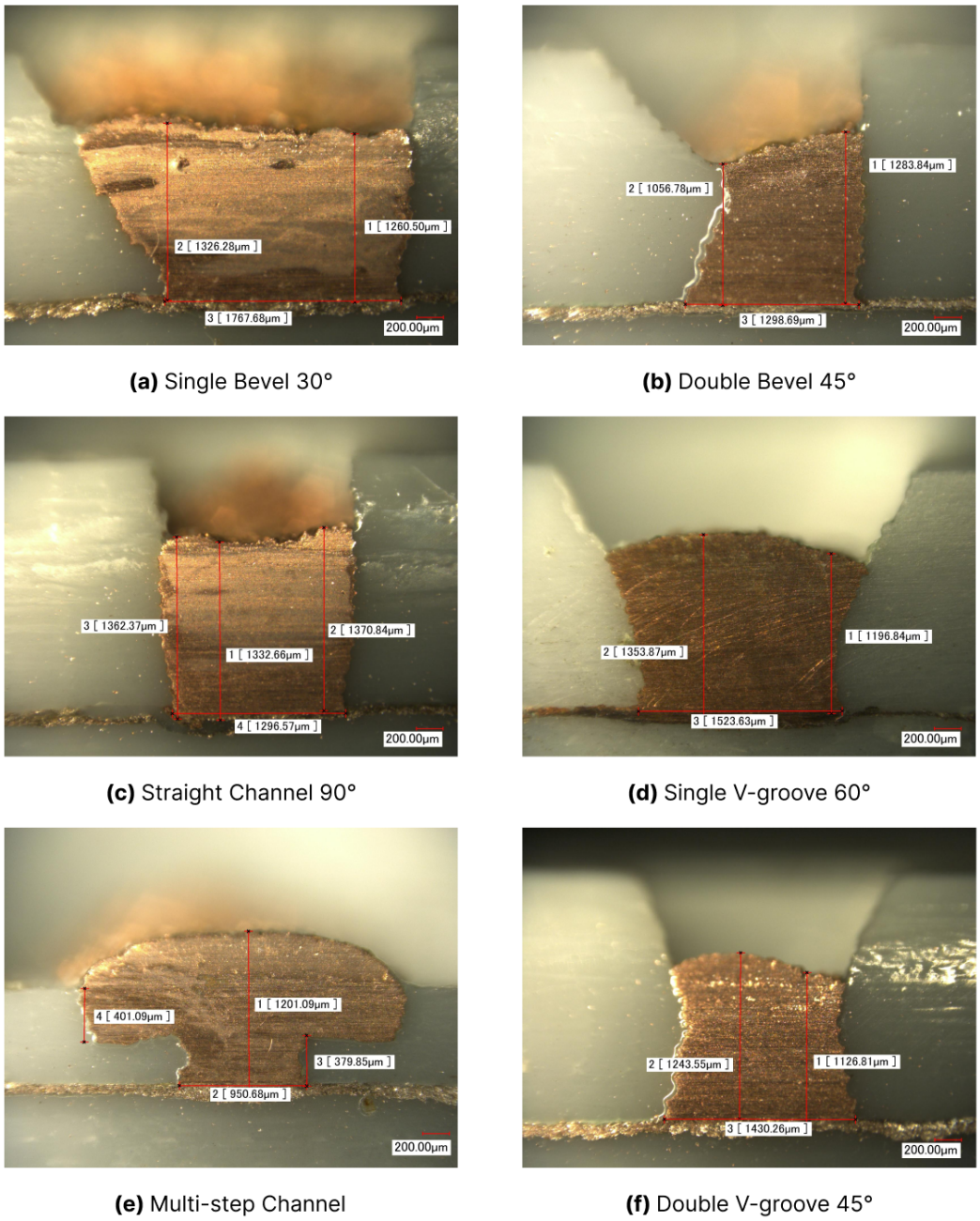

(a) Single Bevel 30°

(b) Double Bevel 45°

(c) Straight Channel 90°

(d) Single V-groove 60°

(e) Multi-step Channel

(f) Double V-groove 45°

Figure 4.4: Different features after electroforming captured by a digital microscope with accompanying measurements.

Subsequent to the electroforming phase, the mold was partitioned into multiple segments to unveil the cross-sectional perspectives of the electroformed geometries.

Each segment was then subjected to polishing to eliminate any debris from the cutting process and to reveal the deposited copper within the distinct channels. Each geometrical feature was separately examined and studied under the microscope.

Figure 4.4 shows microscopic images illustrating various features present within the mold. The ABS mold is depicted in a light grey hue, the interstitial space between the mold layers is represented in a light golden shade (signifying the conductive paint), and the copper deposits, formed bottom-up originating from the conductive paint, cathode, are exhibited. The copper deposition is demonstrated in six different geometries with varying angles. Remarkably, the electroforming process exhibits a high level of precision in depositing copper within the mold. The copper deposits effectively adhered to the structural walls of the top mold layer, even in the smallest cavities and over the imperfections introduced during the FDM printing process. Upon analysis of the geometrical features, no visible voids or cracks are evident within the copper formations across all the featured geometries.

Straight Channel 90°

When comparing the consistency of thickness across the different geometries, it becomes evident that the straight 90° wall channel, as illustrated in figure 4.4(c), exhibits the most consistent surface. In order to gauge the uniformity of deposition thickness within each feature, the maximum and minimum heights of the deposition were measured for every individual feature under the microscope. This assessment aims to determine the degree of uniformity in deposition thickness across the various features. To facilitate the assessment of surface uniformity, the evaluation employs the calculation of percentage non-uniformity (α_t), a parameter that quantifies thickness uniformity [61]:

$$\% \, \alpha_t = (\frac{h_{max} - h_{min}}{h_{min}}) \times 100 \tag{4.2}$$

Where (h_{max}) and (h_{min}) stand for maximum height and minimum height, respectively. The measured h_{max} for the straight channel is 1370.84 μm, and the measured h_{min} is 1332.66 μm. The calculated percentage non-uniformity (α_t) is approximately equal to 3%.

Multi-Step Channel

Regarding the multi-step channel depicted in figure 4.4e), a notable phenomenon emerges wherein the deposit shape transitions from a straight bottom-up filling to a structure commonly referred to as a "mushroom-shaped deposition" in the literature [67]. This phenomenon becomes apparent due to the presence of the conductive surface only at the first step. As the first step becomes completely filled, the deposition of copper atoms, in the second and third step, occurs only on the conductive surface, which is the previously deposited copper.

Consequently, copper atoms accumulate atop each other, deviating from the mold's original geometry and resulting in the formation of a mushroom-like structure. This observation holds substantial implications for the design of metal parts with varying thicknesses throughout their depths. It highlights the limitation of relying on a single cathodic layer at the bottom of the mold, as it can result in uneven thickness distribution and the possibility of incomplete filling in specific areas. This concern becomes particularly relevant when substantial differences in widths exist between two mold layers.

Double Bevel and Double V-groove

The electroforming process demonstrated its capability to successfully deposit copper in regions ranging from narrow to wide and vice versa, even with varying angles. This phenomenon is evident in figures 4.4(b) and 4.4(f), which depict the 45° double bevel and the 45° double v-groove, respectively. In these instances, the copper depo-

sition encompasses wider regions with acute angles, transitions to narrower regions, and then shifts again to wider regions with obtuse angles.

This observation highlights the feasibility of designing molds for the production of intricate 3D components, incorporating varying angles along the walls of the mold. However, different angles and features affect the uniformity of the surface differently in a way which is hard to predict. Thus, studying the deposition in different shapes, angles, and features can provide a base line for mold design consideration when electroforming additively-manufactured molds.

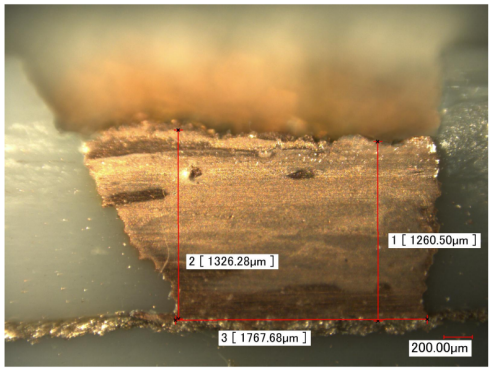

(a) Single Bevel 30°

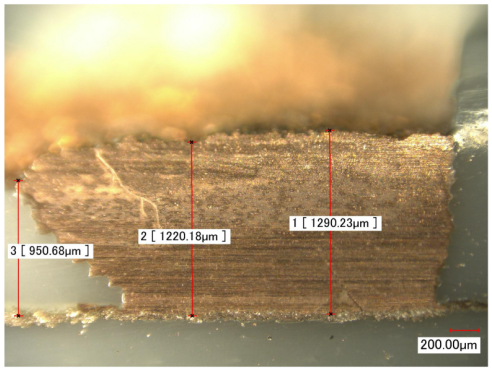

(b) Single Bevel 45°

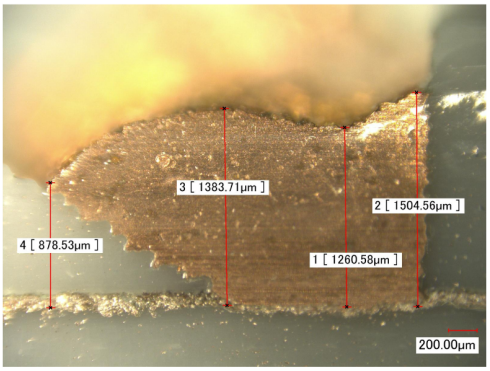

(c) Single Bevel 60°

Figure 4.5: Copper deposition in three single bevels with varying angles, visualized using a digital microscope.

Single Bevels featuring Various Angles

Regarding the influence of distinct angles on copper deposition within the mold, an investigation was conducted focusing on three individual bevel structures featuring varying angles. The three single bevel structures, illustrated in figure 4.5, encompasses overhang angles of 30°, 45°, and 60°, meaning that the actual angles at which copper is deposited are 120°, 135°, and 150°, correspondingly. For the 30° overhang single bevel, depicted in figure 4.5(a), the observed h_{max} measures 1326.28 μm, while the h_{min} equals 1260.50 μm. Thus, the non-uniformity (α_t) approximately amounts to 5%.

The non-uniformity for the 45° overhang single bevel, as shown in figure 4.5(b), is computed to be 35%. The non-uniformity had increased significantly from the 30° single bevel. Furthermore, it is evident that the deposition significantly diverged from uniformity in the case of the 60° overhang single bevel, exhibiting a non-uniformity rate of 70%.

This is a considerable escalation in comparison to the other features. It is also noteworthy that a pattern emerges when the angle becomes too steep, the deposit tends to deviate from following the structure. This dis-connection arises due to the increased non-conductive distance, causing the deposit to fall short of completing the intended structure. Moreover, the surface of the copper deposition, as depicted in figure 4.5(c), showcases a wave-like structure, attributed to the formation on such a steep angle of 150°.

Holes

Finally, with respect to the electroforming of the holes in the mold, it was observed that holes with diameters of 3 mm, 2 mm, 1.75 mm, 1.5 mm, and 1 mm were partially filled with copper deposits. However, smaller holes with diameters of 0.8 mm, 0.6 mm,

0.4 mm, and 0.2 mm were unable to facilitate the formation of copper deposits.

Summary

In summary, the viability of the fabrication approach has been successfully established. The electroforming process, utilizing the specified parameters, has demonstrated its capability to deposit copper formations with thicknesses exceeding 1000 μm, exhibiting acceptable thickness uniformity, and high precision. Among the various structures investigated, the straight 90° channels exhibit the most even surface uniformity. Regarding structures with angles spanning from 30° to 110°, the thickness uniformity remains satisfactory, with a non-uniformity rate (α_t) of less than 10%, corresponding to the specific angle of copper deposition. The study of multi-step channels, devised for producing components with varying thicknesses, has revealed the emergence of mushroom-like formations as the first step becomes fully filled, and the geometry widens in the second and third steps.

Chapter 5

Modeling and Simulation of Electroforming Process

This chapter is focused on modeling and simulating the electrochemical deposition of copper (Cu). The simulation serves to evaluate Cu growth in specific structures and explore the viability of electroforming various geometries. Given that the electroforming process employed in this study is time-intensive due to the substantial thickness of the targeted deposits (> 1000 μm), the simulation of Cu growth offers a time-saving measure and can guide more effective experimental trials.

The quality of electroforming is influenced by various parameters, with the key components being the electrolyte formulation, applied potential, system temperature, and plating time as they significantly impact the behavior of Cu filling and its deposited shape during the process. To understand the copper deposition mechanism, mathematical models were established based on a series of electrochemical equations. These models provide insights into the processes involved in Cu electroplating.

For simulation purposes, finite element models were constructed, incorporating various transport phenomena such as diffusion, migration, and convection, as well as multiple species and reactions. Employing these models, the copper electroforming process was simulated for one of the geometrical features. This simulation provided valuable insights into the electroforming process's behavior and its implications for the precise fabrication of metal parts.

5.1 Electrochemical Model

The basic principle of electrochemical copper (Cu) deposition is straightforward and widely accepted. However, the Cu deposition mechanism is microcosmic and complex, encompassing a series of electrochemical reactions [72]. The simulation is conducted using the Electrochemistry Module of COMSOL Multiphysics software, provided by COMSOL Inc. in Stockholm, Sweden.

Under the influence of direct current, electrolytic reactions occur on the surfaces of both the anode and the cathode. The overall reaction involved in copper electroplating is the conventional redox reaction of copper. The related equation can be expressed as follows:

$$Cu \rightleftharpoons Cu^{2+} + 2e^{-} \tag{5.1}$$

The copper electroplating process involves two distinct charge-transfer steps. The oxidation of copper metal at the anode:

$$Cu \rightarrow Cu^{2+} + 2e^{-} \tag{5.2}$$

The reduction of copper ions at the cathode:

$$Cu^{2+} + 2e^{-} \rightarrow Cu \tag{5.3}$$

These two steps together constitute the overall redox reaction of copper electroplating, wherein copper ions are reduced to form solid copper metal on the cathode surface. The simulation model is designed to operate in an acidic environment with a pH of 4, where copper (Cu^{2+}) and sulfate ($SO_4{}^{2-}$) ions are the dominant species. The deposition of copper at the cathode and the dissolution of copper at the anode are assumed to occur with 100% current yield, implying that the model excludes potential side reactions.

During the process, differences in electrolyte density emerge within the enclosed cell, leading to a higher density at the anode compared to the cathode. This density

variation could induce free convection within the cell. However, under the modeled conditions, the composition differences are small, allowing for the neglect of free convection effects. As the deposition process unfolds, the cathode boundary moves, rendering the process inherently time dependent. The model is constructed based on material balances for the involved ions copper (Cu^{2+}) and sulfate ($SO_4{}^{2-}$) as well as the electro-neutrality condition. These components govern the electrochemical reactions and overall behavior during the copper electroplating process.

The flux for each ionic species in the electrolyte can be determined using the Nernst-Planck equation, which is given by:

$$J_i = -D_i \nabla c_i - z_i u_i F c_i \nabla \phi_l \tag{5.4}$$

Where, (J_i) denotes the transport vector for the ionic species (mol/(m^2·s)), (c_i) represents the concentration of the ionic species in the electrolyte (mol/m^3), (z_i) is the charge of the specific ionic species, (u_i) is the mobility of the charged species (m^2/(s·J·mole)), (F) is Faraday's constant and is equal to (96485.33 A·s/mole), (∇c_i) is the concentration gradient in the electrolyte, and ($\nabla \phi_l$) is the potential gradient in the electrolyte (V). The material balances are expressed through a set of differential equations that govern the concentrations of the involved ionic species:

$$\frac{\partial c_i}{\partial t} + \nabla .\ J_i = 0 \tag{5.5}$$

one for each species, that is $i = 1, 2$. The electro-neutrality condition, which ensures that the overall system remains electrically neutral, is expressed by the following equation:

$$\sum z_i c_i = 0 \tag{5.6}$$

The charge transfer reactions occurring at the interfaces of the cathode and anode can be mathematically described by arbitrary functions. One common and widely used equation to represent the charge transfer current density is the Butler-Volmer equation. This gives the following relation for the local current density as a function

of potential and copper concentration:

$$i_{ct} = i_o \left[\exp(\frac{\alpha_a F \eta}{RT}) \ - \frac{c_{Cu^{2+}}}{c_{Cu^{2+},ref}} \exp(-\frac{\alpha_c F \eta}{RT}) \right] \tag{5.7}$$

Where, (i_o) denotes the exchange current density of copper reduction (A/m^2), (α_a) is the anodic charge transfer coefficient, (α_c) is the cathodic charge transfer coefficient, (R) is the ideal gas constant and is equal to (8.314 J/(mol·K)), (T) is the absolute temperature measured in (K), and (η) denotes the over-potential, and defined as:

$$\eta = \ \phi_s - \phi_l - E_{eq.} \tag{5.8}$$

Where, (ϕ_s) the electric potential of the respective electrode, (ϕ_l) is the electric potential of the electrolyte, and ($E_{eq.}$) the equilibrium potential. This gives the following condition for the cathode:

$$\begin{aligned} J_{Cu^{2+}}.\, \boldsymbol{n} = \ - \frac{i_o}{2F} \Bigg[& \exp(\frac{\alpha_a F \left(\phi_{s,\ cat} - \phi_l - E_{eq.}\right)}{RT}) \\ & - \frac{c_{Cu^{2+}}}{c_{Cu^{2+},ref}} \exp(\frac{\alpha_c F \left(\phi_{s,\ cat} - \phi_l - E_{eq.}\right)}{RT}) \Bigg] \end{aligned} \tag{5.9}$$

Where, ($\boldsymbol{n}$) denotes the normal vector to the boundary. The condition at the anode is:

$$\begin{aligned} J_{Cu^{2+}}.\, \boldsymbol{n} = \ - \frac{i_o}{2F} \Bigg[& \exp(\frac{\alpha_a F (\phi_{s,\ an} - \phi_l - E_{eq.})}{RT}) \\ & - \frac{c_{Cu^{2+}}}{c_{Cu^{2+},ref}} \exp(\frac{\alpha_c F \left(\phi_{s,\ an} - \phi_l - E_{eq.}\right)}{RT}) \Bigg] \end{aligned} \tag{5.10}$$

All boundaries, other than the anode and the cathode, are insulating. For other ions, insulating conditions are applied to the whole model:

$$J_{Cu^{2+}}.\, \boldsymbol{n} = \ 0 \tag{5.11}$$

The initial conditions for the electroactive species concentrations are:

$$c_{Cu^{2+}} = \ c_0 \tag{5.12}$$

$$c_{SO_4{}^{2-}} = c_0 \tag{5.13}$$

The ion fluxes and boundary mesh velocity at the electrode surface boundary node are determined by considering the reaction currents, the number of electrons involved in the reactions, and the specified stoichiometric coefficients of the electrode reactions. The sign of the stoichiometric coefficient for a particular species depends on whether the species undergoes oxidation, positive coefficient, or reduction, negative coefficient, within the reaction. In the case for the total reaction in this model the stoichiometric coefficient is ($N_{Cu^{2+}} = -1$) for the copper ions in the electrolyte, and ($N_{Cu} = 1$) for the copper atoms in the electrodes.

Equation (5.1) through Equation (5.13) are set up utilizing the Tertiary Current Distribution and Nernst-Planck interface, that are pre-defined in the COMSOL software. The Deformed Geometry interface is responsible for monitoring the mesh deformation.

Table 5.1 shows the required parameters to run the simulation. The initial parameters to be configured under the electrode boundaries (cathode, and anode) are the density and molar mass of the dissolving-depositing species of Cu. The density was set at $\rho =$ 8960 kg/m^3 , and the molar mass at M = 0.06355 kg/mol. (C_i) refers to the initial concentration of Cu ions (Cu^{2+}) in the electrolyte. The initial concentration of Cu^{2+} ions was set to 1000 mol/m^3, relevant to the solution used in the electroforming setup. The system temperature is the temperature of the electrolyte during the experiment. Experimentally there were no temperature control, thus the temperature was set to ambient, 296K.

The exchange current density (I_o) is defined as the current exchanged at the electrode-electrolyte interfaces in both directions in equilibrium. The value of I_o changes based on the applied current during electroforming, and the conductivity of the cathode. Current-potential data was used to fit exchange current density. The value of I_o is experimentally determined at 100 A/m^2. In the electroforming experiment, a pulsed deposition technique was employed, alternating between 150 mV and

Table 5.1 Simulation Parameters of Copper Electroforming.

Parameter	**Symbol**	**Value**	**Unit**
Cu density	ρ	8960	kg/m^3
Cu molar mass	M	0.06355	kg/mol
Concentration of Cu in electrolyte	C_i	1000	mol/m^3
System temperature	T	296	K
Exchange current density	I_o	100	A/m^2
Anodic potential	$\phi_{s,\ an}$	0.145	V
Cathodic potential	$\phi_{s,\ cat}$	-0.145	V
Anodic charge transfer coefficient	α_a	1.5	-
Cathodic charge transfer coefficient	α_c	0.5	-
Cu charge	z_Cu	+2	-
SO_4 charge	z_ SO_4	-2	-
Cu diffusivity	D_Cu	2e-9	m^2/s

100 mV for the final 10% of the charge. The anodic and cathodic potentials were set at a weighted average of +145 mV and -145 mV, respectively.

The charge transfer coefficient (α) is defined as the fraction of the electrostatic potential energy affecting the reduction rate in an electrode reaction. The summation of anodic and cathodic transfer coefficients has to be equal to the number, n, of electrons involved in the overall electrode reaction [73].

$$\alpha_a + \alpha_c = n \tag{5.14}$$

Therefore, their summation must be equal to 2. Transfer coefficients for copper ions are derived from their respective Tafel plots [73, 74], and their values are equal to $\alpha_a = 1.5$, and $\alpha_c = 0.5$. Lastly, the copper diffusivity, which is a property of the material in the electrolyte, was set to $2\text{x}10^{-9}$ m^2/s.

5.2 Simulation Model Geometry

The model's geometry is visually depicted in figure 5.1. A multi-step feature geometry, one of the geometrical features implemented in the mold, was chosen for this simulation to be computed by the software. The mold is placed nearly 5 mm away from the copper sheet. In this representation, the upper horizontal boundary symbolizes the anode, which is the copper sheet, while the cathode is positioned at the lower portion corresponding to the conductive plated area of the mold. The vertical walls correspond to the pattern present on the master electrode, and they are insulated.

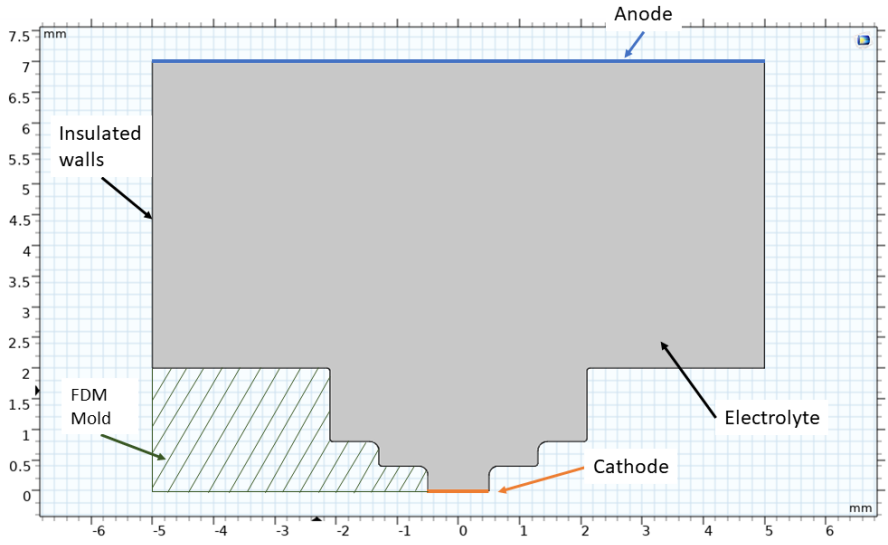

Figure 5.1: Model geometry illustrating the boundaries of the anode, cathode, and vertical insulating walls.

The designed dimensions for the multi-step geometry were incorporated into the simulation by creating the 2D geometry, illustrated in figure 5.1. The geometry was designed on SOLIDWORKS and imported to COMSOL as a DXF file. The top layer of the mold has a thickness of 2 mm. The first step, where the cathode is positioned, measures 1 mm in width. The second step is 2.6 mm wide, and the third step is 4.2 mm wide. The wall thickness between the first and second steps matches that between the second and third steps, at 0.4 mm. For simplification, the anode width was set at 10 mm in width.

The dimensions used in the 2D geometry design of the simulation model are identical to the designed dimensions of the geometrical features mold, as discussed in section 4.1. In the simulation, a user-controlled mesh spacing is maintained, necessitating the specification of five parameters in the Element Size Parameter section. These parameters are the maximum element size, minimum element size, maximum element growth rate, curvature factor, and resolution of narrow regions.

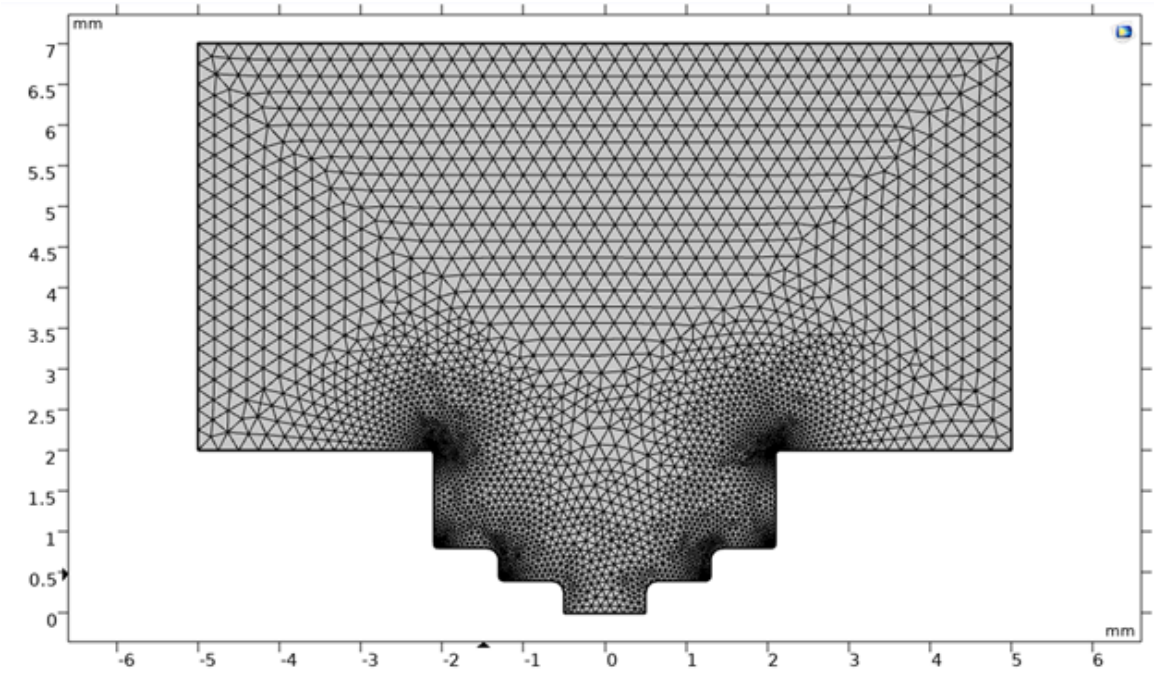

Figure 5.2: Mesh spacing of the 2D model domain.

The maximum element size was set to 0.25 mm and minimum element size was set

to 0.2 μm. The maximum element growth rate represents the extent to which the element size can increase from one element to the next, and it was configured at 1.1, equivalent to a growth of 10%. The curvature factor, which denotes the relationship between the element size and the boundary's curvature radius in the model, was established at 5. In the field designated for the resolution of narrow regions, the value 3 was entered. This setting guarantees that narrow areas will consistently comprise around 3 layers of elements.

The meshed geometry, depicted in figure 5.2, was generated utilizing the aforementioned mesh parameters. Given the primary focus on the deposits formed on the cathode's surface, the mesh on the cathode boundary was finely refined. Emphasis was placed on the mold region situated at the interface between the cathode and the top surface of the mold. Given that copper deposition would occur in the cathodic zone, potentially leading to geometrical distortion in that region, an exceptionally fine mesh was designated for this area. This fine meshing strategy was adopted to avoid any mesh deformation phenomena that might hinder the model from achieving convergence.

After establishing the simulation parameters, boundary conditions, initial values, and mesh, the time dependent study was initiated. The time for the solver to simulate the deposition process was set to 100 hours, corresponding to the real experiment time. The time unit was set to hours and the range was set to (0,1,100), which means that the deposition process is running for 100 hours, storing solutions every 1 hour.

5.3 Simulation Model Validation

The software was utilized for the simulation of the Cu deposition process employing two distinct electroplating methods. The implementation of a moving mesh facilitated the dynamic representation of the cathode boundary's growth throughout the progression of the process. This capability to depict deformed mesh and moving boundary phenomena dynamically enabled the visualization of the transient evolu-

tion of Cu deposition. The symmetry factor plays a pivotal role in influencing both the deposition rate and the symmetrical characteristics of the process.

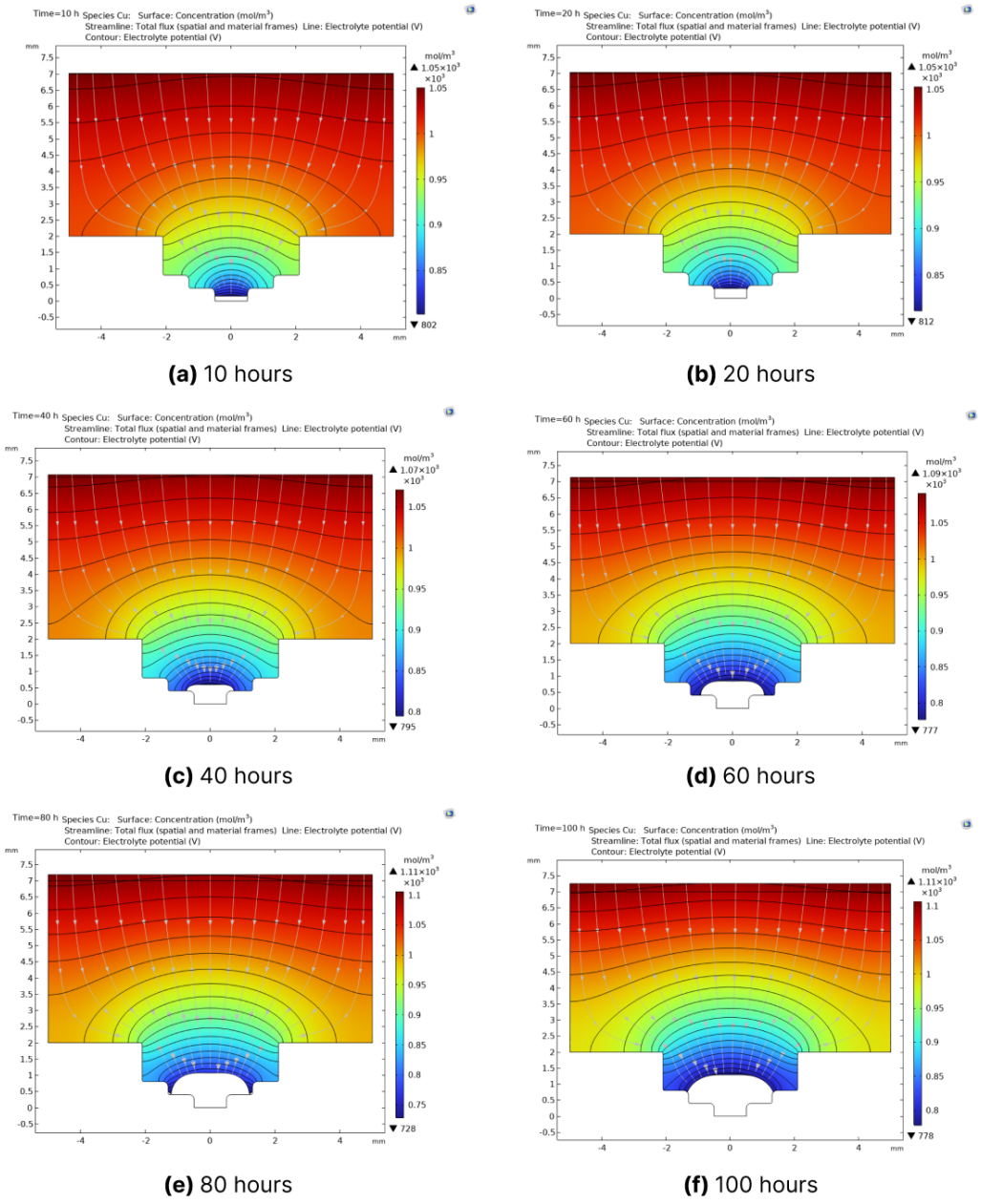

Figure 5.3: Simulation results displaying the copper concentration and its growth in the multi-step channel at various time intervals, ranging from (a) 10 hours to (f) 100 hours.

Figure 5.3 offers a visual representation of the Cu deposition within the multi-step channel for a time of 100 hours. The displayed color gradient serves to illustrate the

concentration of copper in units of mol/m^3. Notably, the maximum concentration resides in proximity to the anode, showcasing an average value of 1070 mol/m^3. Conversely, the minimum concentration is situated near the cathodic surface, with an average value of 770 mol/m^3. A decrement in concentration occurs as ions traverse from the anode to the cathode. The grey arrows, denoted as streamlines, present the filling direction which is directed to the conductive part of the mold and visually indicate the overall flux as it traverses from the anode to the cathode. Additionally, the black-colored contour lines present the electrolyte potential inherent in the electroforming process.

In the initial stages, the growth of the Cu deposit remains uniform within the straight right-angled walls, depicted in figure 5.3(a), and 5.3(b). Once the deposited copper fills the first step and the geometry of the multi-channel expands from 1 mm to 2.6 mm, the Cu deposit shape changes from a bottom-up straight filling to a mushroom-shaped structure, depicted in figure 5.3(c). As discussed in section 4.3, The mushroom-shaped phenomenon becomes apparent as the deposition of copper atoms, in the second and third step, occurs only on the conductive surface, which is the previously deposited copper. In effect, this allows the accumulation of copper atoms upon one another, causing a deviation from the original mold geometry resulting in the formation of a mushroom-like structure.

To validate the simulation model for copper electroforming, the simulation time was set at 100-hour duration, aligning it with the experimental electroforming process of the geometrical features mold. Visually, the simulation results closely resemble the experimental outcomes. However, the model predicts a slightly thicker deposit at the edges of the mushroom-shaped formation. Figure 5.4 provides a comparative view of the simulation of copper deposition in the multi-step channel and the experimental electroforming process. Specifically, figure 5.4(a) shows the simulated Cu deposition in the multi-step channel after 100 hours, while Figure 5.4(c) showcases a graphical representation, extracted from the resulting simulation, of the profile of the deposited

copper in the multi-step channel at intervals of 2 hours.

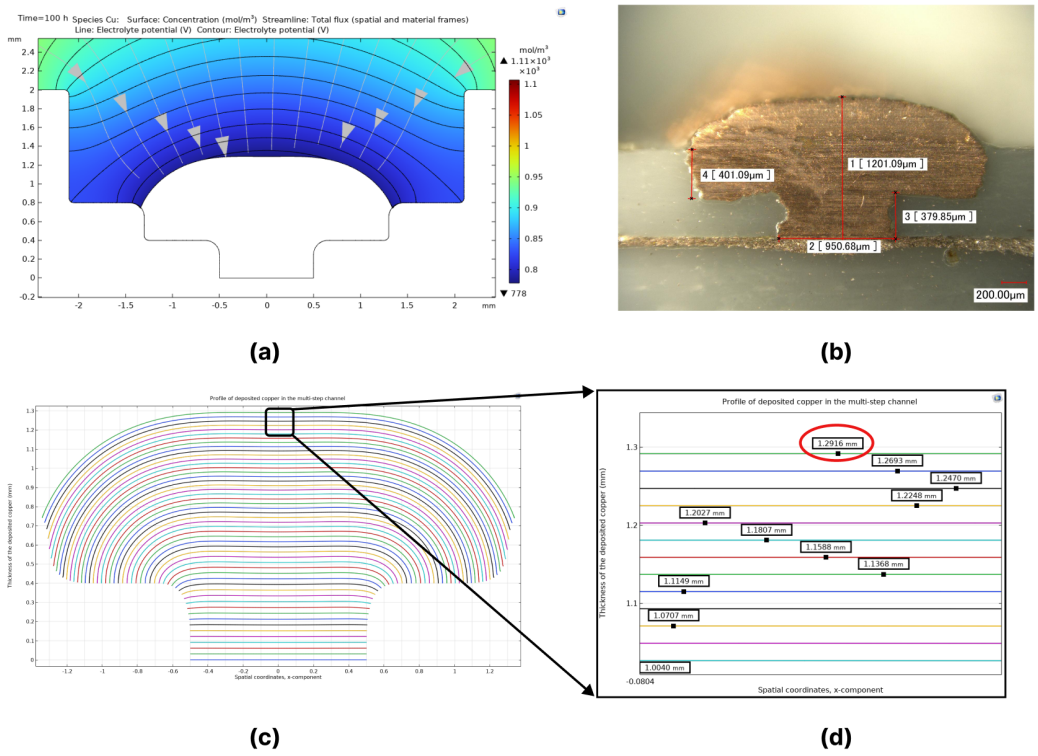

Figure 5.4: (a) Simulation results illustrating the change in total electrode thickness after 100 hours. (b) Experimental results for the electroforming of the multi-step channel. (c) A graphical representation of the deposited copper profile every 2 hours. (d) Maximum point in deposited copper thickness.

In the experimental results, shown in figure 5.4(b), the maximum measured thickness of the electroformed deposit is 1201.09 μm. However, in the simulated model, the maximum thickness of the deposited copper was at 1291.60 μm, depicted in figure 5.4(d). The variance between the model and experimental results is accounted to be 7.536% in terms of the maximum deposition thickness.

The variation between the simulated model and the experimental results is linked to the difference in dimensions between the simulated geometry and the actual geometry of the multi-step channel. The variation in the geometry is due to the quality of FDM printing in the experimental setup.

5.4 Insights from Electroforming Simulations

This section delves into exploring the impact of the conductive paint location subsequent to validating the simulation model. Notably, the position of the paint substantially influences the final shape of the electroform. By manipulating the paint locations, we can simulate the resulting shape to ensure it aligns with the desired outcome. This demonstrates how even a slight alteration in the conductive paint location can significantly change the resulting shape. Furthermore, the effects of insulating and conducting the walls on the electroform shape is examined. Additionally, the section covers design considerations and guidelines for the electroforming process. These guidelines result from a comprehensive synthesis of findings from experimental work and the simulation model.

5.4.1 The Impact of Cathode Location on Electroformed Geometry

The simulation results indicate that the second step in the multi-step structure did not achieve complete filling until approximately 100 hours of deposition. Additionally, the appearance of the mushroom-shaped structure has a substantial impact on the overall uniformity of the resulting structure. Thus, depending on a single cathodic layer for electroforming components with varying thicknesses is considered unreliable. This concern becomes particularly evident when the mold's geometry involves a significant difference in width (W2 – W1) across its various thicknesses, as illustrated in figure 5.5.

As discussed in the findings of section 4.3, a comparative analysis of thickness consistency across various geometries highlights the pronounced uniformity observed in the straight 90° channel. Thus, the proposition of adding an additional cathodic layer for each distinct width within the intended part's geometry emerges as a strategic solution to address the thickness uniformity challenge.

The concept behind this strategy is illustrated in figure 5.5, which visually contrasts

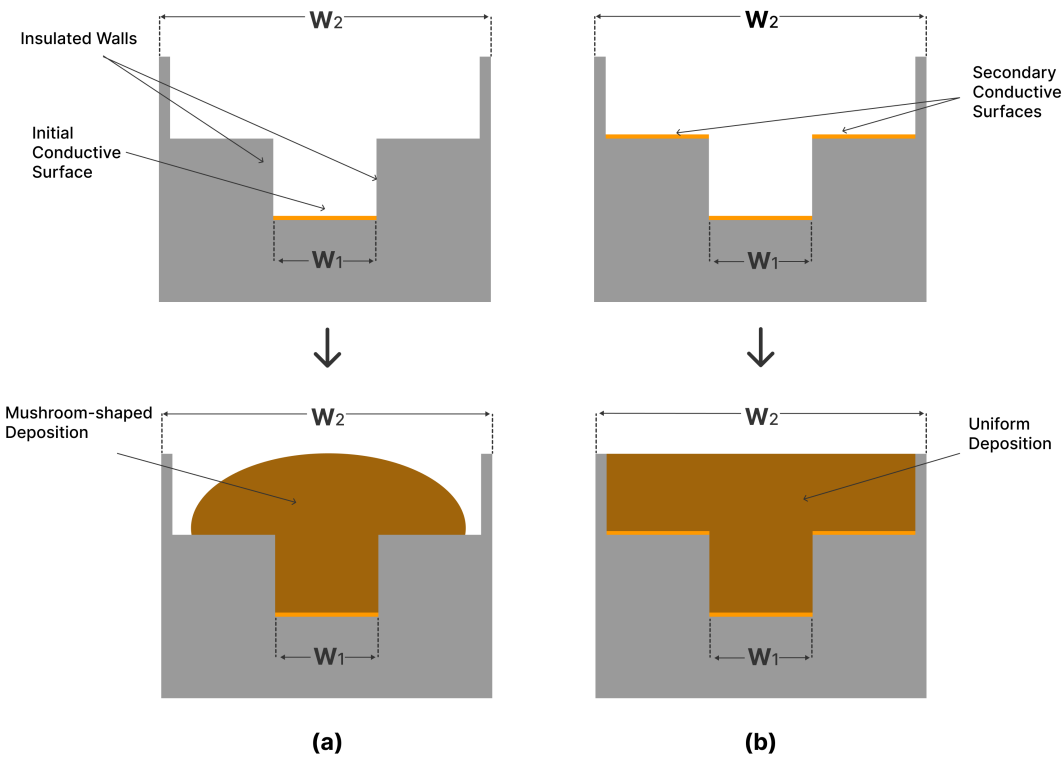

Figure 5.5: A schematic illustrating the electroforming of two different molds: (a) with one conductive surface and (b) with two conductive surfaces.

the outcomes of employing a single conductive surface versus employing two conductive surfaces within the mold designated for the electroforming process. To avoid the formation of mushroom-shaped structures, a solution involves incorporating secondary conductive surfaces (cathodes) onto the multi-level structures, as depicted in figure5.5(b).

Initially, the Cu deposition occurs exclusively on the first step of the structure. As the deposit reaches the same level of the conductive surface on the secondary step, an electrical connection is established between the top surface of the Cu deposit and the secondary conductive surfaces. This approach ensures the entire surface is covered by an electroformed layer, leading to improved surface uniformity and a consistent deposition layer that replicates the mold's contours.

To confirm the viability of employing multiple cathodic layers at each step, the geometry of the multi-step channel is replicated in the model, this time incorporating

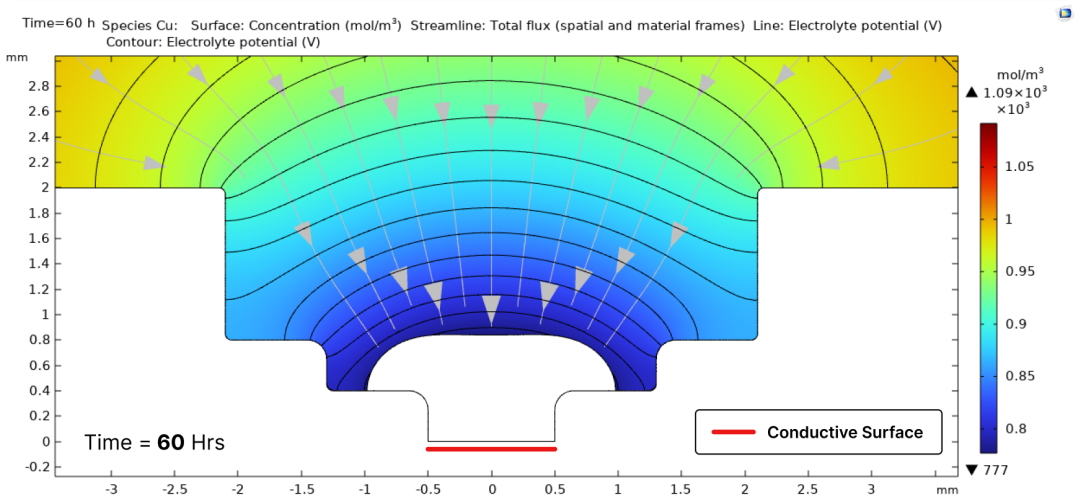

(a) Visualization of the Cu growth with a single conductive surface.

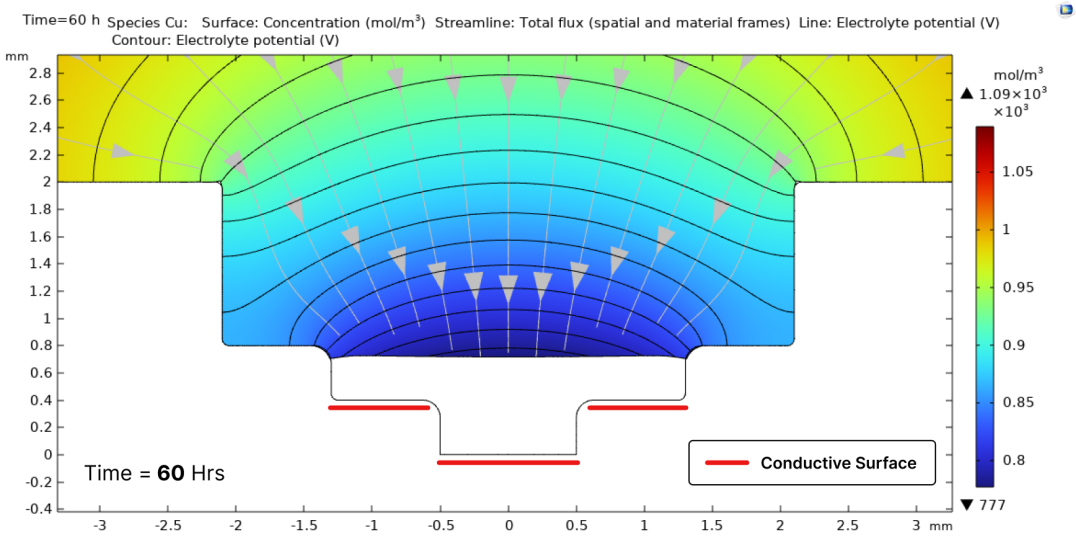

(b) Visualization of the Cu growth with two conductive surfaces.

Figure 5.6: Simulation results depicting the growth of Cu deposits after 60 hours, comparing (a) a mold with one conductive surface to (b) a mold with two conductive surfaces.

the two conductive surfaces is shown in earlier in the schematic. Figure 5.6(b) provides a visual representation of the Cu deposition process within the multi-step channel. The resulting copper structure demonstrates satisfactory thickness uniformity across its width, with an average thickness of 750 μm achieved after 60 hours of electroform-

ing. This aligns with the maximum deposition observed in the mushroom-shaped structure depicted in figure 5.6(a). Therefore, introducing multiple conductive layers, rather than relying on a single layer, leads to improved surface uniformity and the establishment of a consistent deposition layer in the electroforming of multi-thickness structures.

Furthermore, a crucial aspect to take into account is refraining from applying paint to the mold walls. The walls must remain isolated to achieve the intended uniform shape. Any residual paint on the mold walls might result in unintended deposits during electroforming, potentially jeopardizing the quality of the final electroformed part. Equally important is the need to guarantee the proper isolation of mold components from each other. This enables the deposition process to occur in the correct sequence, beginning with the base layer and progressing to the mask layer.

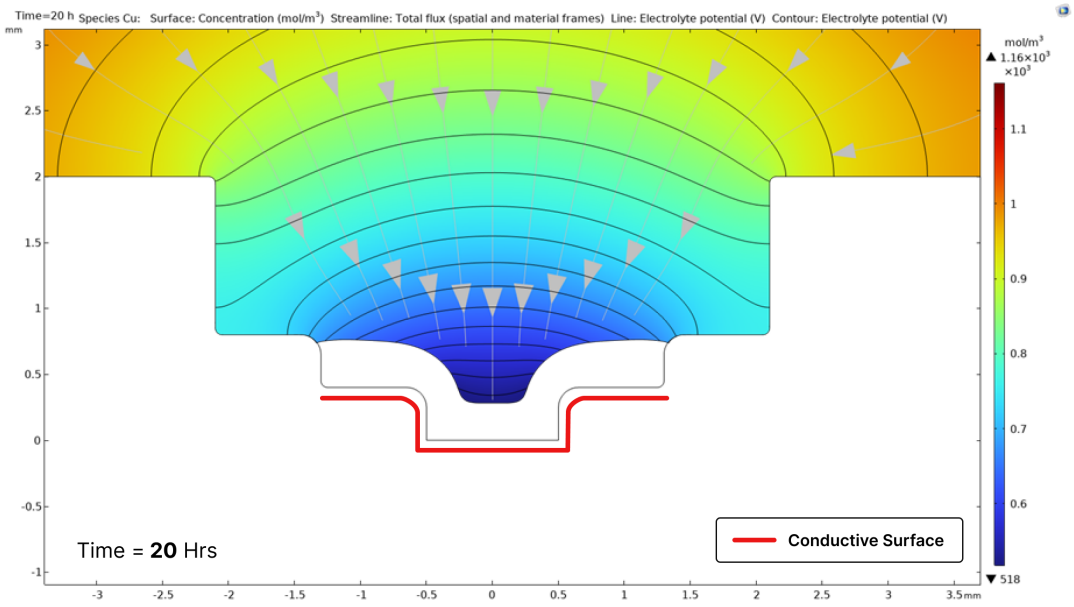

(a) Visualization of the Cu Deposit with Un-insulated Walls

Figure 5.7: Simulation results illustrating the growth of Cu deposits after 20 hours within a mold featuring two conductive surfaces and un-insulated walls.

However, this outcome is contingent on the intended shape of the electroformed part. Applying conductive paint on the mold walls will result in the creation of a

completely distinct geometrical shape. Consequently, the final result is heavily reliant on the desired part geometry. Conductive walls will interconnect all the conductive surfaces, effectively triggering deposit formation on all surfaces simultaneously.

To visualize the resulting shape when applying conductive paint to the walls, the geometry of the multi-step channel was once again replicated in the model. However, this time, the walls were included as a cathodic surface in addition to the two conductive surfaces, thus interconnecting them all. Figure 5.7 illustrates the simulated copper formation within the multi-step channel after 20 hours of electroforming. The resulting deposit shape is notably distinct from the desired uniform surface shape depicted in figure 5.6(b). While this shape may not be suitable for achieving a uniformly flat top surface, it might be precisely what another application requires.

The key takeaway here is that changing the distribution of conductive surfaces within the mold will yield a significantly different electroformed shape. Therefore, the use of simulation is of paramount importance when electroforming a specific part within the mold. Simulation of copper growth enables a visual representation of the final outcome, allowing for precise adjustments to the mold's geometry to achieve the desired shape. Additionally, simulation provides an accurate estimate of the time required to produce the intended electroformed shape. Furthermore, it offers the significant advantage of time savings, as simulations are considerably quicker to set up and execute compared to the time-consuming electroforming process.

5.4.2 Process Design Considerations and Guidelines

By conducting experiments involving the electroforming process in FDM printed molds with varying angles, shapes, and features, and leveraging the simulation model to visualize copper growth, valuable insights were gained for shaping part design considerations in electroforming. In this section, both the experimental and simulated results are leveraged to define the guidelines for the electroforming process. These guidelines serve as a foundational resource for understanding essential aspects of part

design, especially when it comes to electroforming composite structures in AM molds. When designing a part to be manufactured using electroforming technology, several critical considerations warrant attention.

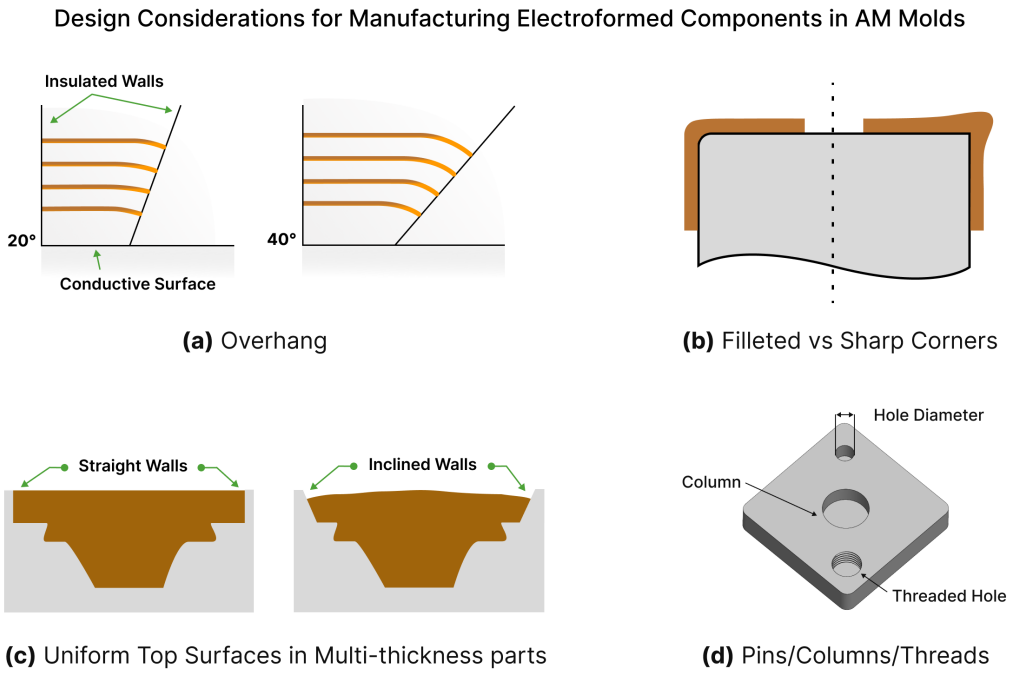

Characteristics of Electroforming Process	
Tolerance	Electroforming replicate features up to 1µm. (Dependent on the mold manufacturing process)
Walls	The process is able to produce supported and unsupported walls.
Dimensional Accuracy	The process replicates the mold. Expect no shrinkage neither warpage.
Repeatability	The electroforming process offers very high repeatability.
Size	The size of the part is only limited by the size of the plating tank.
Part Thickness	Electroforming becomes challenging as the thickness of the part increases.
Materials	Any conductive material, i.e., Copper, Gold, Silver, Iron, Titanium, Nickel, Chromium, Graphite, Zinc and Alloys.

Figure 5.8: Design considerations and guidelines for electroforming within additive manufacturing (AM) molds.

Overhang Angles

The presence of overhangs is a vital factor to address in electroforming part design. Overhangs manifest when a part geometry includes inclined walls that extend beyond the vertical with angles surpassing 90 degrees. This phenomenon first came to attention during the investigation of the influence of angles on copper deposition within the geometrical features of the mold in section 4.3. It became evident that, as the angle of overhang steepness increased, the deposited copper deviates from the intended structure. This deviation was primarily attributed to the expanded non-conductive distance, causing the deposit to fall short of fully realizing the intended shape.

To precisely understand the influence of overhang angles on part formation, multiple simulations were employed to model various angles exceeding 90 degrees. This analysis aimed to establish the maximum allowable overhang angle without compromising part quality and with minimal impact on surface uniformity. The findings indicate that an overhang of up to 20 degrees is the maximum permissible angle without compromising part quality and while maintaining surface uniformity. For visual clarity, Figure 5.8(a) provides a side-by-side comparison of a 20-degree overhang and a 40-degree overhang, the latter being excessive due to the significant disconnection and the amplified non-conductive distance.

Filleted vs Sharp Corners

The design of corners holds notable influence over the formation of deposited copper. Sharp corners can induce irregular deposition and concentration of material around the sharp edge, as shown in figure 5.8(b). Conversely, filleted corners promote a smoother material deposition, facilitating even flow and distribution. This results in a more uniform deposition across all corners. Importantly, these principles apply to both external and internal walls. For optimal electroforming outcomes, it is

advisable to incorporate filleted edges into the mold design. This measure enhances the overall deposition process, ensuring a more uniform and consistent deposition of material.

Parts with Varying Thicknesses (2.5D Structures)

Electroforming parts with varying thicknesses within an AM-mold can pose challenges in achieving a uniform top surface. As previously recommended in the methodology section 3.1, it is prudent to employ a step-like design approach. This involves dividing the part into distinct levels, allowing for gradual changes in thickness. Additionally, special attention should be given to the mask layer, which constitutes the topmost layer of the part. It is essential that this layer features uniform walls, preferably with minimal or no inclinations. This design consideration helps prevent excessive overhang, which could otherwise result in a non-uniform top surface for the electroformed component.

Parts with Columns/Pins/Threads

Designing parts with internal holes or threaded features is entirely feasible with electroforming. This is achieved by integrating core objects that create the negative space for these shapes. FDM, due to its limited precision, may pose challenges when fabricating holes, columns, and threaded features, particularly when their diameters are below 2 mm. Nevertheless, if the design incorporates external columns or threads, electroforming proves capable at manufacturing such features with precision. If the mold itself is produced using FDM technology, it is advisable to drill holes and tap threads as a post-processing step. Copper deposition in holes can be observed in a minimum diameter of 1 mm. When experimenting smaller diameters of 0.2, 0.4, 0.6,

and 0.8 mm, no copper formation is observed in any of them.

Other Electroforming Characteristics

Lastly, electroforming exhibits the remarkable capability of achieving tolerances and dimensional accuracies as tight as 1 μm, ensuring exceptional repeatability. However, this precision is linked to the quality of the mold where the deposition process takes place. Electroforming operates as an additive manufacturing method accumulating atom by atom, thus reproducing intricate surface details from the mold. Consequently, enhancing mold manufacturing processes is key to elevating the overall quality of electroformed parts. For a concise overview of the key characteristics of the electroforming process, figure 5.8 is constructed.

The data presented in figure 5.8 is a product of comprehensive integration of findings from experimental work, the simulation model, and the existing literature. This figure serves as an attempt to consolidate all the observed design guidelines into a single, illustrative resource, aimed at facilitating a better grasp of the electroforming process and defining its guidelines, particularly in the context of manufacturing composite structures within AM molds.

Chapter 6

Applications of Electroforming in AM Molds

Traditional manufacturing techniques for metal parts are often unsuitable for mass personalization due to the added expenses incurred from customer-requested design alterations. However, employing electroforming to additively manufactured molds presents a promising fabrication method for producing personalized metal components. Notably, the additive manufacturing of molds incurs no additional costs arising from design modifications. The potential to combine multiple molds into a singular plating batch enables the parallelization of the process, thereby reducing per-part manufacturing costs irrespective of any design adjustments.

This chapter investigates the fabrication method for producing 2.5D and 3D metal parts by electroforming additively manufactured molds. Two applications were chosen to assess the feasibility of this process for creating such structures. A center wheel is fabricated which serves as an example of a 2.5D structure and is characterized by intricate details that include micron-sized teeth. Additionally, a toroidal propeller is manufactured to illustrate how varying angles can lead to the production of 3D structures utilizing electroforming.

6.1 Center Wheel Design

The center wheel, or sometimes named the second wheel, is one of the main gears in the gear train of mechanical watches and clocks. The central wheel completes a single rotation every hour within the watch's gear train. The pinion of this wheel is engaged by the teeth on the mainspring barrel in watches and spring-driven clocks, and by the weight pulley in weight-driven clocks. The arbor of the central wheel extends through a hole in the watch's face and imparts motion, through a friction coupling, to the cannon pinion which in turn controls the movement of the minute hand. Additionally, it drives the pinion of the third wheel [75].

The center wheel serves as the initial selected application for this fabrication method due to several reasons. Firstly, the center wheel boasts a relatively intricate geometry, featuring 80 micro-sized teeth arranged along its diameter, as well as hollow curved sections at its center. Furthermore, this component exhibits a multi-thickness configuration along its depth, effectively constituting a 2.5D structure. As a result, it stands as an ideal candidate for thoroughly exploring the viability of the presented fabrication approach in creating complex 2.5D structures.

Secondly, the conventional manufacturing of high-precision center wheels within the industry necessitates a series of intricate manufacturing processes that are not only costly but also time-intensive. The traditional approach typically involves Computer-Numerical-Control (CNC) turning, a process used to shape the wheel blanks into the desired thicknesses and subsequently, centering and drilling the center wheel hub. Following this, each wheel undergoes a cleaning process to eliminate any residuals stemming from the turning procedure. Moreover, the wheel blanks are subjected to a pressing tool for stamping to add the internal curved angles to the center wheel. The center wheel blank is then clamped, and teeth generation is accomplished through a gear hobbing process.

The gear teeth undergo a polishing phase involving the use of indexed wooden disks

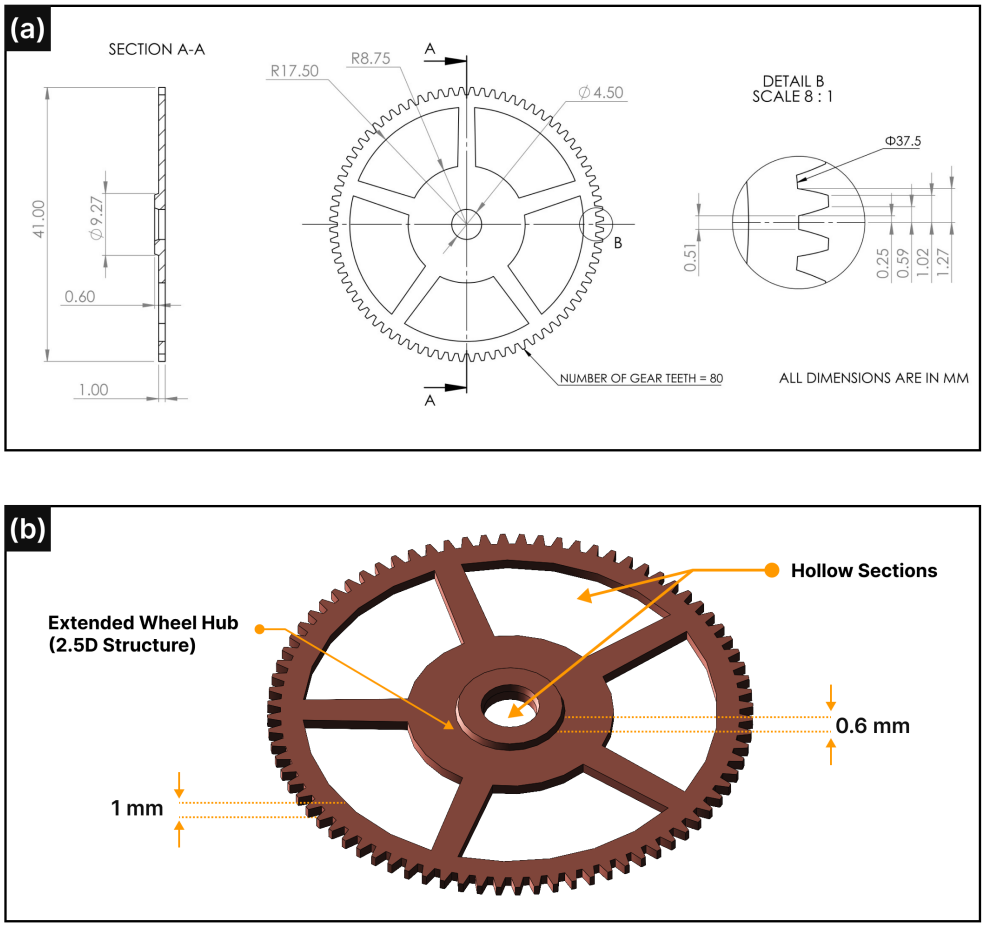

Figure 6.1: (a) An engineering drawing showing the center wheel specifications and dimensions. (b) 3D CAD model of the center wheel.

saturated with polishing compounds. Finally, center wheels are loaded to a plate and are polished using a polishing machine. The traditional method of manufacturing center wheels follows the principles outlined by Watkins [76], the American system of watchmaking. Given the intricate and labor-intensive nature of this conventional approach, the utilization of electroforming in FDM printed molds holds promise as a viable and cost-effective alternative to this resource-intensive and time-consuming process.

The initial step in fabricating the center wheel involves its CAD model design. The standard dimensions of the center wheel were extracted from various resources,

Meyer and Cifrulak [75], as well as insights from experts in the field of watchmaking [77]. The dimensions utilized for the center wheel in this study were scaled to 2x for testing the feasibility of the process as the original dimensions of the teeth posed challenges in terms of compatibility with the FDM printer employed in this study.

The center wheel configuration, visualized in figure 6.1, encompasses 80 teeth, and exhibits a total diameter of 41 mm, alongside a root diameter of 37.5 mm. The overall thickness of the center wheel stands at 1.6 mm, comprising a 1 mm gear body and a 0.6 mm extended hub positioned at the center wheel's midpoint, having a diameter of 9.27 mm. Five spokes extended from a diameter of 17.5 mm and span outward to 35 mm. Additionally, the central hole of the gear measures 4.5 mm in diameter.

To devise a suitable mold design for electroforming the center wheel, the methodology outlined in section 3.2 is adopted. Employing only a substrate layer and a mask layer proves inadequate for manufacturing the center wheel due to its 2.5D structure encompassing multiple thicknesses at varying depths. Hence, the incorporation of multi-layers atop the substrate emerges as a practical solution for several factors:

- **Electroforming of 2.5D Structures**: Given the center wheel's 2.5D structure, adopting multiple layers facilitates the generation of diverse flat features at different depths.
- **Enhanced coating process**: During the coating of the ABS printed mold components, specific layers necessitate conductivity, while others must remain electrically isolated.
- **Improved Deposition Consistency**: As verified through simulations, introducing multiple cathodic surfaces contributes to better surface uniformity and a consistent deposited layer.

The mold is conceptualized to have three-layer design, integrating positive inserts. This configuration consists of a base layer, which acts as a substrate. Positioned

above is an intermediate layer, to match the 0.6 mm thickness of the center wheel's extended hub. The intermediate layer has five positioning recesses as well, designed to accommodate the positive inserts. The extended hub's development initiates at the substrate, ascending to its targeted thickness at the upper part of the intermediate layer.

The gear body electroforming is initiated from the intermediate layer, progressing towards the top layer. The top layer encompasses the negative encounter of the gear teeth. Additionally, upon assembly atop the intermediate layer, the five positive inserts function as negative encounters defining the contours of the hollow curved segments, forming the spokes.

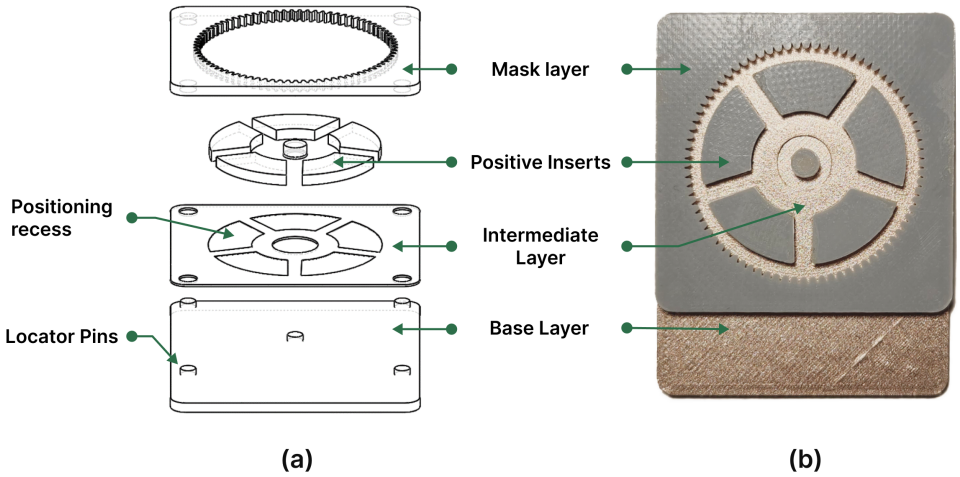

Figure 6.2: (a) A schematic depicting the center wheel mold components. (b) A photograph displaying the fully assembled mold.

The base substrate measures 50 mm x 65 mm and has a thickness of 2 mm. Within this frame, a 50 mm x 50 mm square is designated as the core mold assembly zone. Additionally, an extended segment measuring 50 mm x 15 mm is incorporated to ensure secure mounting throughout the electroforming procedure. The substrate has four locator pins along its sides and one positioning pin in the center. The four locator pins are included to ensure precise alignment and positioning of the intermediate and

mask layer during assembly. However, the pin in the center is for positioning the center core which acts as a negative encounter for the hole in the middle of the center wheel. Figure 6.2 depicts a schematic illustrating the center wheel mold components and the assembled mold after painting and assembly.

The intermediate layer occupies dimensions of 50 mm x 50 mm and features four through holes at its corners. The holes align with the pins in the base layer for easy positioning. Correspondingly, the mask layer also integrates four holes, serving as docking points for the pins, completing the assembly. All mold components are produced utilizing ABS filaments, employing the same FDM printer as mentioned in the experimental procedures section 3.2. The fabrication of mold components is done by adopting the same optimal parameters utilized in this study for consistent results throughout.

6.2 Center Wheel Electroforming Results

Following the preparation of the center wheel mold for electroforming, as illustrated in figure 6.2(b), the mold was subjected to the electroforming process. The targeted deposition thickness was set at 1600 μm, in accordance with the center wheel design specifications. In order to achieve this desired thickness, the number of deposition cycles was set to 32,000. The electroforming process spanned approximately 5 days, corresponding to a total of 120 hours, until the mold completed the designated cycles.

Top Surface Irregularities and Post-processing

Following the electroforming process, the electroformed mold, illustrated in figure 6.3(a), underwent a cleaning procedure involving de-ionized water and subsequent air drying. Examination of the deposited material surface reveals distinct irregularities resulting from the non-uniform electroforming deposition process. These surface irregularities include waviness, bumps, and micro slits, highlighting the influence of process parameters on the extent and distribution of these surface features arising

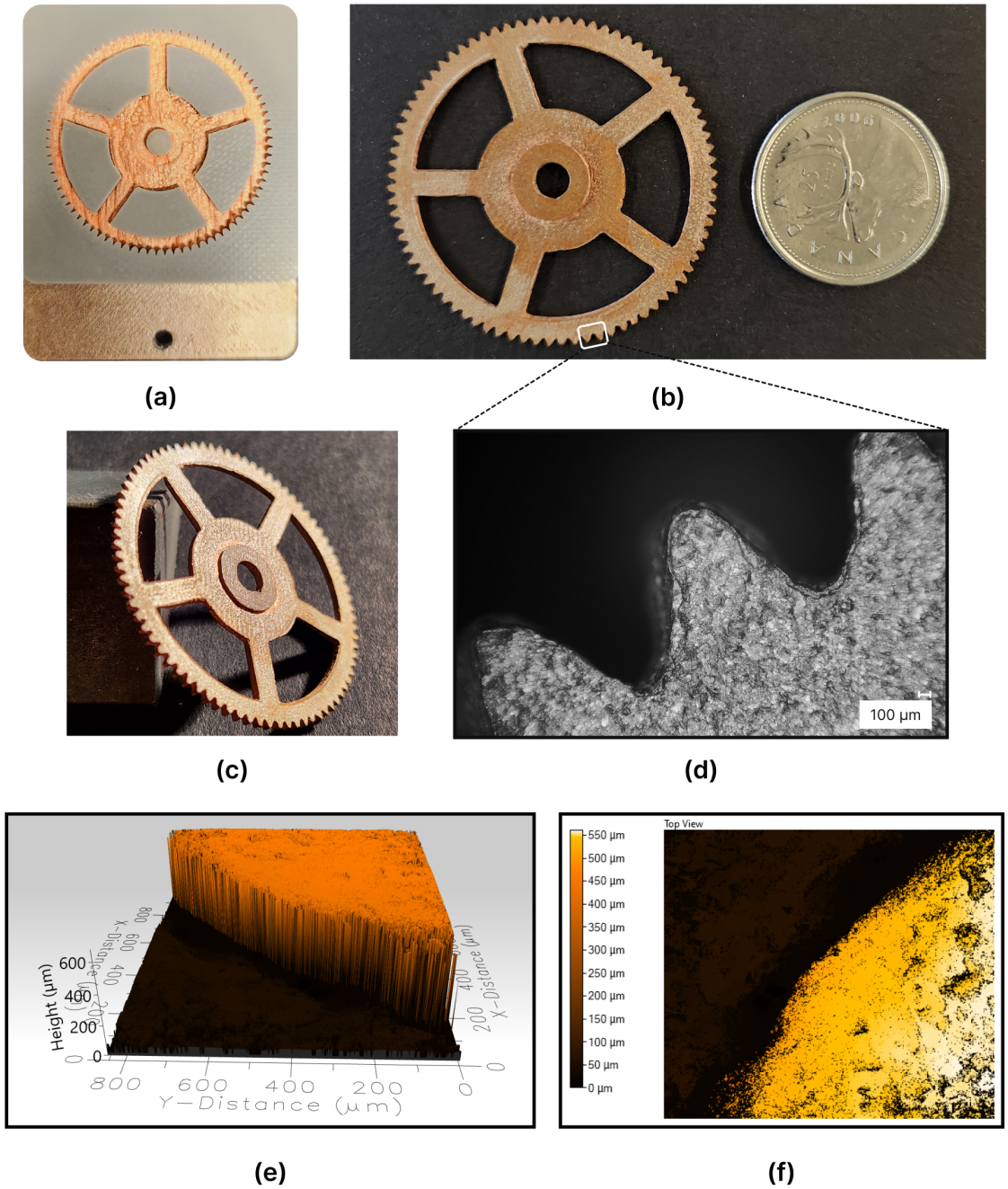

Figure 6.3: (a) The center wheel mold following the electroforming process. (b) The produced 2.5D center wheel. (c) An angled photograph showcasing the center wheel. (d) A microscopic image of the center wheel's teeth under a microscope. (e),(f) An optical scan depicting the center wheel's hub.

from electroforming.

Moreover, the electroforming setup employed at Concordia University is in a pre-

liminary state and would benefit from various enhancements. These improvements include the integration of a filtration system, optimizing electrolyte circulation, and implementing a covering system to minimize the presence of debris and contaminants in the electrolyte. Despite these surface imperfections, the process successfully achieved the fabrication of a structure with an approximate thickness of 1.6 mm. This is a notable accomplishment, given the inherent challenges in electroforming a structure of this thickness.

These findings confirm the importance of surface post-treatments for achieving a controlled, consistent, and repeatable surface morphology in electroformed structures. Given the sensitivity of most mechanical failures to surface properties, it is anticipated that enhancing the performance and functionality of electroformed components can be significantly enhanced by manipulating surface topographical characteristics. Consequently, the adoption of surface post-processing technologies becomes vital in elevating the functionality and longevity of electroformed structures. As a result, mechanical surface treatments such as grinding and polishing have been integrated into this manufacturing process to eliminate surface irregularities on the uppermost surface.

The grinding process was initialized by employing 220 grit sandpaper to remove the material until the surface irregularities were removed and the desired intersection was revealed. Following this, the sample underwent successive polishing stages with 600, 800, and 1200 grit sandpapers to achieve a smoother surface finish. Once the polishing process was completed, both the mold and the electroformed part were immersed in acetone to facilitate the separation of the center wheel from the mold. This separation process lasted approximately 2 hours for the mold to be entirely dissolved in the acetone.

Bottom Surface Characterization

The center wheel underwent an additional cleaning step with acetone to elimi-

nate any remaining paint particles. The bottom surface of the electroformed center wheel is depicted in figure 6.3(b). As anticipated, the electroforming process precisely replicates the surface quality of the mold, resulting in a bottom surface devoid of irregularities. Nevertheless, some minor defects persist in the part, primarily stemming from the printing lines and dots present in the FDM printed mold components, which are mirrored by the electroforming process.

The photo of the center wheel captured at an angle, depicted in figure 6.3(c), shows that the the proposed electroforming technique in AM-manufactured molds effectively produced the center wheel with varying thicknesses throughout its depth, thus achieving the intended 2.5D structure. The extended hub of the center wheel was electroformed initially, followed by the gear body conforming to the molds contours to create the final center wheel shape.

Figure 6.3(d) offers a detailed view of the center wheel teeth, examined through a digital microscope (VHX-1000, Keyence). The teeth of the center wheel closely mirror the shape of the ABS mold. Under microscopic inspection, disparities in dimensions between the designed and fabricated geometry emerge. Furthermore, variations in the quality of fabrication are observable among different teeth. This anticipated variance can be traced back to the dimensional accuracy and the inherent geometrical limitations of the FDM printer employed in this study.

Moreover, a section of the center wheel hub was subjected to scanning using a 3D optical profilometer, Profilm 3D®, which uses white light interferometry to measure surface profiles and roughness down to 0.05 µm. The optical scanner provided visual illustration of the bottom surface of the electroformed structure. The scanned area is presented in figure 6.3(e). This scan reveals the copper growth within the two layers of the center wheel. Additionally, it highlights that the extended hub has a thickness of approximately 560 μm, deviating by around 40 μm from the designed thickness.

To better evaluate the manufacturing technique, surface roughness measurements were conducted on the bottom surface of the center wheel, to evaluate the quality of

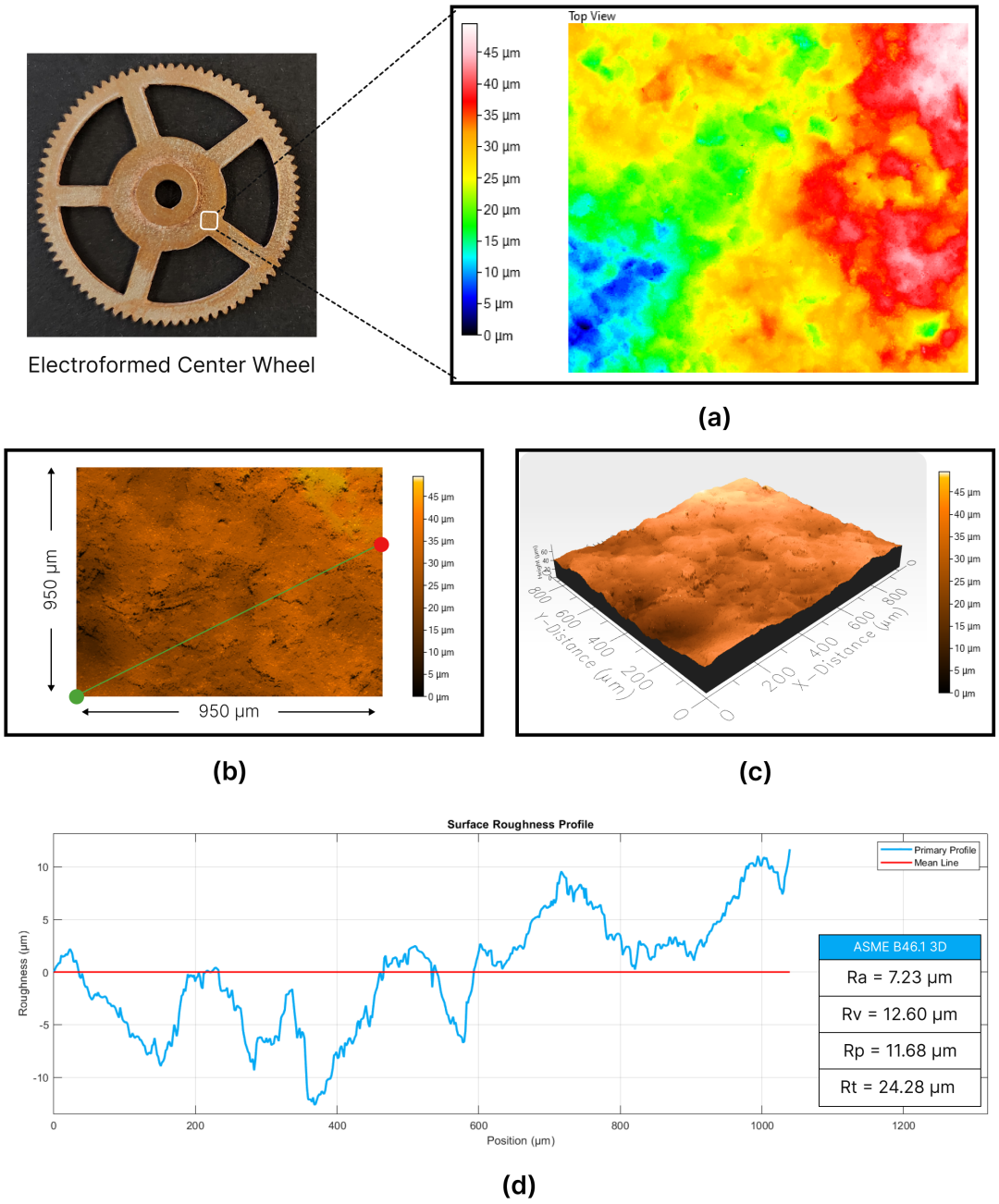

Figure 6.4: Surface topography of the fabricated center wheel. (a) Contour map, (b) and (c) representations of top and isometric surface profiles, and (d) roughness profiles.

the as-deposited copper in the AM mold. The surface topography and roughness measurements were conducted on the same optical scanner, Profilm 3D®. The scanned area is highlighted on the gear photo depicted in figure 6.4. The scanned area is a

square of approximately 950 µm side length.

The contour maps serve as a tool in providing a visual representation of the characteristics on the bottom surface (as-deposited surface) of the center wheel. As depicted in figure 6.4(a), this contour map effectively illustrates elevation differences across the surface. Dark blue regions indicate lower elevations, whereas lighter red areas signify higher elevations. The elevation difference spans approximately 45 µm, indicating variations in surface height. Notably, a substantial portion of the measured area falls within the range of blue, yellow, and green colors, signifying elevations between 15 µm and 40 µm. This range predominantly represents the waviness of the surface, accounting for roughly 25 µm.

To further validate these observations, the top and isometric surface topography representations, presented in figure 6.4(b) and (c), offer an intricate glimpse into the surface characteristics. These visual representations provide additional insights into the surface overall quality and uniformity, reinforcing the observations derived from the contour map analysis. The roughness profile, shown in figure 6.4(d), provides a comprehensive overview of the surface variations along a defined path of 1050 µm. The path is depicted in the top surface topography figure, starting at the red dot and ending at the green dot.

From the roughness profile analysis, several critical roughness parameters are derived in accordance with the ASME B46.1 3D standard. The mean arithmetic roughness, denoted as R_a, is calculated to be 7.23 µm. This parameter offers a measure of the average roughness across the surface. Two other essential parameters include the profile valley depth (R_v), which is measured at 12.60 µm, and the profile peak height (R_p), which is found to be 11.68 µm. These values indicate the depths of the valleys and the heights of the peaks in the surface profile. Additionally, the maximum peak to valley height (R_t) is obtained by summing R_v and R_p, resulting in a value of 24.28 µm. R_t signifies the maximum height difference between the peaks and valleys on the

surface, providing a comprehensive view of the surface irregularities.

Summary

In summary, electroforming of the center wheel, characterized by its 2.5D structure, achieved overall success. Notably, the top surface exhibited defects and surface irregularities, highlighting the necessity of mechanical surface treatment to attain high-quality components. On the other hand, the as-deposited bottom surface displayed acceptable surface roughness, with minor waviness, making it comparable to traditional machining processes. It is worth noting that the FDM printed mold components showed issues related to dimensional and geometrical accuracy. Utilizing higher-quality printing procedures promises significant improvements in the results obtained. These findings emphasize the potential for enhancing the electroforming process for such complex structures.

6.3 Toroidal Propeller Design

In 2017, MIT Lincoln Laboratory re-introduced a concept for propellers configuration called Toroidal Propeller [78]. Distinguished by its unique ring-shaped design, toroidal propellers offer a host of advantages that extend beyond traditional propeller systems. Notably, these propellers excel in producing significantly reduced noise levels, a feature especially prominent within the audible frequency range, spanning from 20 Hz to 20 kHz. Additionally, these propellers assert improved efficiency in both airborne and underwater settings. The intricate shape of toroidal propellers has historically posed significant manufacturing challenges, resulting in very high production costs.

The second application selected for this study involves the fabrication of a toroidal propeller. This choice serves to investigate the process capacity for additively manufacturing metal components with intricate 3D structures. The toroidal propeller features a complex 3D design characterized by three closed loops and a central hub.

The design of the toroidal blade presents significant challenges. Nevertheless, the insights acquired from experimenting and simulating various shapes can be effectively applied to manufacture the toroidal propeller through the electroforming process. This attempt showcases how altering mold surface angles and inducing curves can be potentially used to fabricate intricate 3D structures by electroforming.

The original toroidal propeller design exhibits intricate curvature patterns along its closed loops, with each of these loops serving as a blade for the propeller. Various designs have been proposed for the toroidal blade, ranging from two-blade configurations to those with up to four blades. Across all these designs, they share the common feature of curved enclosed blades. This specific closed-form structure serves to minimize the adverse effects of swirling air currents created at the blade tips and enhances the overall rigidity of the propeller. However, it is essential to note that the design proposed for the present investigation deviates slightly from its original design.

Applying the insights obtained from the design considerations and simulating copper growth, as demonstrated in chapters 4 and 5 respectively, is necessary to electroform a complex 3D structure. Electroforming these intricate blades with steep angles presents challenges that can result in surface irregularities, disconnections in the deposit, and deviations from the intended structural shape. Hence, alterations to the original toroidal propeller design have been made to facilitate its growth within the mold during electroforming. Specifically, the curved blades have been modified to feature less steep angles while maintaining the propeller's functionality.

The CAD model representing the proposed toroidal blade design is illustrated in figure 6.5(b). This specific toroidal blade configuration encompasses three closed loops, each of which functions as an individual blade for the propeller. Additionally, the propeller includes a hub, designed for assembly onto a shaft. The target thickness for the toroidal blade is 1.5 mm. The enclosed 3D blades exhibit varying angles along their dimensions, spanning from 80° to 120°, and differ in width at various

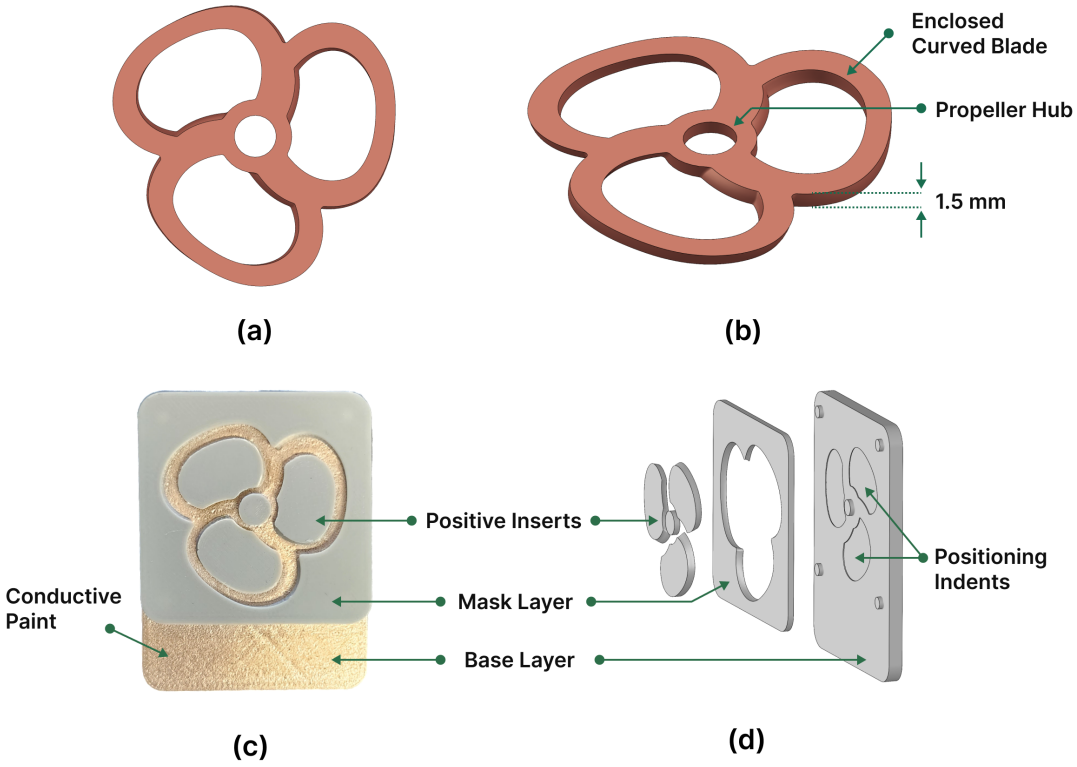

Figure 6.5: (a) and (b) CAD models illustrating the proposed design of the toroidal propeller. (c) A photograph displaying the assembled mold, and (d) a CAD model revealing an exploded view of the mold components.

cross-sections across the blade.

The toroidal blade mold adheres to the mold design previously explained in the methodology section. The mold CAD model and its components are depicted in Figure 6.5(d). Given the uniform thickness of the toroidal propeller design across its cross-section, only a single mask layer is necessary, in addition to the base layer. To accommodate the cut-outs in the closed-loop blades, three positive inserts are designed, along with a cylindrical positive insert to encounter the propeller hub hole. The intricate, multi-angle sections of the blades are seamlessly integrated into the positive inserts and the mask layer, capitalizing on FDM ability to handle such complex profiles. Moreover, the base layer features three 0.1 mm deep positioning indents

to facilitate the assembly of the positive inserts.

Introducing Chemical Vapor Smoothing (CVS)

The mold fabrication process followed the previously outlined experimental technique 3.2, with additional step. In this case, vapor smoothing of the mold components was introduced before applying conductive paint and proceeding with assembly. Vapor smoothing, also recognized as Chemical Vapor Smoothing (CVS), entails subjecting printed parts to vaporized solvent. Recent literature has documented several studies employing chemical solvents, such as acetone, to enhance the surface quality of FDM-printed ABS parts [79, 80]. This process not only minimizes the stair-case effect but also replaces it with a smoother, glossier finish, thereby significantly improving the mold's surface characteristics.

Given the electroforming process sensitivity to mold surface quality, incorporating CVS is notably advantageous. However, it is crucial to note that CVS can potentially impact dimensional accuracy and intricacy in printed parts. Therefore, selecting optimal conditions for CVS becomes essential to mitigate these effects. Singh et al. [79] investigated the impact of CVS on the dimensional accuracy of ABS printed parts and reported critical findings. To minimize these effects, they recommended pre and post cooling of parts at 0°C, maintaining the smoothing temperature at 50°C, and utilizing cycles lasting less than 30 seconds. Following these insights, the mold components were subjected to CVS for 15 seconds during two consecutive cycles, employing pre and post cooling to ensure minimal impact on the dimensions of the parts.

Figure 6.6 provides a comparison between the base layer of the toroidal propeller mold before and after vapor smoothing. In figure 6.6(a), the ABS printed base layer exhibits noticeable printing lines, resulting in a rough surface characterized by peaks and valleys along each line. Microscopic examination reveals gaps between the printing layers, which could detrimentally impact the quality of the electroformed part

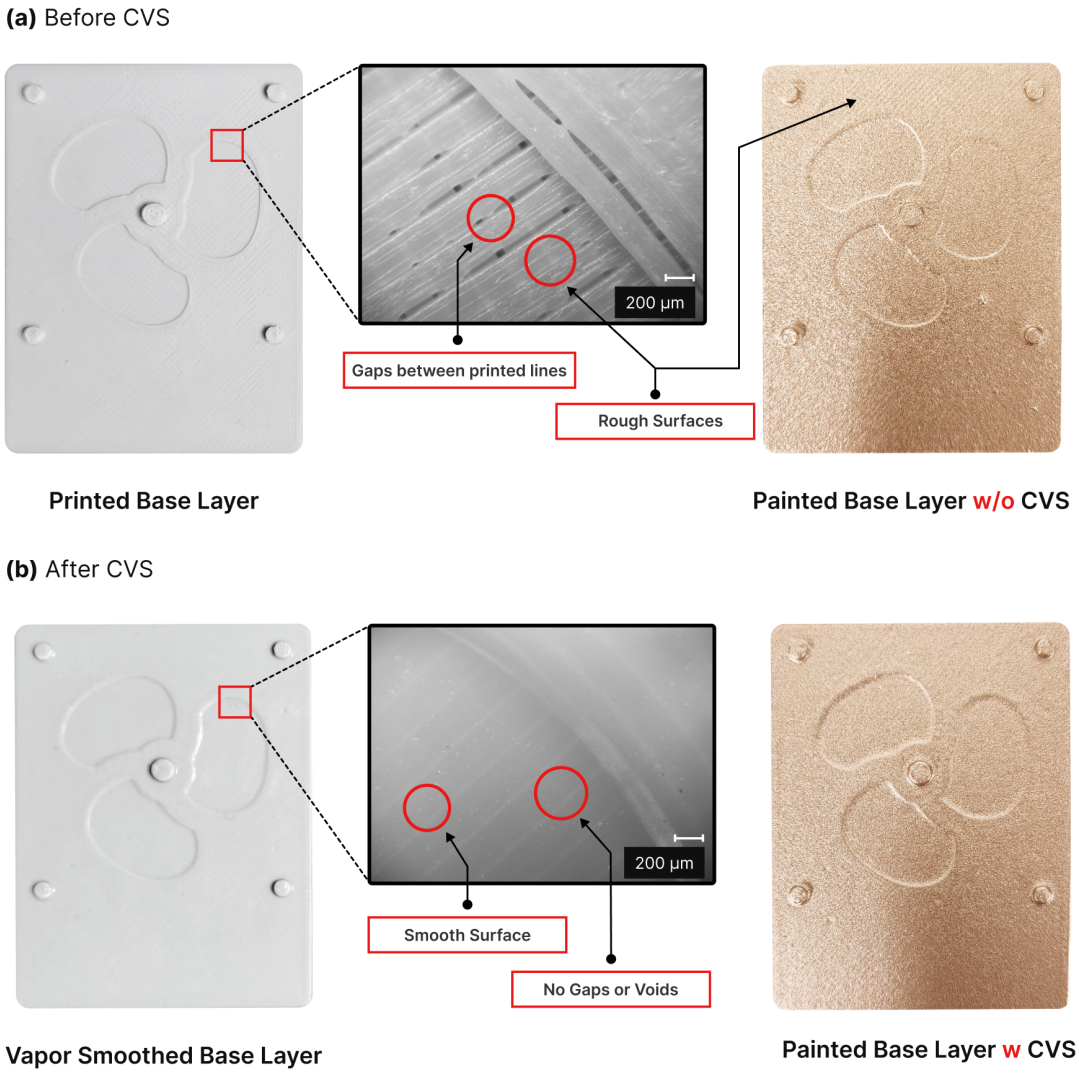

Figure 6.6: Images showing the mold base layer of the toroidal propeller: (a) prior to vapor smoothing, and (b) after vapor smoothing.

within the mold. After the application of conductive paint, the printing lines remain visible in the painted base layer. While the paint might help fill some of the gaps and reduce surface roughness, the overall texture remains relatively rough, still showing signs of the printing lines. In figure 6.6(b), the base layer is presented after undergoing the CVS process. Notably, voids and gaps between the printing lines are no longer visible. The CVS process melted the printed layers, resulting in a significantly smoother surface. Visual inspection reveals that the vapor-smoothed base layer ex-

hibits an overall improved surface finish, devoid of any traces of the original printing lines.

Furthermore, the impact of CVS on the mold dimensions proved to be exceedingly minimal. The assembly of the mold is a precise, snug-fit process utilizing locator pins. During the assembly of the mold components after vapor smoothing, everything proceeded seamlessly, with the components fitting together just as they did before CVS was applied. However, one drawback of the CVS process is its tendency to cause warping in vapor-smoothed components, particularly thin ones. To avoid this warping, the base layer thickness was increased from 1.5 mm to 3.5 mm. This adjustment did not introduce any alterations to the mold design, as the base layer, where the deposit forms to shape the toroidal propeller, does not influence the object dimensions.

6.4 Toroidal Propeller Electroforming Results

After preparing the toroidal propeller mold for electroforming, as depicted in figure 6.5(c), the mold underwent the electroforming process. The aimed deposition thickness was 1500 μm, aligning with the toroidal propeller design specifications. To reach this desired thickness 30,000 deposition cycles were established. The electroforming process spanned around 4.6 days, totaling 110 hours, until the mold had successfully completed the designated cycles, with copper fully filling the mold. After the electroforming process, the electroformed mold underwent a thorough cleaning with de-ionized water and subsequent air drying. To minimize surface irregularities, the same polishing procedure was applied as described in section 6.2, until the intersection between the mold and the deposited material was distinctly revealed.

Figure 6.7(a) illustrates the mold after the electroforming process. Most of the mold surface was adequately covered with copper deposition, with certain areas exceeding the required thickness. However, some voids were visible around the toroidal propeller hub. These voids and surface irregularities were minimized through the

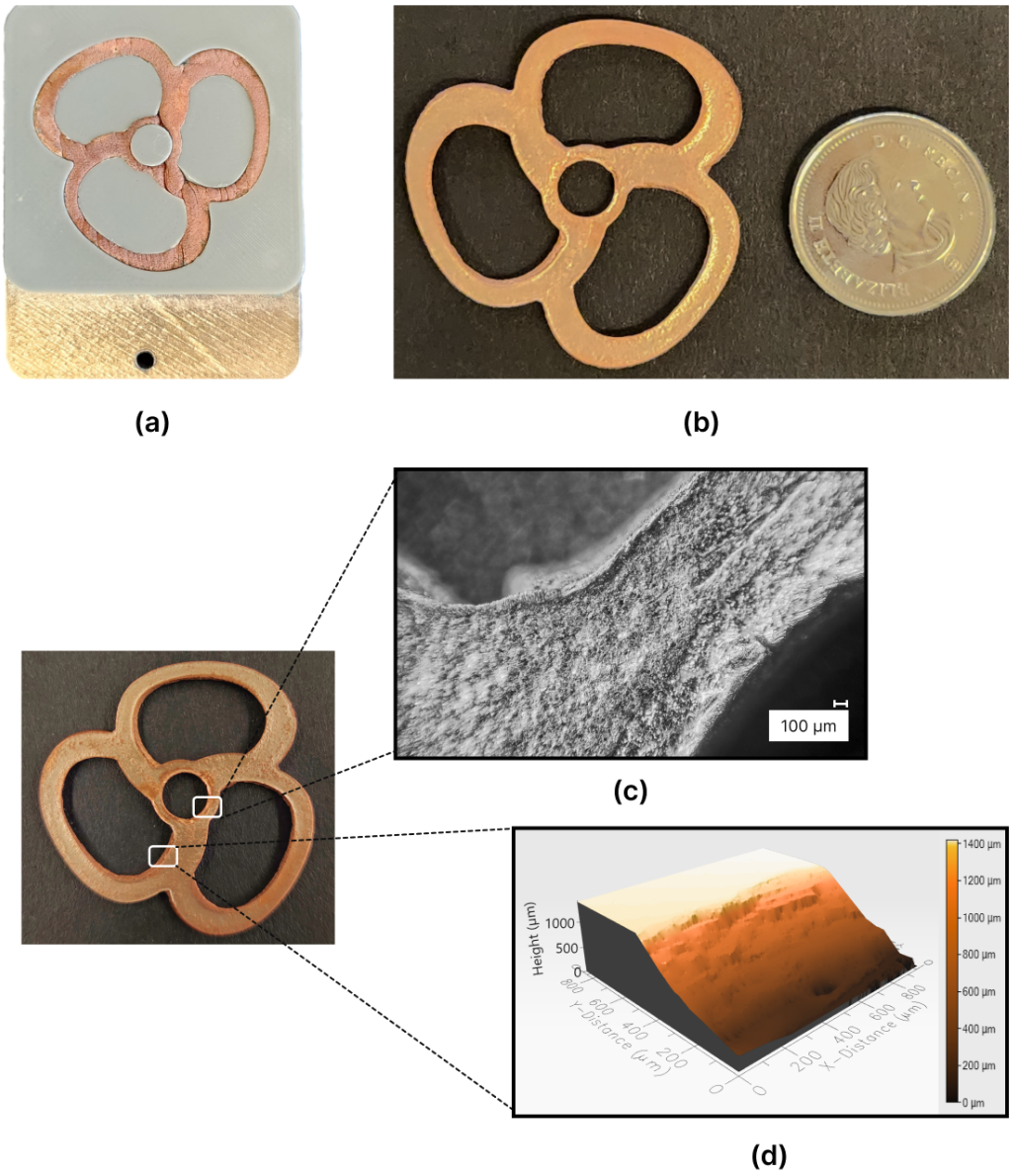

Figure 6.7: Images illustrating the results of electroforming the toroidal propeller: (a) the Toroidal Propeller mold after electroforming, (b) a photo of the fabricated toroidal propeller, (c) microscopic images of the toroidal propeller, and (d) a profile scan of a toroidal propeller blade.

post-electroforming polishing procedure applied to the mold. Subsequently, a similar immersion process in acetone as the one used for the center wheel mold was performed, but this time with the addition of heat and stirring using a magnetic stirrer. Notably, the part separation time was significantly reduced to just 45 minutes, in

contrast to the approximately 2 hours required for separating the center wheel from its mold.

The electroformed toroidal propeller is presented in Figure 6.7(b). The electroforming process effectively replicated the intricate 3D structure with high precision, and the copper deposition in the intricate areas of the blades was notably successful. In Figure 6.7(c), a closer look at the toroidal blade's propeller hub interface with the blade is shown, captured using a digital microscope (VHX-1000, Keyence). This microscopic examination reveals the electroforming process's ability to intricately trace the curvatures of the toroidal propeller design, achieving a high level of accuracy. Furthermore, a section of the toroidal blade was scanned using Profilm 3D®, to visually represent the curvatures and varying angles of the toroidal propeller blade. The optical image obtained is featured in figure 6.7(d).

Bottom Surface Characterization

The evaluation of surface topography for the toroidal propeller was imperative for the purpose of comparing the outcomes resulting from the application of CVS to the mold components, particularly the base layer where the bottom surface takes shape. This process involved the utilization of the same optical scanner, Profilm 3D®, for both surface topography assessment and roughness measurements. The area scanned on the bottom surface of the toroidal propeller is depicted in figure 6.8, representing a square with a side length of 950 μm.

The surface contour maps and topographical representations, as seen in figure 6.8(a),(b), and (c), provide insight into the surface waviness and deviations within the scanned region of the toroidal propeller. The elevation difference spans approximately 35 µm, indicating variations in surface height. Furthermore, a significant portion of the scanned region exhibits yellow and green colors, indicating elevations ranging from 15 μm to 30 μm. This color range predominantly represents the waviness of the surface, accounting for approximately 15 μm, which is a noticeable reduction when

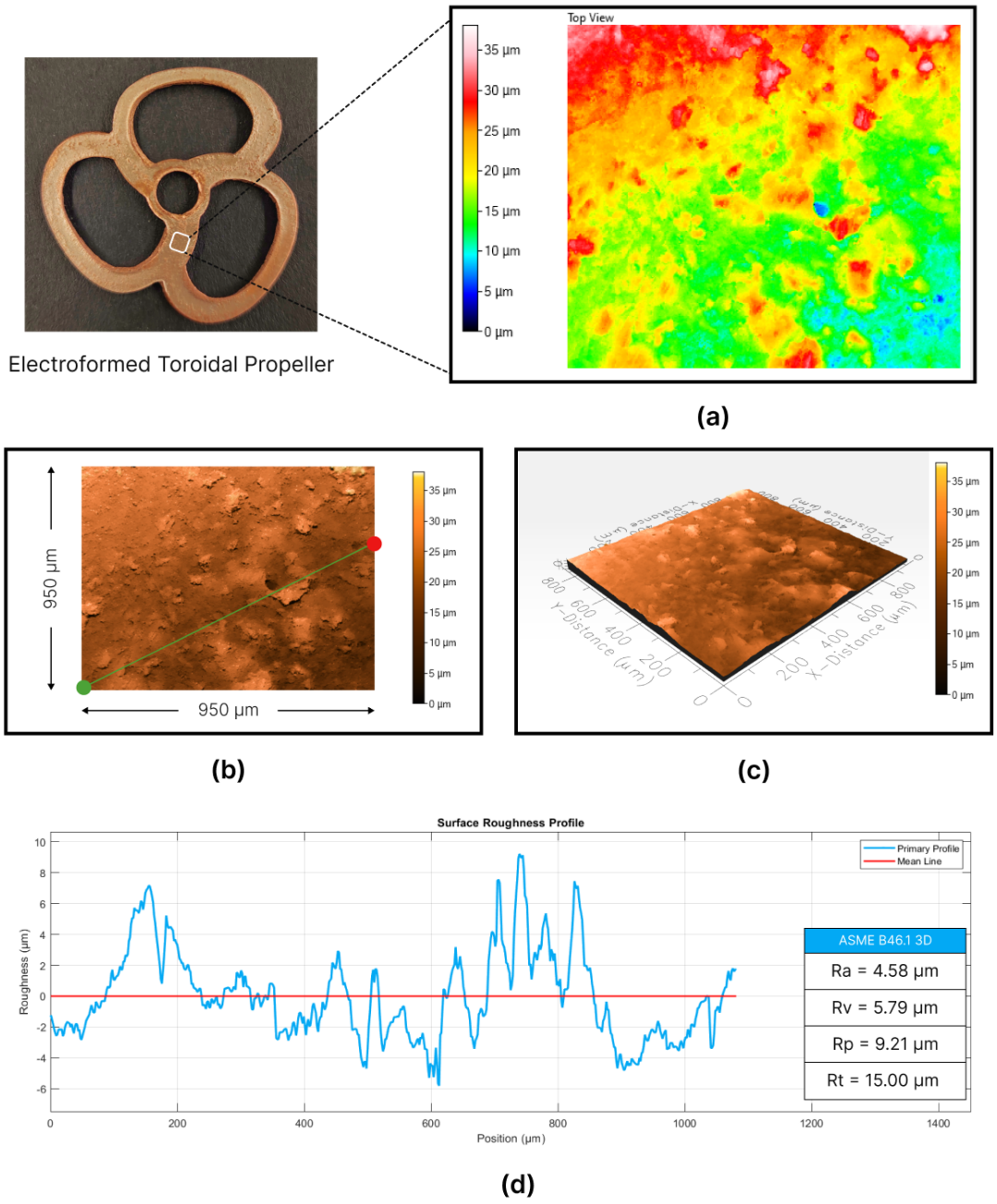

Figure 6.8: Surface topography of the manufactured toroidal propeller. (a) Contour map, (b) and (c) representations of top and isometric surface profiles, and (d) roughness profiles.

compared to the center wheel.

The roughness profile, as depicted in figure 6.8(d), offers a comprehensive representation of surface variations along a defined 1050 μm path. The path is delineated in

the top surface topography figure, commencing at the red dot and concluding at the green dot. The mean arithmetic roughness (R_a) is calculated to be 4.58 μm. Meanwhile, the profile valley depth (R_v) measures 5.80 μm, and the profile peak height (R_p) is determined to be 9.20 μm. Thus, the maximum peak to valley height (R_t) is calculated by summing R_v and R_p, resulting in a value of 15.00 μm.

CVS Enhancements

The results of the surface roughness assessment indicate a significant improvement due to CVS, enhancing the surface roughness by approximately 37%, from 7.23 μm to 4.58 μm. This level of roughness is competitive with what can typically be expected from CNC machining. Furthermore, visual and microscopic inspections reveal that the toroidal propeller is less affected by the printing lines and dots resulting from FDM printing of the mold components, as CVS effectively reduces these imperfections, resulting in smoother and more uniform printed surfaces.

Summary

In summary, the results presented in this chapter highlight the capability of electroforming to produce composite structures, combining both hollow and solid elements, in both 2.5D and 3D configurations. The use of multi-layer mold components, in conjunction with selective application of the conductive paint, has demonstrated that various 2.5D structures with multiple levels can be successfully electroformed in additive manufacturing molds. Furthermore, the introduction of altered angles and curvatures in the mold design has enabled the electroforming of intricate 3D structures. The application of Chemical Vapor Smoothing (CVS) has proven effective in melting mold layers and creating smoother surfaces for the mold components, thereby enhancing the overall quality of the electroformed parts within the mold.

Electroforming in additive manufacturing molds offers a cost-effective method for producing metal parts with diverse geometric shapes, at a lower cost and better qual-

ity compared to traditional additive manufacturing techniques. It is notably more economical than metal AM techniques, both in terms of setup and production expenses. While electroforming may be time-consuming for individual parts, the ability to batch multiple molds concurrently allows for process parallelization, reducing both manufacturing time and costs. It is important to note that electroforming is no longer limited to producing thin-walled and hollow structures; it has demonstrated its capacity to additively manufacture solid, hollow, and composite structures on both micro and macro scales, with relatively limited thicknesses.

The process requires further refinement to improve the surface quality of manufactured parts, eliminating the necessity for mechanical surface treatments. Additionally, there is a need to enhance the process for reduced fabrication times, thereby unlocking the potential for greater thicknesses. Moreover, exploring additional design considerations is necessary to address the geometric limitations of the process. This will enable the fabrication of more intricate and complex structures. Finally, electroforming of structural materials, including titanium, stainless steel, steel, and iron, deserves attention. As this exploration will significantly broaden the range of applications for this manufacturing process.

Chapter 7

Summary and Future Outlook

The aim of this research was to establish design procedures for molds, used for electroforming mainly 2.5D and potentially 3D metal parts. The designed molds are fabricated utilizing additive manufacturing. This was done to enable electroforming of personalized miniature composite metal parts in different shapes and configurations. This investigation involved a modular mold design, experimental mold assembly procedures, electroforming tests encompassing various geometries and thicknesses exceeding 1000 μm, and the development of a simulation model for visualizing the deposition process. The critical findings and the significance of this research are summarized as follows:

- **Modular Mold Design**: The mold design introduced modularity, accommodating electroforming for a wide array of geometries, including 2D, 2.5D, and 3D solid and composite structures. The molds, fabricated economically via FDM printing with ABS filaments, feature sacrificial properties, simplifying part separation post-electroforming.

- **Experimental Approach for Mold Development and Electroforming**: This comprehensive procedure guided the entire process, spanning mold fabrication, conductive coating application, component assembly, electroforming, and mechanical surface treatments applied to the electroformed parts.

- **Design Considerations and Guidelines for Electroforming**: Successful

electroforming of structures exceeding 1000 μm thickness led to essential guidelines. Notably, straight walls exhibited the most uniform top surfaces, while structures within the range of 30° to 110° angles displayed satisfactory thickness uniformity. Multi-step structures revealed mushroom-like formations, and filleted corners facilitated smoother material deposition.

- **Simulation Model Development**: A validated simulation model was developed, which provided valuable insights into electroforming in the developed molds. It clarified the impact of conductive paint location on the electroformed structure and facilitated the production of 2.5D and 3D structures with uniform top surfaces. The model also offers time-saving advantages compared to experimental electroforming.

- **Applications of the Proposed Method**: Composite structures with both configurations of 2.5D and 3D were manufactured successfully using electroforming in the developed molds. Applications include a center wheel and a toroidal propeller. The resulting structures have an average thickness of 1500 μm which is challenging to produce using electroforming. Parts exhibited high quality with minimal waviness on the bottom surface (R_a= 7.23 μm) and a mechanically treated top surface. The introduction of Chemical Vapor Smoothing to the mold components melted the printing lines and dots, and further reduced the roughness by 37%, thus elevating overall part quality.

In conclusion, electroforming in additively manufactured molds provides a cost-effective method for manufacturing metal parts with diverse geometric shapes. This method is more cost-efficient and offers higher quality parts, specifically limited thickness ones, compared to traditional metal additive manufacturing techniques. Electroforming stands out as an economical alternative, including setup and production expenses. The potential for parallelization makes it efficient, especially for batch processing.

In existing literature, the application of electroforming has been primarily associated with the fabrication of thin-walled hollow structures, 2D components, and applications at the nanoscale. However, this study has successfully demonstrated the adaptability of electroforming to produce solid and composite structures, both in 2.5D and 3D configurations, spanning micro and macro scales. Notably, the applications explored in this research feature thicknesses exceeding 1000 μm, a formidable challenge for electroforming due to its inherent difficulty in achieving uniform surfaces at such thicknesses. Moreover, the methodologies employed in mold design, experimental application, and the simulation model not only overcome this challenge but also pave the way for the realization of true mass personalization across diverse applications. This signifies electroforming's potential to evolve into a dependable, robust, and versatile metal additive manufacturing technique.

Future Outlook

As this study concludes, it leads to the horizon of future work in the domain of electroforming as an additive manufacturing technique. It is highly promising to explore advanced FDM printing technologies that combine ABS and conductive filaments. Multi-head FDM printers capable of simultaneously extruding mold components in ABS and conductive filament layers promise increased flexibility and precision during mold fabrication. To realize this potential, careful selection of a highly conductive filament is essential to enable the electroforming. This approach not only enhances mold quality but also enables the development of intricate and complex metal parts.

Furthermore, integrating advanced AM technologies, such as digital light processing (DLP), can dramatically enhance precision and dimensional accuracy, outperforming FDM by a factor of five. This technology paves the way for creating precise, complex structures, especially micro parts, expanding the boundaries of mold fabrication and electroforming.

Efficiency of the electroforming process can be greatly enhanced by refining the

existing setup. Implementing a filtration system, optimizing electrolyte circulation, and minimizing contaminants in the electrolyte through a covering system hold the potential to enhance process predictability, efficiency, and the delivery of high-quality results.

Additionally, the scope of electroforming can be broadened by exploring alternative conductive materials such as titanium, graphite, steel, and various alloys. These materials can meet the requirements of applications demanding durability, strength, and rigidity, thus widening the range of compatible materials for electroforming. Furthermore, delving into the mechanical characteristics of electroformed parts offers insights into their structural integrity and mechanical behavior. Such investigations can greatly influence the design, application, and overall performance of electroformed components.

Bibliography

[1] G. Xiong *et al.*, "From mind to products: Towards social manufacturing and service," *IEEE/CAA Journal of Automatica Sinica*, vol. 5, no. 1, pp. 47–57, 2017.

[2] M. Ozdemir, "Design for mass personalization in digital manufacturing context," 2022.

[3] L. Chong, S. Ramakrishna, and S. Singh, "A review of digital manufacturing-based hybrid additive manufacturing processes," *The International Journal of Advanced Manufacturing Technology*, vol. 95, pp. 2281–2300, 2018.

[4] R. Matsuzaki, T. Kanatani, and A. Todoroki, "Multi-material additive manufacturing of polymers and metals using fused filament fabrication and electroforming," *Additive Manufacturing*, vol. 29, p. 100 812, 2019.

[5] K. Angel, H. H. Tsang, S. S. Bedair, G. L. Smith, and N. Lazarus, "Selective electroplating of 3d printed parts," *Additive Manufacturing*, vol. 20, pp. 164–172, 2018.

[6] S. M. Aghili, Z. Zheng, and R. Wüthrich, "Fabrication of low-cost molds for manufacturing of high precise micro parts by electroforming," *ECS Transactions*, vol. 97, no. 7, p. 515, 2020.

[7] P Hernández *et al.*, "Electroforming applied to manufacturing of microcomponents," *Procedia engineering*, vol. 132, pp. 655–662, 2015.

[8] S. Roy and E. Andreou, "Electroforming in the industry 4.0 era," *Current Opinion in Electrochemistry*, vol. 20, pp. 108–115, 2020.

[9] X. Zhan, Q. D. Cao, K. Trieu, and X. Zhang, "Microstructure and mechanical properties of copper microtubes fabricated via the electroforming process," *Journal of Materials Engineering and Performance*, vol. 29, pp. 1741–1750, 2020.

[10] A. Ramesh, Z. Qin, and Y. Lu, "Digital thread enabled manufacturing automation towards mass personalization," in *International Manufacturing Science and Engineering Conference*, American Society of Mechanical Engineers, vol. 84263, 2020, V002T07A008.

[11] S. Ahmad, R. G. Schroeder, and D. N. Mallick, "The relationship among modularity, functional coordination, and mass customization: Implications for competitiveness," *European Journal of Innovation Management*, vol. 13, no. 1, pp. 46–61, 2010.

[12] R. Volti, *An introduction to the sociology of work and occupations*. Sage Publications, 2011.

[13] R. K. Sikhwal and P. R. Childs, "Towards mass individualisation: Setting the scope and industrial implication," *Design Science*, vol. 7, e16, 2021.

[14] R. Ogunsakin, *Towards a Highly Flexible Manufacturing System for Mass Personalisation: Exploring Nature-Inspired Models*. The University of Manchester (United Kingdom), 2020.

[15] S. J. Hu, "Evolving paradigms of manufacturing: From mass production to mass customization and personalization," *Procedia Cirp*, vol. 7, pp. 3–8, 2013.

[16] T. S. Harzer, "Value creation through mass customization: An empirical analysis of the requisite strategic capabilities," Ph.D. dissertation, Aachen, Techn. Hochsch., Diss., 2013, 2013.

[17] H. Zhao, L. McLoughlin, V. Adzhiev, and A. Pasko, "" why do we not buy mass customised products?"-an investigation of consumer purchase intention of mass customised products," *International Journal of Industrial Engineering and Management*, vol. 10, no. 2, pp. 181–190, 2019.

[18] P. K. Paritala, S. Manchikatla, and P. K. Yarlagadda, "Digital manufacturing-applications past, current, and future trends," *Procedia engineering*, vol. 174, pp. 982–991, 2017.

[19] Y. Lu, X. Xu, and L. Wang, "Smart manufacturing process and system automation–a critical review of the standards and envisioned scenarios," *Journal of Manufacturing Systems*, vol. 56, pp. 312–325, 2020.

[20] Y. Wang, H.-S. Ma, J.-H. Yang, and K.-S. Wang, "Industry 4.0: A way from mass customization to mass personalization production," *Advances in manufacturing*, vol. 5, pp. 311–320, 2017.

[21] F. Zhou, Y. Ji, and R. J. Jiao, "Affective and cognitive design for mass personalization: Status and prospect," *Journal of Intelligent Manufacturing*, vol. 24, pp. 1047–1069, 2013.

[22] R. Ogunsakin, C. A. Marin, and N. Mehandjiev, "Towards engineering manufacturing systems for mass personalisation: A stigmergic approach," *International Journal of Computer Integrated Manufacturing*, vol. 34, no. 4, pp. 341–369, 2021.

[23] Y. Koren, M. Shpitalni, P. Gu, and S. Hu, "Product design for mass-individualization," *Procedia Cirp*, vol. 36, pp. 64–71, 2015.

[24] L. R. Novais, J. M. Maqueira, and S. Bruque, "Supply chain flexibility and mass personalization: A systematic literature review," *Journal of Business & Industrial Marketing*, vol. 34, no. 8, pp. 1791–1812, 2019.

[25] J. Morgan, M. Halton, Y. Qiao, and J. G. Breslin, "Industry 4.0 smart reconfigurable manufacturing machines," *Journal of Manufacturing Systems*, vol. 59, pp. 481–506, 2021.

[26] S. Aghili, Z. Zheng, and R. Wüthrich, "Low-cost manufacturing of high-precision personalized flexures by a hybrid 3d printing-electroforming technique," *The International Journal of Advanced Manufacturing Technology*, pp. 1–14, 2023.

[27] C. R. Boër and S. Dulio, "Footwear mass customization in practice," *Mass Customization and Footwear: Myth, Salvation or Reality? A Comprehensive Analysis of the Adoption of the Mass Customization Paradigm in Footwear, from the Perspective of the EUROShoE (Extended User Oriented Shoe Enterprise) Research Project*, pp. 89–151, 2007.

[28] S. I. Abdul Kudus, "The value of personalised consumer product design facilitated through additive manufacturing technology," Ph.D. dissertation, Loughborough University, 2017.

[29] L. Deloitte, *The deloitte consumer review made-to-order: The rise of mass personalization*, 2015.

[30] S. Chen and M. M. Tseng, "Aligning demand and supply flexibility in custom product co-design," *International Journal of Flexible Manufacturing Systems*, vol. 19, pp. 596–611, 2007.

[31] A. Albers, N. Bursac, H. Scherer, C. Birk, J. Powelske, and S. Muschik, "Model-based systems engineering in modular design," *Design Science*, vol. 5, e17, 2019.

[32] M. A. Cusumano, "Shifting economies: From craft production to flexible systems and software factories," *Research policy*, vol. 21, no. 5, pp. 453–480, 1992.

[33] T. Blecker and G. Friedrich, *Mass customization: challenges and solutions*. Springer Science & Business Media, 2006, vol. 87.

[34] S. Aheleroff, R. Philip, R. Y. Zhong, and X. Xu, "The degree of mass personalisation under industry 4.0," *Procedia CIRP*, vol. 81, pp. 1394–1399, 2019.

[35] H. E. Quinlan, T. Hasan, J. Jaddou, and A. J. Hart, *Industrial and consumer uses of additive manufacturing: A discussion of capabilities, trajectories, and challenges*, 2017.

[36] H. Watschke, A.-K. Bavendiek, A. Giannakos, T. Vietor, *et al.*, "A methodical approach to support ideation for additive manufacturing in design education," in *DS 87-5 Proceedings of the 21st International Conference on Engineering Design (ICED 17) Vol 5: Design for X, Design to X, Vancouver, Canada, 21-25.08. 2017*, 2017, pp. 041–050.

[37] G. Shang and C. Sun, "Effect of 3d printing technology on 3c product manufacturing," *World Journal of Engineering and Technology*, vol. 8, no. 4, pp. 712–719, 2020.

[38] K. V. Wong and A. Hernandez, "A review of additive manufacturing," *International scholarly research notices*, vol. 2012, 2012.

[39] I. Gibson *et al.*, *Additive manufacturing technologies*. Springer, 2021, vol. 17.

[40] I. Gibson and M. Savalani, "Rapid manufacture and garpa," *Rapid Prototyping Journal*, vol. 12, no. 3, 2006.

[41] A. Vafadar, F. Guzzomi, A. Rassau, and K. Hayward, "Advances in metal additive manufacturing: A review of common processes, industrial applications, and current challenges," *Applied Sciences*, vol. 11, no. 3, p. 1213, 2021.

[42] E. Bogdan and P. Michorczyk, "3d printing in heterogeneous catalysis—the state of the art," *Materials*, vol. 13, no. 20, p. 4534, 2020.

[43] D. Pham and S. S. Dimov, *Rapid manufacturing: the technologies and applications of rapid prototyping and rapid tooling*. Springer Science & Business Media, 2012.

[44] A. Majeed, A. Ahmed, J. Lv, T. Peng, and M. Muzamil, "A state-of-the-art review on energy consumption and quality characteristics in metal additive manufacturing processes," *Journal of the Brazilian Society of Mechanical Sciences and Engineering*, vol. 42, pp. 1–25, 2020.

[45] A. Boschetto, V. Giordano, and F. Veniali, "Surface roughness prediction in fused deposition modelling by neural networks," *The International Journal of Advanced Manufacturing Technology*, vol. 67, pp. 2727–2742, 2013.

[46] P. K. Gurrala and S. P. Regalla, "Part strength evolution with bonding between filaments in fused deposition modelling," *Virtual and Physical Prototyping*, vol. 9, no. 3, pp. 141–149, 2014.

[47] H. Platform, *What is fdm (fused deposition modeling) 3d printing?* [Online]. Available: https://www.hubs.com/knowledge-base/what-is-fdm-3d-printing/.

[48] A. Garg, A. Bhattacharya, and A. Batish, "On surface finish and dimensional accuracy of fdm parts after cold vapor treatment," *Materials and Manufacturing Processes*, vol. 31, no. 4, pp. 522–529, 2016.

[49] M. Doshi, A. Mahale, S. K. Singh, and S. Deshmukh, "Printing parameters and materials affecting mechanical properties of fdm-3d printed parts: Perspective and prospects," *Materials Today: Proceedings*, vol. 50, pp. 2269–2275, 2022.

[50] S. Wickramasinghe, T. Do, and P. Tran, "Fdm-based 3d printing of polymer and associated composite: A review on mechanical properties, defects and treatments," *Polymers*, vol. 12, no. 7, p. 1529, 2020.

[51] M. J. Sole, "Electroforming: Methods, materials, and merchandise," *Jom*, vol. 46, pp. 29–35, 1994.

[52] R. Parkinson, *Electroforming: A Unique Metal Fabrication Process*. Nickel Development Institute Toronto, ON, Canada, 1998.

[53] C. Huang, H. Y. Li, M. J. Zhu, and M. M. Yu, "Present research situation and new trends of electroforming," *Applied Mechanics and Materials*, vol. 278, pp. 401–405, 2013.

[54] Y. Mo, C. Shen, and D. Zhu, "Study of copper electrodeposition at a very low temperature near the freezing point of electrolyte," *Micromachines*, vol. 13, no. 12, p. 2225, 2022.

[55] H. Li, K. Jiang, Y. Guo, and Y. Peng, "Research on bipolar pulse current electroforming in precision molds and dies," *Tsinghua Science and Technology*, vol. 14, no. S1, pp. 144–148, 2009.

[56] *Expert manufacturing of precision thin film amp; electroformed components*, 2023. [Online]. Available: http://www.metrigraphicsllc.com/.

[57] J. McGeough, M. Leu, K. Rajurkar, A. De Silva, and Q. Liu, "Electroforming process and application to micro/macro manufacturing," *CIRP Annals*, vol. 50, no. 2, pp. 499–514, 2001, ISSN: 0007-8506. DOI: https://doi.org/10.1016/S0007-8506(07)62990-4. [Online]. Available: https://www.sciencedirect.com/science/article/pii/S0007850607629904.

[58] H. Zhang, N. Zhang, M. Gilchrist, and F. Fang, "Advances in precision micro/nano-electroforming: A state-of-the-art review," *Journal of Micromechanics and Microengineering*, vol. 30, no. 10, p. 103 002, 2020.

[59] J. Hannavy, *Encyclopedia of nineteenth-century photography*. Routledge, 2013.

[60] K. C. Chan, N. Qu, and D. Zhu, "Quantitative texture analysis in pulse reverse current electroforming of nickel," *Surface and Coatings Technology*, vol. 99, no. 1-2, pp. 69–73, 1998.

[61] B.-y. Jiang, C. Weng, M.-y. Zhou, H. Lv, and D. Drummer, "Improvement of thickness deposition uniformity in nickel electroforming for micro mold inserts," *Journal of Central South University*, vol. 23, no. 10, pp. 2536–2541, 2016.

[62] M.-C. Chou, H Yang, and S.-H. Yeh, "Microcomposite electroforming for liga technology," *Microsystem technologies*, vol. 7, pp. 36–39, 2001.

[63] T.-H. Tsai, H Yang, and R Chein, "New electroforming technology pressure aid for liga process," *Microsystem technologies*, vol. 10, no. 5, pp. 351–356, 2004.

[64] L. Du *et al.*, "Study on improving thickness uniformity of microfluidic chip mold in the electroforming process," *Micromachines*, vol. 7, no. 1, p. 7, 2016.

[65] C.-W. Park and K.-Y. Park, "An effect of dummy cathode on thickness uniformity in electroforming process," *Results in Physics*, vol. 4, pp. 107–112, 2014.

[66] F Eisner, "Thickness distribution for gold and copper electroformed hohlraums," *Fusion technology*, vol. 35, no. 2, pp. 81–84, 1999.

[67] G. S. Phull, S. Kumar, and R. S. Walia, "Nickel deposition optimization on plastic substrate produced by additive manufacturing," *International Journal of Manufacturing Science and Engineering*, vol. 8, no. 2, pp. 119–125, 2017.

[68] B. Zharylkassyn, A. Perveen, and D. Talamona, "Effect of process parameters and materials on the dimensional accuracy of fdm parts," *Materials Today: Proceedings*, vol. 44, pp. 1307–1311, 2021.

[69] K. M. Agarwal, P. Shubham, D. Bhatia, P. Sharma, H. Vaid, and R. Vajpeyi, "Analyzing the impact of print parameters on dimensional variation of abs specimens printed using fused deposition modelling (fdm)," *Sensors International*, vol. 3, p. 100 149, 2022.

[70] G. S. Phull, S. Kumar, and R. S. Walia, "Electroforming defects during metal deposition on plastic substrate produced by additive manufacturing," *Int. J. Sci. Res. Sci. Technol*, vol. 2, no. 4, pp. 1179–1188, 2018.

[71] P. Fallah, L. A. Hof, and R. Wuthrich, "Fabrication of high-thickness and low surface roughness metal parts by a hybrid electrochemical manufacturing process," *Advances in Industrial and Manufacturing Engineering*, vol. 2, p. 100 034, 2021.

[72] R. Schuster, V. Kirchner, P. Allongue, and G. Ertl, "Electrochemical micromachining," *Science*, vol. 289, no. 5476, pp. 98–101, 2000.

[73] R. Guidelli *et al.*, "Defining the transfer coefficient in electrochemistry: An assessment (iupac technical report)," *Pure and Applied Chemistry*, vol. 86, no. 2, pp. 245–258, 2014.

[74] E Mattsson and J. Bockris, "Galvanostatic studies of the kinetics of deposition and dissolution in the copper+ copper sulphate system," *Transactions of the Faraday Society*, vol. 55, pp. 1586–1601, 1959.

[75] G. M. DE, "The adams & perry watch co. and the early watch companies of lancaster, pa," 2022.

[76] R. Watkins, "Watchmaking," 2009.

[77] *"center wheel," adventures in watchmaking.* [Online]. Available: https://watchmaking.weebly.com/center-wheel.html.

[78] T. Sebastian and C. Strem, *Toroidal propeller*, U.S. Patent 15/803,961, Nov. 2017. [Online]. Available: https://patents.google.com/patent/US10836466B2/en.

[79] J. Singh, R. Singh, and H. Singh, "Repeatability of linear and radial dimension of abs replicas fabricated by fused deposition modelling and chemical vapor smoothing process: A case study," *Measurement*, vol. 94, pp. 5–11, 2016.

[80] J. S. Chohan, R. Singh, and K. S. Boparai, "Vapor smoothing process for surface finishing of fdm replicas," *Materials Today: Proceedings*, vol. 26, pp. 173–179, 2020.